

AD-A053 520

MASSACHUSETTS INST OF TECH CAMBRIDGE DEPT OF PHYSICS

F/G 20/8

PRISM PLOT ANALYSIS OF THE REACTION  $\pi(-)P$  YIELDS  $P$   $\pi(+)\pi(-)P$ --ETC(U)

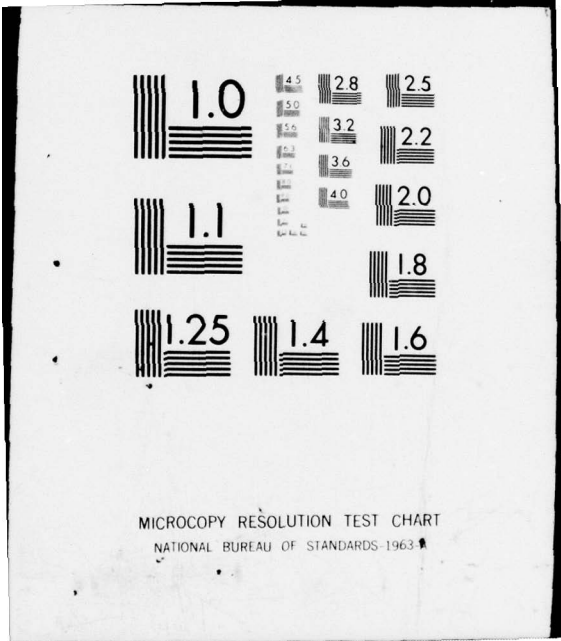
MAY 77 T LAINIS

UNCLASSIFIED

NL

1 OF 2  
AD  
A053 520





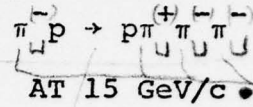
MICROCOPY RESOLUTION TEST CHART  
NATIONAL BUREAU OF STANDARDS-1963-A

AD A 053520

AD NO. DDG FILE COPY

6

PRISM PLOT ANALYSIS OF THE REACTION



by yields

pi

10

THOMAS LAINIS

B.S., United States Military Academy (1971)

SUBMITTED IN PARTIAL FULFILLMENT OF THE REQUIREMENTS FOR THE DEGREE OF

9

Master's thesis MASTER OF SCIENCE

12

11

at the

MASSACHUSETTS INSTITUTE OF TECHNOLOGY

11

May 1977

Signature of Author

Thomas Lainis

Department of Physics, May

Certified by

Irvin A. Pleas

Thesis S

Accepted by

George Fred Koster

Chairman, Departmental Com Graduate

442735

DISTRIBUTION STATEMENT A

Approved for public release; Distribution Unlimited

## PRISM PLOT ANALYSIS OF THE REACTION

$$\pi^- p \rightarrow p \pi^+ \pi^- \pi^-$$

AT 15 GeV/c

by

THOMAS LAINIS

Submitted in partial fulfillment of the requirements for the Degree of Master of Science to the Department of Physics on May 24, 1977.

## ABSTRACT

The four body final state  $\pi^- p \rightarrow p \pi^+ \pi^- \pi^-$  has been analyzed at incident beam momentum of 15 GeV/c.

The data are taken from 460,000 photographs of the SLAC 82-inch Hydrogen Bubble Chamber. All events were measured by the M.I.T. PEPR (Precision Encoding and Pattern Recognition) system, and processed through the CERBERUS-GEOMAT-SQUAW chain.

The four body final state  $\pi^- p \rightarrow p \pi^+ \pi^- \pi^-$  is analyzed by means of the Prism Plot technique. Cross sections, invariant mass spectra and angular distributions for all channels contributing to the final state are presented. The dominant channels are found to be the diffraction dissociation of the beam and nucleon. A new, broad, three pion enhancement, first reported by other groups [2,3], is clearly seen in the data with a cross section of  $132 \pm 56 \mu\text{b}$ . Its mass distribution centers about  $1.7 \text{ GeV}/c^2$ , and it decays through the  $\rho^0 \pi^-$  mode.

Thesis Supervisor: Irwin A. Pless  
Title: Professor of Physics

ACCESSION #	
NTIS	Write Section <input checked="" type="checkbox"/>
DDC	Work Section <input type="checkbox"/>
UNCLASSIFIED	<input type="checkbox"/>
NOTICE/DISPATCH	
<i>Letter on file</i>	
BY	
RESTRICTION/AVAILABILITY CODES	
Dist.	AVAIL. and/or SPECIAL
A	

## TABLE OF CONTENTS

	<u>Page</u>
ABSTRACT	2
ACKNOWLEDGEMENTS	4
I. INTRODUCTION	6
II. DATA	9
III. THE PRISM PLOT	13
IV. CROSS SECTION	17
V. DISTRIBUTIONS	20
VI. THE A'	23
VII. SUMMARY AND CONCLUSIONS	27
VIII. APPENDICES	
A. Observations and Problems During Data Reduction	29
B. The Prism Plot	31
C. The Overlap Matrix	42
REFERENCES	44
LIST OF TABLES	45
FIGURE CAPTIONS	55
FIGURES	61-113

## ACKNOWLEDGEMENTS

When I began this project, I felt as if I were attempting to untie the Gordian knot. Fortunately, there were many who aided this novice in his endeavor to master the tools of the experimentalist's trade. It would be impossible to mention each person individually, but I shall try to give my personal thanks and acknowledgements to most members of the vast army of technicians, physicists and administrators who made this experiment and report possible.

In general, I need to first thank the staff of SLAC who controlled the pion beam and the bubble chamber, for without them this exploration of the subatomic world could not have been attempted. To the entire LNS and APC group I express my gratitude for their efforts in running the computer, scanning and measuring the thousands of photographs in such an efficient manner. Special thanks are accorded to Marianne Von Randow and Ragnhild Gundersen for ensuring the continuous flow of work. There are my fellow students whose knowledge and experience eased the agony of computer battles and defeats. I should like to give personal recognition to Patrick Miller, for his methodical analysis of computer-oriented problems and inconsistencies, and to Jerome Silverman, from whom I drew as much knowledge and guidance as was physically possible from a true friend and professional associate. I certainly will never

forget the professors and post doctorates working on the floor whose insight, sense of humor and suggestions made the world of physics so much more enjoyable and rewarding, especially Dr. Pierre Trepagnier, who did the initial data reduction for the experiment, and my supervisor, Professor Irwin Pless. It was his skepticism, guidance, wit and experimental know-how that inspired me to join the group and complete this thesis.

The last individual I would like to thank is Phyllis Cusanelli whose quick and efficient typing skills allowed me to share these results with the rest of the world.

## I. INTRODUCTION

The year 1975 marked the completion of the data reduction stage of a 15 GeV/c  $\pi^-p$  experiment for the Accelerator Physics Collaboration (APC) group centered at M.I.T. The initial study of the data [1] was the prism plot analysis (PPA) of the reactions:

$$\pi^-p \rightarrow p\pi^-\pi^0$$

$$\pi^-p \rightarrow n\pi^+\pi^-$$

For a subsequent study, the four prong four constraint reaction  $\pi^-p \rightarrow p\pi^+\pi^-\pi^-$  appeared to be the natural choice, particularly since it is so amenable to prism plot analysis. This selection became particularly interesting in 1976 when the Aachen-Berlin-Bonn-Cracow-Heidelberg-Warsaw consortium reported on the indication of a new, broad, three pion enhancement at 1800 MeV which they labelled as the A' [2,3]. Their conclusions were based on two experiments. The first was a study of the reaction  $\pi^+p \rightarrow p\pi^+\pi^+\pi^-$  at 16 GeV/c incident momentum. The enhancement peaked at 1800 MeV with an approximate width of 580 MeV and a cross section of  $93 \pm 12$   $\mu\text{b}$  [2]. The second report was based on the reaction  $\pi^-p \rightarrow p\pi^+\pi^-\pi^-$  at 16 GeV/c. The A' found in that experiment centered about

2000 MeV, peaked at 1800 MeV, and had a width of about 1 GeV. In both experiments, the A' was found to decay into  $\rho\pi$ . The reports were based on a prism plot analysis of the data.

The primary purpose of this work was to conduct a prism plot analysis of the reaction  $\pi^-p \rightarrow p\pi^+\pi^-\pi^-$  at 15 GeV/c and to confirm or deny the possible existence of this new three pion enhancement.

Section II reviews the origin and reduction of the data. It is augmented by Appendix I which discusses the problems involved during the processing of the data.

Section III presents the effects of overlap between reaction channels in the prism plot technique. It discusses an overlap matrix which can be used to estimate the importance of overlap to a particular channel.

Appendix II elaborates more fully on the PPA with respect to the variables, procedures, and parametrizations used. This is done not only for the reader who wishes to evaluate the technique in depth, but also for the experimentalist who desires to duplicate any or all parts of the analysis.

Section IV gives the final cross sections found for the various channels. The overall cross section for the reaction  $\pi^-p \rightarrow p\pi^+\pi^-\pi^-$  is  $1.02 \pm .03$  mb, giving  $0.165 \pm .005$   $\mu$ b per event or  $6.06 \pm .18$  events/ $\mu$ b.

Section V presents the various distributions found for

the channels considered. The results are purer than those obtained by other means of separation (e.g. longitudinal phase space techniques). This can be seen from the cleanliness of the distributions.

Section VI presents a detailed analysis of the so-called A' enhancement. The results of this experiment confirm the existence of this enhancement, which, at this stage of the analysis, is found (when fit to a gaussian curve) to have a central value of  $1728 \pm 16$  MeV, a width of  $830 \pm 24$  MeV, and a cross section of  $132 \pm 56$   $\mu$ b. These results are in agreement with the aforementioned reports.

## II. DATA

The data for this experiment consists of 460,000 pictures taken at the SLAC 82-inch hydrogen bubble chamber with an incident  $\pi^-$  beam of 15 GeV/c momentum. For technical reasons, the data was taken in two separate runs and listed in APC documentation as Experiments 7 and 13. The two experiments were treated separately in the data reduction stage, but combined for final analysis.

Figure 1 shows the beam layout. Figure 2 depicts a schematic of the chamber. A detailed description of the data collection and reduction may be found in [1]. Figure 3 shows a schematic of the data processing chain while Table 1 gives the approximate time schedule for the experiments. Referring to the schematic will aid in understanding the processing of events in this experiment, as described below:

The film (three views per bubble chamber expansion) is initially scanned by an individual using an image plane digitizer (IPD). The scanner may reject an event for any of the following reasons:

(1) The event is not within a fixed area of the film (which converts into a fiducial volume in three dimensions). This ensures that all tracks are long enough for adequate identification and measurement.

(2) The picture is of poor quality. This eliminates

events with more than 12 incoming beam tracks, with tracks too faint for measurement or with gross visible distortions.

(3) The event is too difficult to be measured by PEPR (an acronym explained below). This excludes events with outgoing tracks less than 3 mm long or within 1.5 mm of each other in the chamber. This rejection is biased against events with low  $|t|$  (the four-momentum transfer between the target and the outgoing proton), high multiplicity or closely correlated tracks. This is characteristic of beam diffraction and is a point that will be referred to later.

Any event not rejected is digitized by coding the location on the film of the primary and secondary vertices, outgoing tracks and an ionization reference track which may or may not be the incoming beam. This information is recorded on magnetic tape via an online PDP 8.

The IPD tape is processed through a program called PREP which converts the film coordinates into PEPR's input format. PEPR stands for Precision Encoding and Pattern Recognition. It is a semi-automatic device designed by Prof. I.A. Pless and documented in [4]. Briefly, PEPR scans the film using a cathode ray tube and records the precision measurements on tape.

A program entitled CERBERUS combines the still separated (by film views) precision measured events into one convenient tape record. Geometric reconstruction of the tracks

in space is performed by GEOMAT, while kinematic fitting is done by SQUAW. SQUAW attempts fits to the following hypotheses for four prong events:

HYPOTHESIS	CONSTRAINTS
$\pi^- p \rightarrow p \pi^+ \pi^- \pi^-$	4
$\pi^- p \rightarrow p \pi^+ \pi^- \pi^- \pi^0$	1
$\pi^- p \rightarrow p \pi^+ \pi^- \pi^- \mu\mu$	0
$\pi^- p \rightarrow n \pi^+ \pi^+ \pi^- \pi^-$	1
$\pi^- p \rightarrow \pi^+ \pi^+ \pi^- \pi^- \mu\mu$	0
$\pi^- p \rightarrow p k^+ k^- \pi^-$	4

Finally, the events are run through ARROW, which creates the Data Summary Tape (DST), by selecting the most highly constrained successful SQUAW fits. Tests are imposed on the proton and the  $\pi^+$  when ambiguities arise. An ambiguous event is an event which has more than one successful hypothesis of the same constraint class. In the reaction  $\pi^- p \rightarrow p \pi^+ \pi^- \pi^-$ , an ambiguity may occur if a successful fit is obtained when the roles of the proton and the  $\pi^+$  are reversed. At low momentum (less than 1.0 GeV/c) protons and pions are distinguishable on the basis of the ionization information included in the data. At higher momenta, resolution of the ambiguity by other means is necessary. In this experiment, the ambiguities were resolved by selecting the event with the least  $\chi^2$ .

The final DST contains 6183 events of the reaction  $\pi^- p \rightarrow p \pi^+ \pi^- \pi^-$ , of which 128 were ambiguous.

Appendix I reviews the problems encountered during these stages that may have affected this work, and the means taken to test their effects.

## III. THE PRISM PLOT

Prism Plot Analysis (PPA) is an iterative process in which Monte Carlo events, created to kinematically reproduce the results of the previous iteration, are compared to actual data. It has been described in detail in [1,5,6,7]. The theory, as well as the parametrization used, is summarized in Appendix II. This section discusses overlap between channels.

The overlap region for two reaction channels is that volume of phase space kinematically shared by events in both channels. It is events of this type which PPA has difficulty separating. By studying the degree of overlap between the reaction channels one may estimate the purity of separation. A matrix has been derived to evaluate the significance of overlap regions [2]. Appendix III defines and summarizes the meaning of the matrix while Table 2 reproduces the numerical results for the reaction channels in the present analysis.

From the table, we see that the percentage of overlap varies between 1% and 47%. However, a high degree of overlap is expected between certain channels. For example, the diffraction dissociation of the proton into ( $\Delta^{++}\pi^-$ ) or ( $p\pi^+\pi^-$ ) is impossible to separate. This is obvious not only from the values of the overlap matrix (47% and 44%) but also from observation of the mass distributions of the ( $p\pi^+$ ) for these

channels. The strong  $\Delta^{++}$  signal coexisting with the threshold kinematic limits of the  $(p\pi^+)$  makes the two channels indistinguishable and suggests combining the results for both channels. This has been done and the combined channel will be referred to as  $\pi^-p \rightarrow (\Delta^{++}\pi^-)_{DD}\pi^-$ .

The  $A_1$  and  $A_2$  also display a high degree of overlap (36% and 44%). Coupled with the results of a partial wave analysis [8], which showed that there is a strong interference effect between the two states, the observations suggested combining the results of the  $A_1$  and  $A_2$ . It is felt that the  $A_3$  which decays through a  $(f^0\pi^-)$  mode is still pure enough to discuss separately. The  $A'$  also displays a high degree of overlap with the  $A_1$  and  $A_2$ ; this is probably not due to true overlap, but rather to the parametrization of the  $A'$  which resulted in too many events being weighted as the  $A'$ . The cross section for the  $A'$  of  $132 \pm 56 \mu\text{b}$ , which is surprisingly high for an enhancement only recently discovered, adds credence to this conjecture. PPA would be more accurate if the shape of the  $A'$  were known and fixed in the prism plot program [see Appendix III]. If the entire A sample of events ( $A_1 A_2 A_3 A'$ ) were used as input into another analysis (e.g. partial wave analysis) more accurate results should be expected. This suggestion implies that the total A sample is well separated from other channels and therefore is reasonably pure. This hypothesis can be tested. We can group the various

reaction channels according to vertex mechanisms:

<u>pion diffraction</u>	<u>proton diffraction</u>	<u>Reggeon exchange</u>
$\pi^- p \rightarrow pA_1$	$\pi^- p \rightarrow (\Delta^{++} \pi^-)_{DD} \pi^-$	$\pi^- p \rightarrow \Delta^{++} \pi^- \pi^-$
$\rightarrow pA_2$		$\rightarrow \Delta^0 \rho^0$
$\rightarrow pA_3$		$\rightarrow (p\pi^-) f^0$
$\rightarrow pA'$		

Table 3 reproduces the values of the overlap matrix for these three groupings. The two diffractive processes are extremely well separated from each other, while the Reggeon exchange events have a 15% overlap with those of the other two processes. This result, while non-negligible, is felt to be within acceptable limits.

An interesting aspect of the overlap matrix is that it gives one an upper limit on the importance of interference, which is ignored in the current formulation of PPA. Consider a final state with only two channels, e.g.,

$$\pi^- p \rightarrow pX \quad (a)$$

$$\pi^- p \rightarrow pY \quad (b)$$

The differential cross section is:

$$d\sigma = M_a^2(\vec{x}) + M_b^2(\vec{x}) + 2M_a(\vec{x})M_b(\vec{x}) \cos(\theta_a - \theta_b)$$

where  $M_j(\vec{x})$ ,  $j = a, b$ , is the amplitude for reaction  $j$  to occur at position  $\vec{x}$  in phase space (as discussed in Appendix II,  $\vec{x}$  may be characterized by  $3N - 5$  coordinates), and  $\theta_a - \theta_b$  is the phase difference between the two amplitudes. If the product of  $M_a(\vec{x})M_b(\vec{x})$  is zero, the interference term is zero regardless of the phase angle. (Presently, PPA arbitrarily assumes the difference to be  $\pi/2$ .) The overlap matrix indicates the degree to which  $M_a(\vec{x})$  and  $M_b(\vec{x})$  are simultaneously non-zero in the interference term.

## IV. CROSS SECTION

The total cross section is:

$$\sigma = \frac{AN}{\rho A_0 \beta f \ell}$$

where:

$\sigma$  is the cross section

A is the atomic weight of H = 1.008 gm/mole

$\rho$  is the density of liquid hydrogen = 0.0594  $\pm$   
.001 gm/cm<sup>3</sup>

$\beta$  is the average beam tracks per picture

f is the number of frames in the experiment

$\ell$  is the track length corrected for attenuation

$A_0$  is Avogadro's number

N is the number of events found by the scanners and corrected for scanner efficiency and missing low |t| elastics.

Such a calculation [1] yields a total cross section of 26.21  $\pm$  1.0 mb. As this is in agreement with a high precision counter experiment [9], the results have been normalized to their findings and summarized in Table 4.

For this paper,  $\sigma/N$  for four prong events is found most simply by:

$$\frac{\sigma_{4p}}{N_{4p}} = \frac{4 \text{ Prong Cross Section}}{\text{Total 4 Prong Events}} = \frac{9.36 \text{ mb}}{56333} = 0.165 \pm .0005 \frac{\mu\text{b}}{\text{events}}$$

This yields as the cross section:

$$\sigma(\pi^- p \rightarrow p\pi^+\pi^-\pi^-) = (0.165)(6183) = 1.02 \pm 0.03 \text{ mb}$$

where the error quoted is purely statistical. In addition, systematic errors (due to processing biases and beam contamination) are estimated to be 1.2% [1].

The 6183 events were separated into their channels by the prism plot as described in the previous sections. The resultant cross sections are given in Table 5. In general, these results compare quite favorably with published data as can be seen in the same table.

However, the cross section for the pion diffraction ( $A_1 A_2 A_3 A'$  production) is noticeably lower than that found in [2]. Comparison of the raw  $(\pi^+\pi^-\pi^-)$  invariant mass distributions for this experiment and for [2] shows that there are relatively fewer events in the A region in this experiment. A possible explanation for this discrepancy lies in the scanning biases described in Section II, which would preferentially reject events in the A region. Another source of problems may be GEOMAT, as explained in Appendix I.

It is interesting to compare the cross sections found in this analysis for the diffraction dissociation of the upper

and lower vertices, to those found in a  $\pi^+p$  experiment as the mechanisms are theoretically independent of charge. Such a comparison may be found in Table 6. Within two standard deviations, and considering the possible biases discussed above, the cross sections are seen to be independent of the charge of the beam.

## V. DISTRIBUTIONS

The distributions of the separated samples in mass, decay angles and  $t$  are shown as follows:

<u>Channel</u>	<u>Figures</u>
(1) $\pi^- p \rightarrow (\Delta^{++} \pi^-)_{DD} \pi^-$	5 - 8
(2) $\pi^- p \rightarrow \Delta^{++} \pi^- \pi^-$	9 - 11
(3) $\pi^- p \rightarrow \Delta^0 \rho^0$	12 - 14
(4) $\pi^- p \rightarrow (p \pi^-) f^0$	15 - 18
(5) $\pi^- p \rightarrow p A_1$	19 - 21
(6) $\pi^- p \rightarrow p A_2$	22 - 24
(7) $\pi^- p \rightarrow p A_3$	26 - 28
(8) $\pi^- p \rightarrow p A'$	30 - 43

Table 7 compares the slopes for  $\frac{d\sigma}{dt}$  found in this analysis with those found in other works.

The  $(\Delta^{++} \pi^-)_{DD}$  channel appears to indicate the presence of  $N^*$  (1688). This is expected as the parametrization of the DD channel is such that it will pick up any low mass  $(p \pi^+ \pi^-)$  enhancement. The  $\cos \theta_{GJ}$  of the DD peaks extremely forward,

in agreement with [3]. It may also be noted that the striking similarity between this distribution and that of  $\pi^+p \rightarrow (\Delta^{++}\pi^-)_{DD}\pi^-$  [2] lends additional credence to the theory that the reaction mechanism for this channel is charge independent.

The invariant mass of the  $(p\pi^+)$  in reaction 2 has a narrow width and appears to be rather clean (Figure 9). This observation and the small asymmetry in  $\cos \theta_{GJ}$  suggest that contamination from other channels is not significant.

Indications from the mass distribution of reactions 3 and 4 imply that, in addition to  $\Delta^0$  (1232), higher mass isobars may be present (Figures 12 and 15, respectively). The restriction on the mass of the  $(p\pi^-)$  in the Monte Carlo program for channel 3 is the probable cause for the lower cut-off in the  $(p\pi^-)$  mass distribution as compared to that of channel 4 (see Appendix II). While the  $\cos \theta_{Hel}$  distributions for the  $(p\pi^-)$  in both channels are quite similar, the  $\cos \theta_{GJ}$  appears to be peaked more forward for reaction 3 than for reaction 4. This is in agreement with the results published in [3].

The  $A_3$  invariant mass distribution appears to be quite broad, as expected. The  $(\pi^+\pi^-)$  invariant mass shows some contamination from a  $\rho^0$  source, presumably another A. The  $\cos \theta_{GJ}$  distributions are in excellent agreement with published results [3].

No particular comments will be made about the individual distributions for the  $A_1$  and  $A_2$ , as overlap and interference

have made separation difficult (see Section III). These distributions have been given for comparison with the A'. Since this enhancement, by virtue of its recent discovery, is the most interesting, it is discussed separately in the next section.

## VI. THE A'

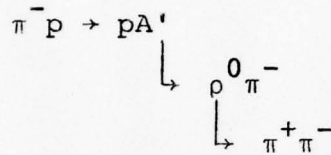
There are 802 weighted events designated as A'. The cross section is  $132 \pm 56 \mu\text{b}$ . Before continuing the discussion, however, the reader is reminded that the events designated as A' may not be pure (see Section V). There is probably contamination from both the  $A_1$  and  $A_2$  channels.

The obvious question is whether or not the events tagged as the A' are events originating from a single particle or enhancement, or are they a conglomeration of independent events whose only common factor is a similar phenomenological occupation of phase space. To classify events, one usually observes the various invariant mass combinations. The distributions for events tagged as A' are given in Figures 30 - 34. There only appears to be a minute percentage of  $\Delta^{++}$  events present. The  $(p\pi^-)\rho^0$  and  $(p\pi^-)f^0$  channels are ruled out, not because there is no indication of  $\rho^0$  [primarily present] or an  $f^0$  [negligibly present], but because the mass distribution  $(p\pi^-)$  fails to indicate any structure. One might argue that a non-negligible fraction of DD is present (6%), but this hardly explains the data. Finally, on the basis of their  $3\pi$  effective mass distribution, these events cannot all be  $A_1$ ,  $A_2$  or  $A_3$  which have masses lower than that found for the A'. Also, the  $A_3$  decays into  $f^0\pi^-$ .

If we suppose that the events are a unique combination of many channels, then we might expect that while the mass distributions will not indicate which reaction channel the

events originated from, the decay properties might demonstrate the lack of cohesive structure.

The first property observed is the imposed decay mode, namely:



This condition was deemed applicable for two reasons:

- (1) The A' originally appeared in the A<sub>1</sub> channel which decays via  $\rho^0$  mode.
- (2) Prior to tagging for the A', a clear  $\rho^0$  signal was obvious in the untagged events.

We note that the  $\rho^0$  signal (Figure 31) is rather pure.

We can also study the decay angular distributions. As shown in literature [10,11, for example], the spin of an enhancement may be obtained from the angular distributions of the outgoing particles. The two more common reference frames in which one can project the angular distributions are the helicity frame (s channel) and Jackson frame (t channel). The reaction  $\pi^- p \rightarrow p A'$  is diagrammed in Figure 35 with the angles in the reference frames defined and depicted.

As a first order approximation, if one goes to the Jackson frame (Figure 36), the highly peaked forward and

backward  $\cos \theta_{GJ}$  distribution suggest a spin on the order of two or greater.

While the Jackson frame is usually assumed simplest for peripheral collisions, the helicity distributions are of interest for other reaction mechanisms. Figure 37 shows the  $\cos \theta_{Hel}$  and  $\phi_{Hel}$  distributions for the A' with the similar trend toward forward and backward peaking.

The distributions  $\frac{d\sigma}{dt'}$  and  $\frac{d\sigma}{dpt^2}$  (Figures 37 and 39) are interesting as their slopes are predicted by theories. Figures 38 and 40 compare both slopes with their counterparts of the A<sub>1</sub>, A<sub>2</sub> and A<sub>3</sub>. All are compatible which may be an indication of similar reaction mechanisms. A striking similarity among the three is the sharp decline at  $|t'| < .02 \text{ GeV}/c^2$ . This may indicate not only a similar mechanism, but also missing events, as mentioned previously. Lastly, the rapidity, Feynman x (where  $x = P_{||}^{cm}/P_{max}^{cm}$ ) and longitudinal momentum distributions are given. They indicate that the A' is produced forward, as expected if beam diffraction is the process, but not as much as either the A<sub>1</sub> or A<sub>2</sub>. A check of the rapidity of the individual pions reveals that this forwardness is not so great as to rule out all but the lightest exchange particle (Figure 43). Until purification is achieved to a higher degree, analysis of the reaction mechanism is difficult.

In summary:

(1) A significant number of events survived the iterative process of PPA as the A'.

(2) The rather pure decay mode ( $\rho^0 \pi^-$ ) of the events so tagged suggests that independent phase space events cannot be claimed as their origin.

(3) There are indications that the A' has a high spin as revealed by the  $\cos \theta_{GJ}$  and  $\cos \phi_{Hel}$  distributions.

(4) There is a remarkable similarity in the slopes of  $\frac{d\sigma}{dt'}$  and  $\frac{d\sigma}{dpt^2}$  between the A' and the  $A_1$ ,  $A_2$  and  $A_3$ .

The A', in view of the above, is an enhancement in its own right. Credit for its discovery must be given to the ABBCCHW collaboration, however, as this work is only confirmatory in nature.

## SUMMARY AND CONCLUSIONS

It has been shown that a Prism Plot Analysis of the reaction  $\pi^- p \rightarrow p \pi^+ \pi^- \pi^-$  at 15 GeV/c is successful and advantageous. It can reveal hidden processes when used correctly. The peripheral nature of events for higher energy reactions makes the analysis difficult and demands the use of a varying box size.

The  $(\Delta^{++} \pi^-)_{DD} \pi^-$  channel appears to be well separated as does the  $\Delta^{++} \pi^- \pi^-$  channel. A  $\Delta^0$  (1232), along with indications of higher mass isobars, appears in the  $(p \pi^-) \rho^0$  and  $(p \pi^-) f^0$  channels. The  $A_1$  and  $A_2$  are too difficult to separate due to their overlapping kinematics and strongly interfering mechanisms.

The  $A'$  has been found to have a central value of  $1738 \pm 16$  MeV and a width of  $830 \pm 24$  MeV. Although it cannot be claimed that the  $A'$  sample is pure (i.e., free from contamination from the  $A_1$  and  $A_2$ ) it is clear that the  $A'$  decays via a  $\rho^0$  mode, that it has a spin of at least 2, and may have a production mechanism similar to that of the  $A_1, A_2$  and  $A_3$ . The cross section of  $132 \pm 56$   $\mu\text{b}$  is surprisingly high for an enhancement that has not been noticed until the past year. Restricting the  $A'$  invariant mass may be necessary in future use of PPA but a more exact separation would probably be obtained if one used the total Prism Plot results for pion diffraction as

input to an analysis technique that takes interference into account. It can be stated, however, that the existence of the A', first reported by the ABBCCCHW collaboration, is now confirmed.

## APPENDIX I

The following comments are pertinent to the history of the data reduction:

A. IPD: The prong count was not originally listed, which complicates the computation of scanner efficiency. As a consequence, if an event was found in both the original scan and the rescan, the prong count of the rescan was used (as the information was included during this scan). Events found in the original scan but not in the rescan were individually checked by either checking the film or the same event further along in the reduction stage.

B. GEOMAT: Prior to computing the curvatures, the program was originally conceived as being able to throw out the points of poorest quality (up to a maximum of three). Unfortunately, an error in programming caused the wrong point to be deleted. This proved to have some effect on the results for 4P 4C events, but the degree has not been ascertained as of yet. A total of 10,329 four prong events were run through a corrected GEOMAT and SQUAW yielding 728 4P 4C events with  $\chi^2 < 23.7$ , corresponding to a confidence level of  $10^{-8}$ . Within statistical errors, the results were not conclusive. A second problem in GEOMAT may be with respect to stopping protons. Analysis of the effect on this experiment was not possible within a reasonable time frame. However, it is precisely these

events - slow proton and highly correlated forward pions that would enhance the region of phase space containing the  $A_1$ ,  $A_2$ ,  $A_3$  and  $A'$ .

C. SQUAW: The program imposed a confidence level of  $10^{-8}$ . Although this is an acceptable practice, the data should be checked for distortions due to this cut. Fifty percent of Experiment 13 was run through SQUAW again with a confidence level cut of  $10^{-16}$ . No significant biases were noted in the data as seen in Figures 44 - 50. The confidence level of  $10^{-8}$  was, therefore, retained.

D. Experiment 7 distinguished between a proton and a  $\pi^+$  with momentum below 1.0 GeV/c on the basis of an ionization scan performed by hand. Experiment 13 discriminates on the lacunarity as measured by PEPR.

E. Experiment 7 and Experiment 13 appear to have similar raw data (indicating no imposed biases) except for the three pion invariant mass distributions (see Figure 50). While both experiments have approximately 48% of the data below 2 GeV, Experiment 7 has 29% below 1.4 GeV while Experiment 13 has only 25% below this level. Kinematic and angular distributions fail to indicate a reason for this difference, and a review of the history of the analysis shows no obvious error.

## APPENDIX II

## PRISM PLOT

A. VARIABLES: For N particles to be fully described kinematically, it is necessary to have 4N independent variables. If the masses of the particles are known, this reduces to 3N variables as  $E^2 - P^2 = M^2$  where E is energy, P is momentum and M is mass. Conservation of energy, conservation of momentum and, for an unpolarized beam and target, an isotropic azimuthal angle dependency, reduce this number to 3N - 5 variables. Prism Plot Analysis involves looking at all 3N - 5 variables simultaneously, unlike other techniques which consider the projections of only a few variables.

For this analysis, the variables chosen were:

$$X_1 = P_{\pi_1}^T + P_{\pi_2}^T$$

$$X_2 = \frac{1}{4} [3 P_P^L - P_{\pi^+}^L - P_{\pi_1^-}^L - P_{\pi_2^-}^L]$$

$$X_3 = \frac{1}{4} [3 T_P - T_{\pi^+} - T_{\pi_1^-} - T_{\pi_2^-}]$$

$$X_4 = \sqrt{\frac{1}{8}} [2 P_{\pi^+}^L - T_{\pi_1^-} - P_{\pi_2^-}^L]$$

$$X_5 = \sqrt{\frac{1}{8}} [2 T_{\pi^+} - T_{\pi_1^-} - T_{\pi_2^-}]$$

$$X_6 = P_{\pi_1^-}^L - P_{\pi_2^-}^L$$

$$X_7 = T_{\pi_1^-} - T_{\pi_2^-}$$

where

$P_i^L$  is the longitudinal momentum of the  $i^{\text{th}}$  particle  
in the CM

$P_i^T$  is the transverse momentum of the  $i^{\text{th}}$  particle in  
the CM

$T_i$  is the kinetic energy of the  $i^{\text{th}}$  particle in the CM  
and  $\pi_1^-$  and  $\pi_2^-$  have been subscripted to differentiate between  
the two  $\pi^-$  particles.

#### B. PROCEDURE:

(1) The 3N - 5 prism plot coordinates for each event  
are calculated and scaled so as to span from 0 to 2000.

(2) The important channels are "guessed".

(3) The initial angular distributions (production angle  
and decay angles  $\theta_{GJ}$  and  $\phi_{TY}$ ) are presumed to be isotropic.  
A reasonable mass shape is also initially presumed.

(4) Using the distributions from (3) as input, Monte  
Carlo events are created and their prism plot coordinates are  
calculated.

(5) A "box" around each Monte Carlo event is constructed.

That is, about each coordinate, a tolerance is given. Mathematically, about a point described by  $(a_1 a_2 a_3 a_4 a_5 a_6 a_7)$  the tolerance used is  $(a_1 \pm \delta, a_2 \pm \delta, a_3 \pm \delta, a_4 \pm \delta, a_5 \pm \delta, a_6 \pm \delta, a_7 \pm \delta)$ . Any real event lying within this box is flagged and that real event is now referred to as a tagged event.

(6) A weight is assigned to each real event for each reaction channel "j". This is the probability that the real event belongs to that channel and is calculated as:

$$W_j = \frac{\text{number of hits from Monte Carlo events for channel } j}{\text{total number of hits from all Monte Carlo events}}$$

(7) The relative total fraction of events belonging to each channel j is calculated as the sum over all events of  $W_j$ .

(8) New mass and angular distributions are calculated and plotted using  $W_j$  as a weighting factor. These distributions are used as input to step (4).

(9) This process continues until the relative total fractions of (7) are the same for several iterations. A state of "stabilization" is said to now exist.

C. SIGNIFICANCE OF THE BOX SIZE [13]: The box size (that is, the tolerance described in the section on Procedure) has the effect of expanding the limits placed on distributions,

and therefore affects the resolution of the separation. This is especially evident for the mass distributions. For clarity of understanding, the 3 pion effective mass (i.e.,  $A_1, A_2, A_3$  and  $A'$ ) will be explored:

Consider the following variables:

$E_i^*$  is the center of mass energy of the  $i^{\text{th}}$  particle  
 $P_i^*$  is the center of mass four vector of the  $i^{\text{th}}$  particle  
 $M_i$  is the mass of the  $i^{\text{th}}$  particle  
 $\Delta_{\text{box}}$  is the box size used

In terms of these variables,

$$\begin{aligned} M_{3\pi}^2 &= (P_{\pi^+}^* + P_{\pi^-}^* + P_{\pi^0}^*)^2 \\ &= (P_{\text{total}}^* - P_p^*)^2 \\ &= P_{\text{total}}^{*2} + P_p^{*2} - 2 E_{\text{total}}^* E_p^* \\ &= s + M_p^2 - 2\sqrt{s} E_p^* \end{aligned}$$

Differentiating:

$$\begin{aligned} 2M_{3\pi} \delta M_{3\pi} &= -2\sqrt{s} \delta E_p^* \\ M_{3\pi} &= -\frac{\sqrt{s} \delta E_p^*}{M_{3\pi}} \end{aligned}$$

$\delta M_{3\pi}$  represents the incremental addition to the mass expressed in terms of  $\delta E_p^*$  - the incremental center of mass prism plot energy. In the present analysis:

$$\Delta \text{box} = \frac{2.147}{\text{MeV}} \delta E_p^*$$

and substitution yields:

$$\delta M_{3\pi} = \frac{-\sqrt{s} \Delta \text{box}}{M_{3\pi} (2.147)}$$

As a concrete example of how resolution is affected, we shall consider the  $A_2$ :

$$\begin{aligned} \sqrt{s} &= 5400 \text{ MeV} \\ M_{A_2} &= 1310 \text{ MeV} \\ \Delta \text{box} &= 100 \text{ [5\% of the energy range]} \\ |M_{3\pi}| &= \frac{5400 \cdot 100}{1310 [2.147]} = 192 \text{ MeV} \end{aligned}$$

Thus, a real event whose  $3\pi$  effective mass is nearly 200 MeV away from a Monte Carlo event could still be tagged (depending on the other variables). Utilizing a varying box technique, one is able to start with a small box (thus, limiting the value of  $\delta$ ). After all possible events have been tagged, the larger box may be used on the remaining untagged events.

D. PARAMETRIZATION OF CHANNELS: Initially, the analysis began with the following parameters:

Channel	Resonance Parametrization
$\pi^- p \rightarrow$ Phase Space	isotropic
$\rightarrow (\Delta^{++} \pi^-)_{DD} \pi^-$ $\downarrow$ $p \pi^+$	DD fixed [13] BW (1232 MeV) $\Gamma = 120$ MeV
$\rightarrow pA_1$ $\downarrow$ $\rho^0 \pi^-$ $\downarrow$ $\pi^+ \pi^-$	G (1100 MeV) $\Gamma = 300$ MeV
$\rightarrow pA_2$ $\downarrow$ $\rho^0 \pi^-$ $\downarrow$ $\pi^+ \pi^-$	G (1310 MeV) $\Gamma = 100$ MeV BW (770 MeV) $\Gamma = 150$ MeV
$\rightarrow pA_3$ $\downarrow$ $f^0 \pi^-$ $\downarrow$ $\pi^+ \pi^-$	G (1640 MeV) $\Gamma = 120$ MeV BW (1270 MeV) $\Gamma = 150$ MeV
$\rightarrow \Delta^0 \rho^0$ $\downarrow$ $\rho^0$ $\downarrow$ $\pi^+ \pi^-$ $\downarrow$ $p \pi^-$	BW (770 MeV) $\Gamma = 150$ MeV BW (1232 MeV) $\Gamma = 120$ MeV
Box size = 10% spanned space = 200	BW = Breit Weigner G = Gaussian

After five iterations, it became obvious that several channels were missing and that the box size needed to be reduced.

The  $p\pi^+\pi^-$  effective mass spectrum of the proton diffraction dissociation channel was given an extended tail and the following channels were added:

Channel	Resonance Parametrization
$\pi^- p \rightarrow (p\pi^-) \rho^0$ $\quad \quad \quad \downarrow$ $\quad \quad \quad \pi^+\pi^-$	$(p\pi^-)$ floated BW (770 MeV) $\Gamma = 150$ MeV
$\rightarrow (p\pi^-) f^0$ $\quad \quad \quad \downarrow$ $\quad \quad \quad \pi^+\pi^-$	$(p\pi^-)$ floated BW (1270 MeV) $\Gamma = 150$ MeV
$\rightarrow \Delta^{++} \pi^- \pi^-$ $\quad \quad \quad \downarrow$ $\quad \quad \quad p\pi^+$	BW (1232 MeV) $\Gamma = 120$ MeV

Box size = 5.5% spanned space  
= 110

The term "floating" means that the mass distribution from one iteration is used as input to the next iteration, in contrast to using a fixed shape, e.g. a Breit Weigner.

After ten iterations, the following observations were made:

(1) Phase space can be thought of as a separate channel whose weight can be calculated just as the other channels' probabilities are, or it may be considered as all events not tagged by any reaction channel. The former method entails increasing the box size until all events are tagged by either a reaction channel or phase space, which has the severe

disadvantage of reducing resolution and increasing the amount by which the separated channels are mixed as discussed in the previous section. The second method is, therefore, deemed more appropriate for highly peripheral reactions. Initially, phase space was considered as a separate channel. Pursuant to evidence of a great deal of overlap, the second concept was chosen and the programs so modified. In addition, programming flexibility was added. The box size could now be altered from iteration to iteration.

(2) The separated  $A_1$  contained many fewer events than found in similar experiments [3,14]. In addition, the separated  $A_3$  appeared to be contaminated by events from other channels. A phase shift analysis [8] has shown that the  $A_1$  is not gaussian in shape. The report by the ABBCCHW collaboration [2,3] of a new enhancement at 1800 GeV also suggested that further modifications should be made. It was, therefore, decided that the  $A_1$  and  $A_3$  invariant mass distributions would be allowed to float (as explained above) and the Monte Carlo widths of known resonances ( $A_2 \Delta^0 \rho^0 f \Delta^{++}$ ) were decreased to account for PPA incremental increases (i.e., resolution problems) as explained in Section C of this Appendix. This resulted in the  $A_1$  channel picking up a second peak as shown in Figure 27. Consequently, the  $A_1$  was parameterized as in [8] and the  $A'$  was allowed to float until it appeared to be peaking in the  $A_1$  region. It was then parameterized as a

gaussian with a central mass of 1660 MeV and a width of 800 MeV.

(3) The channel  $(p\pi^-)\rho^0$  gave a strong indication (in its  $3\pi$  invariant mass distribution) that the events so tagged belonged to other channels. It was therefore dropped.

(4) It was during the exploration of the A' that a more powerful varying box technique was developed in which the box size is changed not from iteration to iteration, but within a single iteration. Events are initially tagged utilizing a small box (2% of the range of the  $3N - 5$  variables). Having tagged all possible events, one now increases the box size and looks at the remaining untagged events. This procedure was repeated four times, until the box spanned 10% of the range of each variable. The reason for the emphasis on box size and on mass widths is that as the  $s$  value of an experiment increases, the reactions tend to become more and more peripheral [15]. The more localized at the kinematic boundaries the reactions become, the more difficult it becomes to separate channels with a single box. This dilemma can be solved by two means. One can increase the number of Monte Carlo events in an attempt to fill up the space in which a reaction channel occurs, allowing the use of a smaller box and yielding a more reliable probability for an event "i" to belong to reaction channel "j". The second solution is to make several passes in each iteration through the tagging

process with increasing box sizes, as previously mentioned, each time considering only those events which are untagged by the smaller box. The limiting and deciding factor is computer time.

The final parameterizations used are:

Channel	Parametrization
$\pi^- p \rightarrow (\Delta^{++} \pi^-)_{DD} \pi^-$ $\downarrow$ $p \pi^+$	DD fixed [11] see Table 8 BW (1232 MeV) $\Gamma = 120$ MeV
$\rightarrow \Delta \begin{matrix} 0 & 0 \\ \rho & \rho \end{matrix}$ $\downarrow$ $\pi^+ \pi^-$ $\downarrow$ $p \pi^-$	BW (770 MeV) $\Gamma = 150$ MeV BW (1232 MeV) $\Gamma = 120$ MeV
$\rightarrow p A_1$ $\downarrow$ $\rho \begin{matrix} 0 & - \\ \pi & \pi \end{matrix}$ $\downarrow$ $\pi^+ \pi^-$	$A_1$ fixed [8] see Table 9 BW (770 MeV) $\Gamma = 150$ MeV
$\rightarrow p A_2$ $\downarrow$ $\rho \begin{matrix} 0 & - \\ \pi & \pi \end{matrix}$ $\downarrow$ $\pi^+ \pi^-$	G (1310 MeV) $\Gamma = 60$ MeV BW (770 MeV) $\Gamma = 150$ MeV
$\rightarrow p A_3$ $\downarrow$ $f \begin{matrix} 0 & - \\ \pi & \pi \end{matrix}$ $\downarrow$ $\pi^+ \pi^-$	$A_3$ floated BW (1270 MeV) $\Gamma = 100$ MeV
$\rightarrow p A'$ $\downarrow$ $\rho \begin{matrix} 0 & - \\ \pi & \pi \end{matrix}$ $\downarrow$ $\pi^+ \pi^-$	G (1660 MeV) $\Gamma = 800$ MeV BW (770 MeV) $\Gamma = 100$ MeV
$\rightarrow (p \pi^-) f^0$ $\Delta \begin{matrix} ++ & - & - \\ \pi & \pi & \pi \end{matrix}$ $\downarrow$ $p \pi^+$	$(p \pi^-)$ floated BW (1270 MeV) $\Gamma = 100$ MeV BW (1232 MeV) $\Gamma = 120$ MeV

Using the varying box technique, the size of the box was varied from 2.5% to 10% of the spanned space (i.e., 50, 100, 150, 200).

Figure 52 illustrates the chronology of the Prism Plot parametrizations and results in this experiment.

APPENDIX III  
THE OVERLAP MATRIX [2]

A means is desired by which one can estimate the purity of separation of a particular reaction channel. The overlap matrix has been formulated for this reason:

$$OV_{ij} = \frac{1}{N_i} \sum_{k=1}^{N_i} \left( 1 - \frac{|w_i^k - w_j^k|}{w_i^k + w_j^k} \right)$$

where the index  $k$  runs through all events  $N_i$  having  $w_i^k \neq 0$ , where  $w_i^k$  is the weight (probability) that event  $k$  belongs to reaction channel  $i$ .

If all events  $k$  have  $w_i^k = 1$ , then:

$$OV_{ij} = \frac{1}{N_i} \sum_{k=1}^{N_i} \left( 1 - \frac{|1 - 0|}{1} \right) = 0$$

This zero value conveys the meaning of a pure sample.

If all events  $k$  have all weights equal for the ten channels,  $w_i^k = 1/10 = 0.1$ .

$$\begin{aligned} OV_{ij} &= \frac{1}{N_i} \sum_{k=1}^{N_i} \left[ 1 - \frac{|0.1 - 0.1|}{0.1 + 0.1} \right] = \frac{1}{N_i} \sum_{k=1}^{N_i} 1 \\ &= \frac{N_i}{N_i} = 1 \end{aligned}$$

In summary,  $OV_{ij}$  indicates the degree of overlap by

means of a scale on which 0.0 is a pure sample and 1.00 is an entirely mixed sample. This mixing also indicates the maximum degree to which interference may take place. It conveys the degree to which the product  $M_a M_b$  in the expression  $2 M_a M_b \cos (\theta_a - \theta_b)$  is not zero. Section III discusses the meaning of this term in greater detail.

## REFERENCES

1. P.C. Trepagnier, Ph.D. thesis, M.I.T. (1976).
2. A-B-B-C-C-H-W Collaboration, Nucl. Phys. B-99, 397 (1975).
3. A-B-B-C-C-H-W Collaboration, Prism Plot Analysis of the Reaction  $\pi p \rightarrow p\pi\pi\pi$  at 16 GeV/c, CERN/EP/Phys 76-41 submitted to Nuclear Physics B, June 30, 1976.
4. F.C. Winkelmann, Ph.D. thesis, M.I.T., p. 57 (unpublished) and references cited therein (1977).
5. F.T. Dao et al., Definitions and Conventions of N-Body Prism Plots, PEPR Programming Note-101, M.I.T. Laboratory for Nuclear Science, January 15, 1971 (unpublished).
6. H.E. Haber et al., The N-Body Prism Plot Ordering Equations, PEPR Prog. Note-102, M.I.T. Laboratory for Nuclear Science, May 1973 (unpublished).
7. J.E. Brau et al., Phys. Rev. Lett. 27, 1481 (1971).
8. A-B-B-C-H Collaboration, Nucl. Phys. B80, 284 (1972).
9. K.J. Foley et al., Phys. Rev. Lett. 19, 330 (1967).
10. K. Gottfried et al., Nuovo Cimento 33, 309 (1964).
11. H.B. Crawley, Decay Angular Distributions and Production Processes, M.I.T. paper (unpublished).
12. P.A. Miller, private communication.
13. G. Berlad et al., Nuc. Phys. B103, 12 (1976).
14. S. Ballum et al., Phys. Rev. D4, 1946 (1971).
15. W.R. Frazer et al., Reviews of Modern Physics 14, 284 (1972).
16. G.W. Brandenburg et al., Nucl. Phys. B16, 287 (1970).
17. C. Case et al., Nuovo Cimento 47, 675 (1967).
18. G. Ascoli et al., Phys. Rev. D7, 669 (1973).

## LIST OF TABLES

1. Approximate Time Schedule for the Reduction of Data
2. Overlap Matrix  $OV_{ij}$  indicating the Overlap in Phase Space between Channels  $i$  and  $j$
3. Overlap Matrix indicating the Overlap in Phase Space between the Quasi Two-Body Channels  $i$  and  $j$
4. Topological Cross Sections
5. Summary of Partial Cross Sections for the Reaction Channels considered in this Analysis compared to Published Reports for the Same Reaction
6. Comparison of Diffraction Cross Sections with Results from a  $(\pi^+ p)$  Experiment at 16 GeV/c
7. Comparison of  $\frac{d\sigma}{dt}$  of the  $A_1$ ,  $A_2$  and  $A_3$  for this Experiment with those of Published Works
8. Histogram Values used as Input to the Monte Carlo Program for the Reaction  $\pi^- p \rightarrow (\Delta^{++} \pi^-)_{DD} \pi^-$
9. Histogram Values used as Input to the Monte Carlo Program for the Reaction  $\pi^- p \rightarrow pA_1$

TABLE 1  
Approximate Time Schedule for the  
Reduction of Data

	<u>Experiment 7</u>	<u>Experiment 13</u>
SLAC Run	Oct. 1970	Mid 1972
IPD	June 1971	Sept. 1972
PEPR	Oct. 1971	Feb. 1973
GEOMAT and SQUAW	June 1975	Aug. 1975

TABLE 2

Overlap Matrix  $OV_{ij}$  (see Appendix III) Indicating the  
 Overlap in Phase Space between Channels  $i$  and  $j$ , Normalized to the  
 Total Number of Events in Channel  $i$

Channel "J"	Channel "i"								
	$(\Delta^{++}\pi^-)_{DD}$	$(p\pi^+\pi^-)_{DD}$	$\Delta^{++}$	$(p\pi^-)^0$	$(p\pi^-)f^0$	$A_1$	$A_2$	$A_3$	$A'$
$(\Delta^{++}\pi^-)_{DD}$	--	.47	.22	.06	.07	.01	.01	.03	.06
$(p\pi^+\pi^-)$	.44	--	.16	.10	.10	.02	.01	.02	.06
$\Delta^{++}$	.12	.09	--	.02	.04	.03	.03	.05	.07
$(p\pi^-)^0$	.04	.07	.02	--	.21	.05	.05	.08	.10
$(p\pi^-)f^0$	.05	.07	.05	.24	--	.04	.02	.11	.08
$A_1$	.01	.02	.05	.09	.06	--	.44	.24	.28
$A_2$	.01	.01	.04	.07	.03	.36	--	.17	.22
$A_3$	.02	.02	.07	.10	.12	.18	.15	--	.24
$A_4$	.07	.08	.15	.21	.14	.33	.31	.38	--

TABLE 3

Overlap Matrix  $OV_{ij}$  (see Appendix III)  
 Indicating the Overlap in Phase Space Between  
 the Quasi Channels  $i$  and  $j$ , Normalized  
 to the Total Number of Events in Channel  $i$

Channel j	Proton Diffraction	Pion Diffraction	Reggeon Exchange
Proton Diffraction	--	.04	.14
Pion Diffraction	.07	--	.18
Reggeon Exchange	.17	.13	--

TABLE 4  
Topological Cross Sections  
 $\sigma$  (mb)

2 Prongs	4 Prongs	6 Prongs	8 or More Prongs	Total
$10.35 \pm .27$	$9.36 \pm .16$	$4.69 \pm .09$	$1.41 \pm .05$	$25.02 \pm .08$

TABLE 5

Summary of Partial Cross Sections for the Reaction Channels Considered in this Analysis Compared to Published Results for the Same Reaction

This Experiment		[3] P (beam) = 16 GeV/c		[12] P (beam) = 16 GeV/c		
Reaction Channel	No. of Events	$\sigma$ ( $\mu\text{b}$ ) **	$\sigma$ ( $\mu\text{b}$ )	method*	$\sigma$ ( $\mu\text{b}$ )	method*
$(\Delta^{++}\pi^-)$ DD	1718	$284 \pm 5$	$312 \pm 27$	PPA	$261 \pm 29$	LPS
$\Delta^{++}$	471	$78 \pm 3$	$44 \pm 10$	"	} $207 \pm 23$	"
$(p\pi^-)\rho^0$	486	$80 \pm 3$	$91 \pm 15$	"		
$(p\pi^-)f^0$	423	$70 \pm 3$	$30 \pm 9$	"		
$(A_1, A_2)$	1638	$270 \pm 6$	482	"		
$A_3$	497	$82 \pm 3$	$80 \pm 14$	"		
$A'$	802	$132 \pm 4$	56	"		
(all A)	2937	$485 \pm 8$	$619 \pm 40$	"	$477 \pm 53$	"
Phase Space	147	$24 \pm$				

\* PPA = Prism Plot Analysis

LPS = Longitudinal Phase Space Analysis

\*\* Errors quoted are statistical only.

TABLE 6

Comparison of Diffraction Cross Sections  
with Results from a  $\pi^+p$  Experiment  
at 16 GeV/c

Channel	This Experiment	$\pi^+p \rightarrow p\pi^+\pi^-\pi^-$	
	$\sigma(\mu\text{b})^*$	$\sigma(\mu\text{b})$	method**
$(\Delta^{++}\pi^-)_{DD}$	$284 \pm 5$	$266 \pm 19$	PPA
$(A_1 A_2)$	$270 \pm 6$	$426 \pm 16$	PPA
$A_3$	$82 \pm 3$	$71 \pm 11$	PPA
$A'$	$132 \pm 4$	93	PPA
(All A)	$485 \pm 8$	$590 \pm 29$	PPA

\* Errors quoted are statistical only.

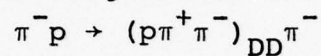
\*\* PPA = Prism Plot Analysis

TABLE 7  
 Comparison of  $\frac{d}{dt}$  of the  $A_1, A_2, A_3$   
 for this Experiment with those of Published Works

<u>Channel</u>	<u>This Experiment</u>	<u>Published Works</u>			
		Slope	P (beam) (GeV/c)	Type Beam	Ref.
$A_1$	$9.65 \pm .41$	$9.6 \pm .4$	16	$\pi^+$	8
		$10.4 \pm .3$	16	$\pi^+$	2
		$10.3 \pm .9$	13	$\pi^-$	16
		$13.0 \pm 1.4$	20	$\pi^-$	16
		$10.6 \pm 1.2$	11	$\pi^-$	17
$A_2$	$8.12 \pm .48$	$7.3 \pm 1.0$	13	$\pi^-$	16
		$7.4 \pm 0.9$	20	$\pi^-$	16
		$5.8 \pm 1.1$	11	$\pi^-$	17
$A_3$	$6.35 \pm .45$	$6.2 \pm .4$	16	$\pi^+$	8
		$6.6 \pm .4$	16	$\pi^+$	2
		$7.7 \pm .8$	16	$\pi^+$	18

TABLE 8

Histogram Values used as Input to the  
Monte Carlo Program for the Reaction

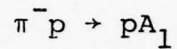


Value of the Lower Bin Edge (MeV)	No. of Events*	Value of the Lower Bin Edge (MeV)	No. of Events*
1280.	1.10	2480.	2.50
1320.	3.60	2520.	2.25
1360.	9.50	2560.	2.00
1400.	12.90	2600.	1.50
1440.	12.20	2640.	1.44
1480.	13.40	2680.	1.38
1520.	16.89	2720.	1.32
1560.	17.79	2760.	1.26
1600.	18.79	2800.	1.20
1640.	21.59	2840.	1.14
1680.	24.29	2880.	1.08
1720.	23.29	2920.	1.02
1760.	12.00	2960.	0.96
1800.	10.30	3000.	0.90
1840.	12.80	3040.	0.84
1880.	9.50	3080.	0.78
1920.	8.60	3120.	0.72
1960.	5.50	3160.	0.66
2000.	5.50	3200.	0.60
2040.	5.25	3240.	0.54
2080.	5.00	3280.	0.48
2120.	4.75	3320.	0.42
2160.	4.50	3360.	0.36
2200.	4.25	3400.	0.30
2240.	4.00	3440.	0.24
2280.	3.75	3480.	0.18
2320.	3.50	3520.	0.12
2360.	3.25	3560.	0.06
2400.	3.00	3600.	
2440.	2.75		

\* The program renormalizes the distribution to the sum of the bin values.

TABLE 9

Histogram Values used as Input to the  
Monte Carlo Program for the Reaction



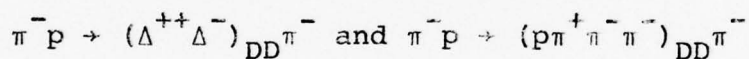
Value of the Lower Bin Edge (MeV)	No. of Events*
800.	7.5
900.	6.5
1000.	12.0
1100.	14.5
1200.	13.0
1300.	7.5
1400.	3.7
1500.	2.4
1600.	2.6
1700.	1.8
1800.	2.0
1900.	1.5
2000.	

\* The program renormalizes the  
distribution to the sum of the  
bin values.

## FIGURE CAPTIONS

1. Plan view of the beam line serving the SLAC 82-inch chamber.
2. Sketch of the 82-inch chamber.
3. Flow chart for the data scanning, measuring and reduction chain.
4. Comparison of the invariant mass of the  $(p\pi^+)$  for the channels  $\pi^-p \rightarrow (\Delta^{++}\pi^-)_{DD}\pi^-$  (left) and  $\pi^-p \rightarrow (p\pi^+\pi^-)_{DD}\pi^-$  (right).

The following figures are for the combined reactions



5. Invariant mass of the
  - a.  $(p\pi^+\pi^-)$
  - b.  $(p\pi^+)$
6. a. Cosine of the Gottfried Jackson angle  
b. The Treiman Yang angle
7.  $\frac{d\sigma}{dt}$  versus  $t$  the solid line is a fit to  $Ae^{-b|t|}$  over the interval

$$.02 \leq |t| \leq .24 \text{ GeV}^2/c^2$$

The following figures are for the reaction  $\pi^-p \rightarrow \Delta^{++}\pi^-\pi^-$

8. Invariant mass of the  $(p\pi^+)$
9. a. Cosine of the Gottfried Jackson angle  
b. The Treiman Yang angle

10.  $\frac{d\sigma}{dt}$  versus  $t$ . The solid line is a fit to  $Ae^{-b|t|}$  over the interval

$$.02 \leq |t| \leq .24 \text{ GeV}^2/c^2$$

The following figures are for the reaction  $\pi^- p \rightarrow \Delta^0 \rho^0$

11. Invariant mass of the:
- $(p\pi^-)$  for the  $\Delta^0$
  - $(\pi^+\pi^-)$  for the  $\rho^0$
12. Cosine of the Gottfried Jackson angle
- $(\Delta^0)$
  - $(\rho^0)$

The Treiman Yang angle

- $(\Delta^0)$
  - $(\rho^0)$
13. a.  $\frac{d\sigma}{dt}$  versus  $t$
- b.  $\frac{d\sigma}{dt'}$  versus  $t'$ . The solid line is a fit to  $Ae^{-b|t'|}$  over the interval
- $$.02 \leq |t'| \leq .40 \text{ GeV}^2/c^2$$

The following figures are for the reaction  $\pi^- p \rightarrow (p\pi^-) f^0$

14. Invariant mass of the
- $(p\pi^-)$  for the baryonic enhancement
  - $(\pi^+\pi^-)$  for the  $f^0$
15. Cosine of the Gottfried Jackson angle
- $(p\pi^-)$
  - $(f^0)$

The Treiman Yang angle

c.  $(p\pi^-)$

d.  $(\rho^0)$

16. a.  $\frac{d\sigma}{dt}$  versus  $t$   
 b.  $\frac{d\sigma}{dt'}$  versus  $t'$ . The solid line is a fit to  $Ae^{-b|t'|}$   
 over the interval

$$.02 \leq |t'| \leq .40 \text{ GeV}^2/c^2$$

The following figures are for the reaction  $\pi^- p \rightarrow pA_1$

17. Invariant mass of the  
 a.  $(\pi^+ \pi^- \pi^-)$   
 b.  $(\pi^+ \pi^-)$  in the  $\rho^0$
18. a. Cosine of the Gottfried Jackson angle  
 b. The Treiman Yang angle
19.  $\frac{d\sigma}{dt'}$  versus  $t'$ . The solid line is a fit to  $Ae^{-b|t'|}$   
 over the interval

$$.02 \leq |t'| \leq .40 \text{ GeV}^2/c^2$$

The following figures are for the reaction  $\pi^- p \rightarrow pA_2$

20. Invariant mass of the  
 a.  $(\pi^+ \pi^- \pi^-)$   
 b.  $(\pi^+ \pi^-)$  in the  $\rho^0$
21. a. Cosine of the Gottfried Jackson angle  
 b. The Treiman Yang angle
22.  $\frac{d\sigma}{dt'}$  versus  $t'$ . The solid line is a fit to  $Ae^{-b|t'|}$

over the interval

$$.02 \leq |t'| \leq .40 \text{ GeV}^2/c^2$$

23. Combined invariant masses for  $\pi^- p \rightarrow pA_1$  and  $\pi^- p \rightarrow pA_2$
- $(\pi^+ \pi^- \pi^-)$
  - $(\pi^+ \pi^-)$  in the  $\rho^0$

The following figures are for the reaction  $\pi^- p \rightarrow pA_3$

24. Invariant mass of the
- $(\pi^+ \pi^- \pi^-)$
  - $(\pi^+ \pi^-)$  in the  $f^0$
25. a. Cosine of the Gottfried Jackson angle  
b. The Treiman Yang angle
26.  $\frac{d\sigma}{dt'}$  versus  $t'$ . The solid line is a fit to  $Ae^{-b|t'|}$   
over the interval

$$.02 \leq |t'| \leq .40 \text{ GeV}^2/c^2$$

27. Comparison of the invariant mass of the  $(\pi^+ \pi^- \pi^-)$  for the  $A_1$  (before the  $A'$  channel was considered) when the  $A_1$  was parameterized as a
- Gaussian distribution
  - Floating distribution

The following figures are for the reaction  $\pi^- p \rightarrow pA'$

28. Invariant mass of the  $(\pi^+ \pi^- \pi^-)$

29. Invariant mass of the  $(\pi^+\pi^-)$  in the  $\rho^0$
30. Invariant mass of the
- $p\pi^+$
  - $p\pi^-$
31. Invariant mass of the
- $(\pi^+\pi^-)$  not in the  $\rho^0$
  - $(\pi^-\pi^-)$
32. Invariant mass of the
- $p\pi^+\pi^-$
  - $p\pi^-\pi^-$
33. Schematic depicting the cosine and  $\phi$  angles in the
- Helicity reference frame
  - Jackson reference frame
34. a. Cosine of the Gottfried Jackson angle
- b. The Treiman Yang angle
35. a. Cosine of the Helicity angle ( $\cos \theta_{\text{Hel}}$ )
- b. The  $\phi_{\text{Hel}}$  distribution
36.  $\frac{d\sigma}{dt'}$  versus  $t'$ . The solid line is a fit to  $Ae^{-b|t'|}$  over the interval
- $$.02 \leq |t'| \leq .40 \text{ GeV}^2/c^2$$
37. Comparison of  $\frac{d\sigma}{dt'}$  versus  $t'$  for the  $A_1, A_2, A_3$  and  $A'$ .
38.  $\frac{d\sigma}{dpt^2}$  versus transverse momentum squared [ $Pt^2$ ]. The solid line is a fit to  $Ae^{-bPt^2}$  over the interval
- $$.02 \leq Pt^2 \leq .32 \text{ GeV}^2/c^2$$
39. Comparison of  $\frac{d\sigma}{dpt^2}$  versus  $Pt^2$  for the  $A_1, A_2, A_3$  and  $A'$

- 40. a. Rapidity
- b. Feynman x
- 41. Longitudinal Momentum
- 42. a. Rapidity of the  $\pi^+$  of the A'
- b. Rapidity of the  $\pi^-$  of the A'

The following figures compare the entire sample's invariant masses listed for

- a.  $\chi^2 < 23.7$
- b.  $\chi^2 > 23.7$

- 43. ( $p\pi^+$ )
- 44. ( $p\pi^-$ )
- 45. ( $\pi^+\pi^-$ )
- 46. ( $\pi^-\pi^-$ )
- 47. ( $p\pi^+\pi^-$ )
- 48. ( $p\pi^-\pi^-$ )
- 49. ( $\pi^+\pi^-\pi^-$ )
  
- 50. Comparison of the invariant mass of the ( $\pi^+\pi^-\pi^-$ ) for
  - a. Experiment 7
  - b. Experiment 13
  
- 51. (a, b, c) Schematic depicting the chronology of the prism plot results as a function of iteration number versus fraction of the data tagged as one of the reaction channels.

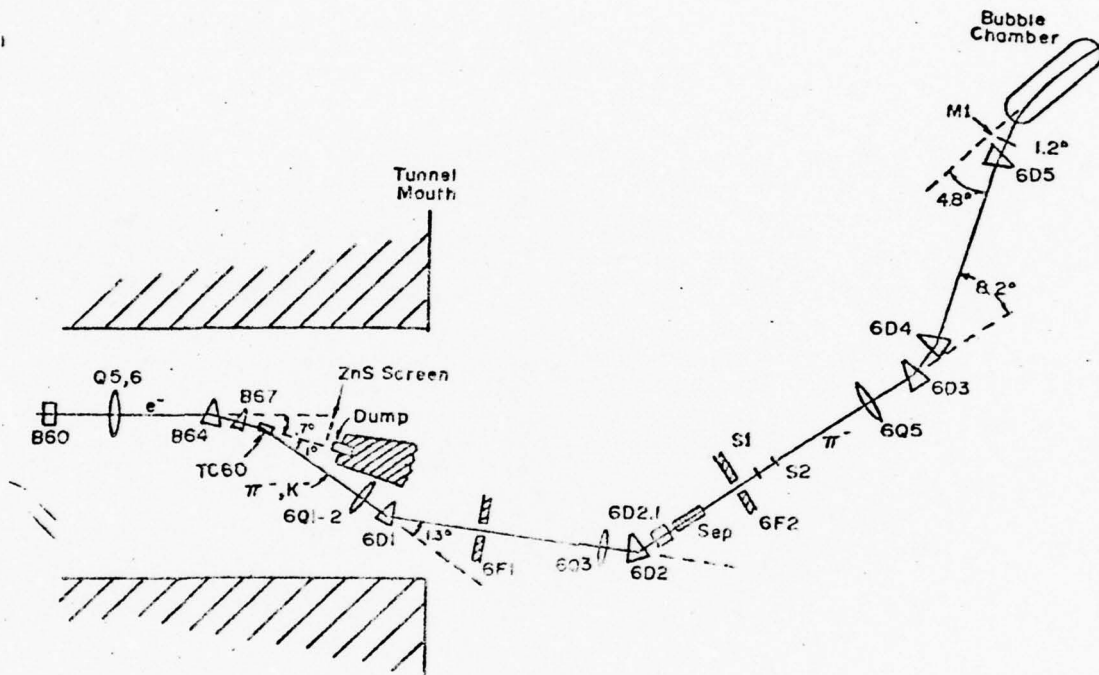


Figure 1

62

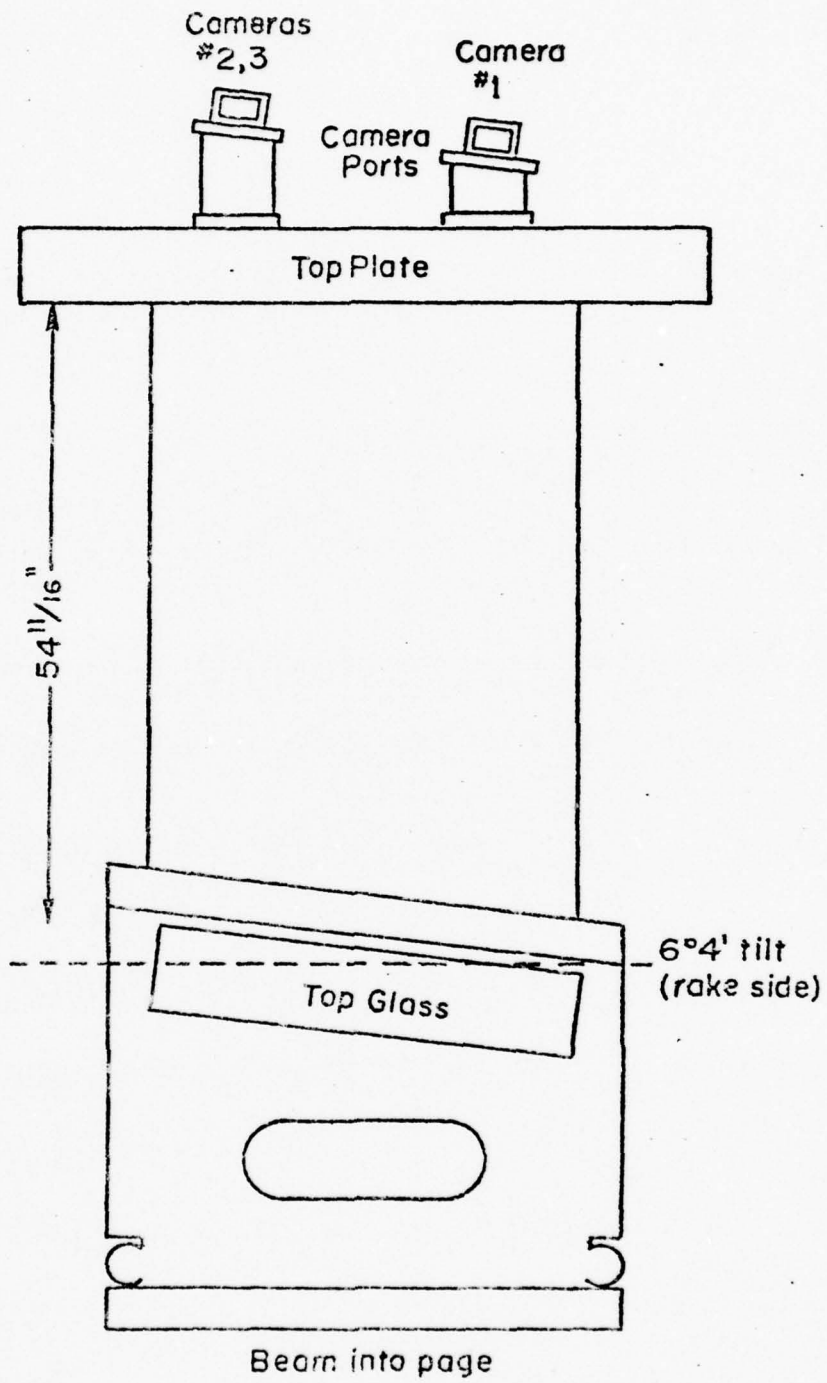


Figure 2

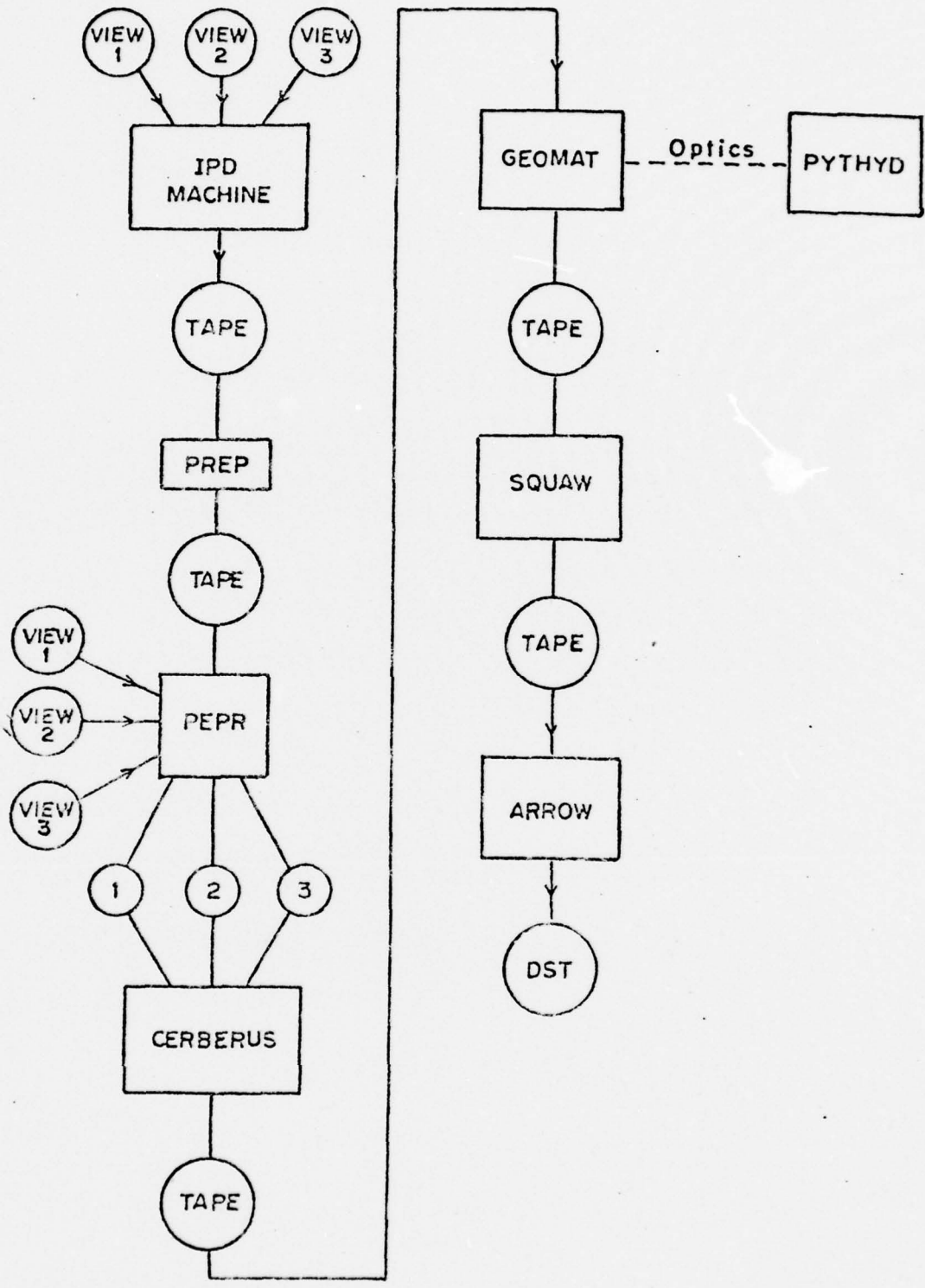


Figure 3

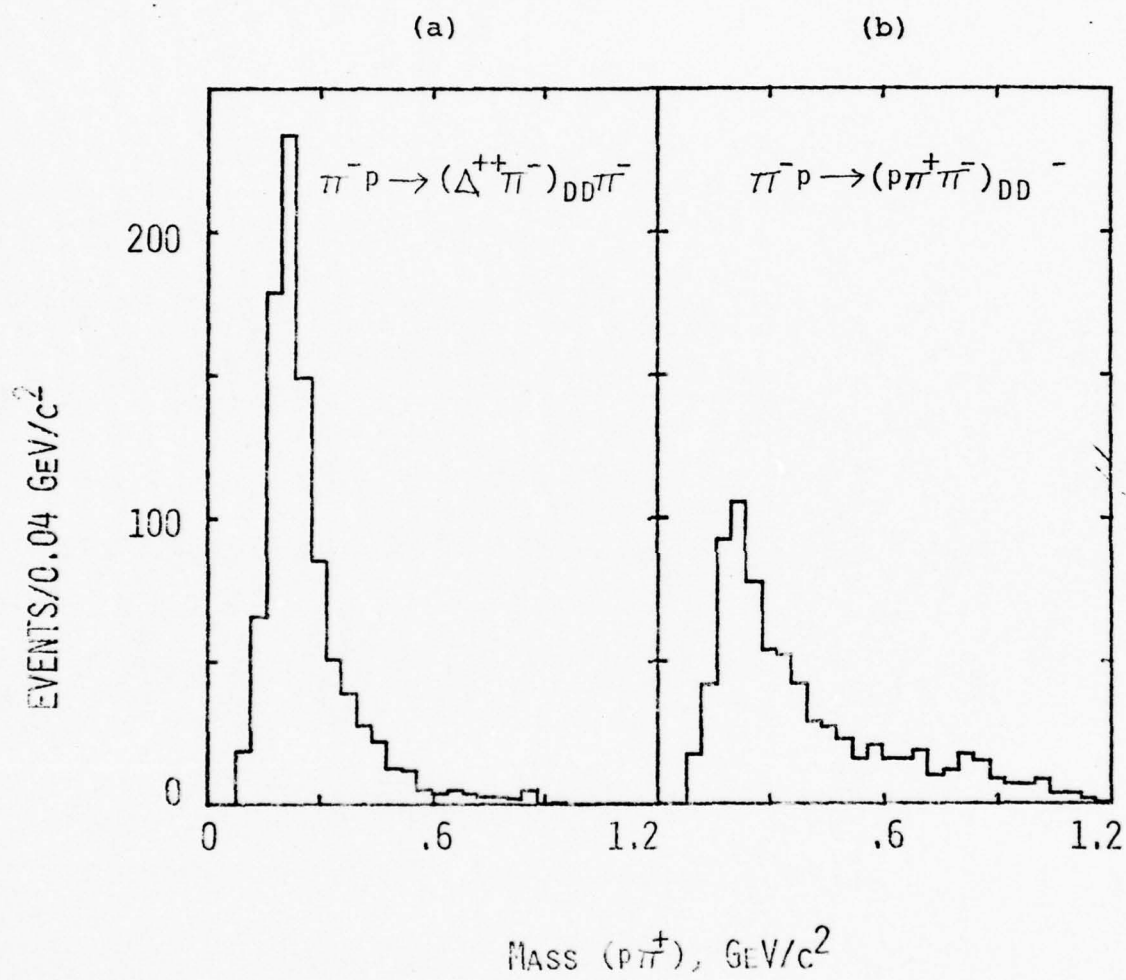


Figure 4

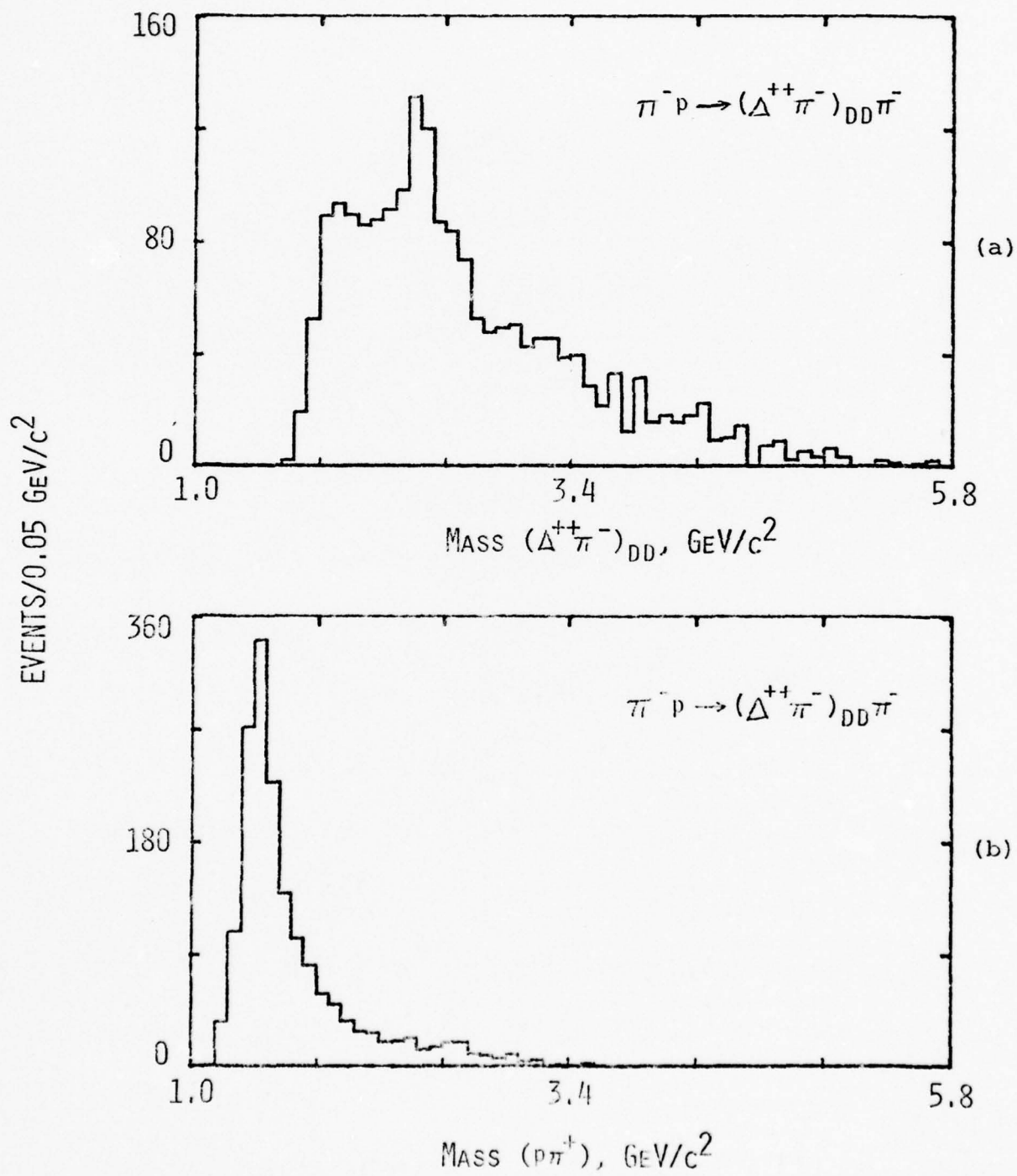


Figure 5

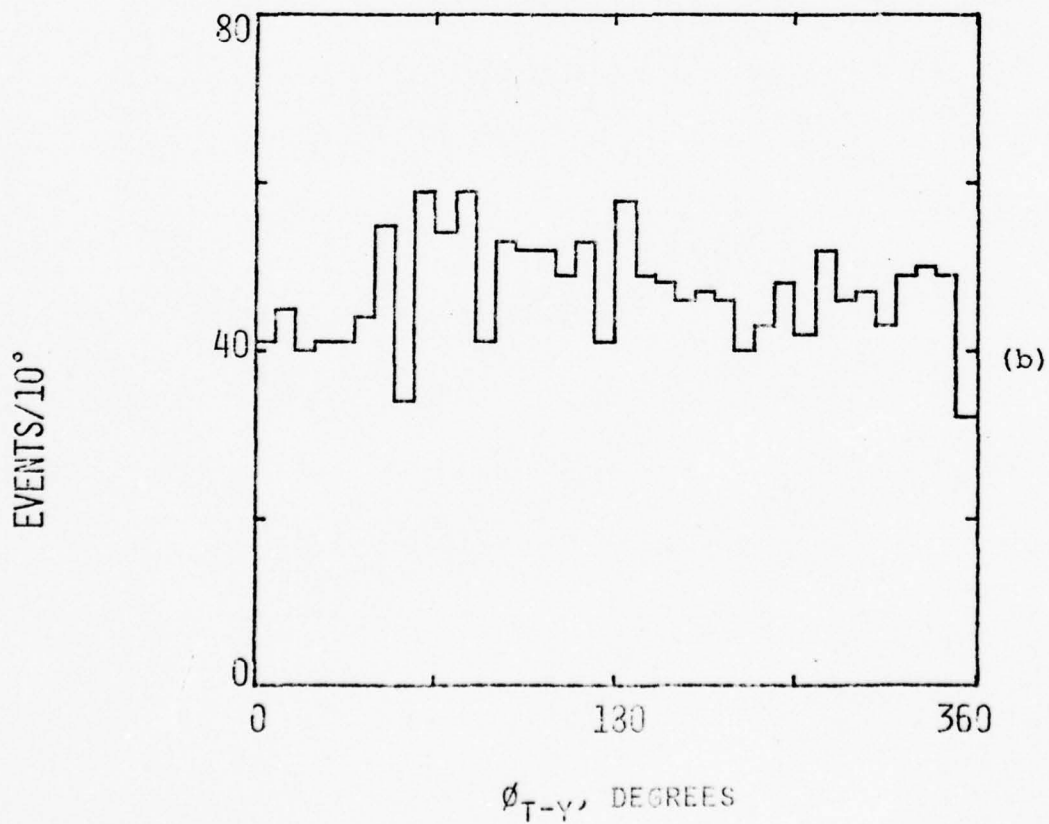
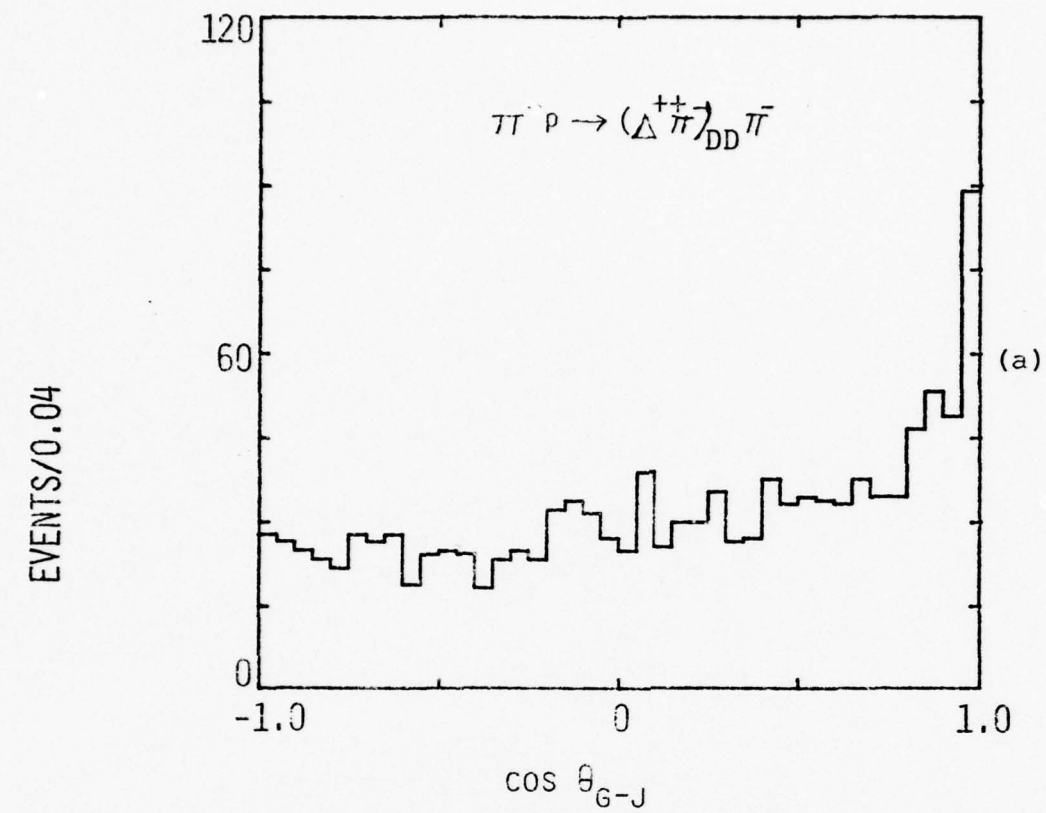


Figure 6

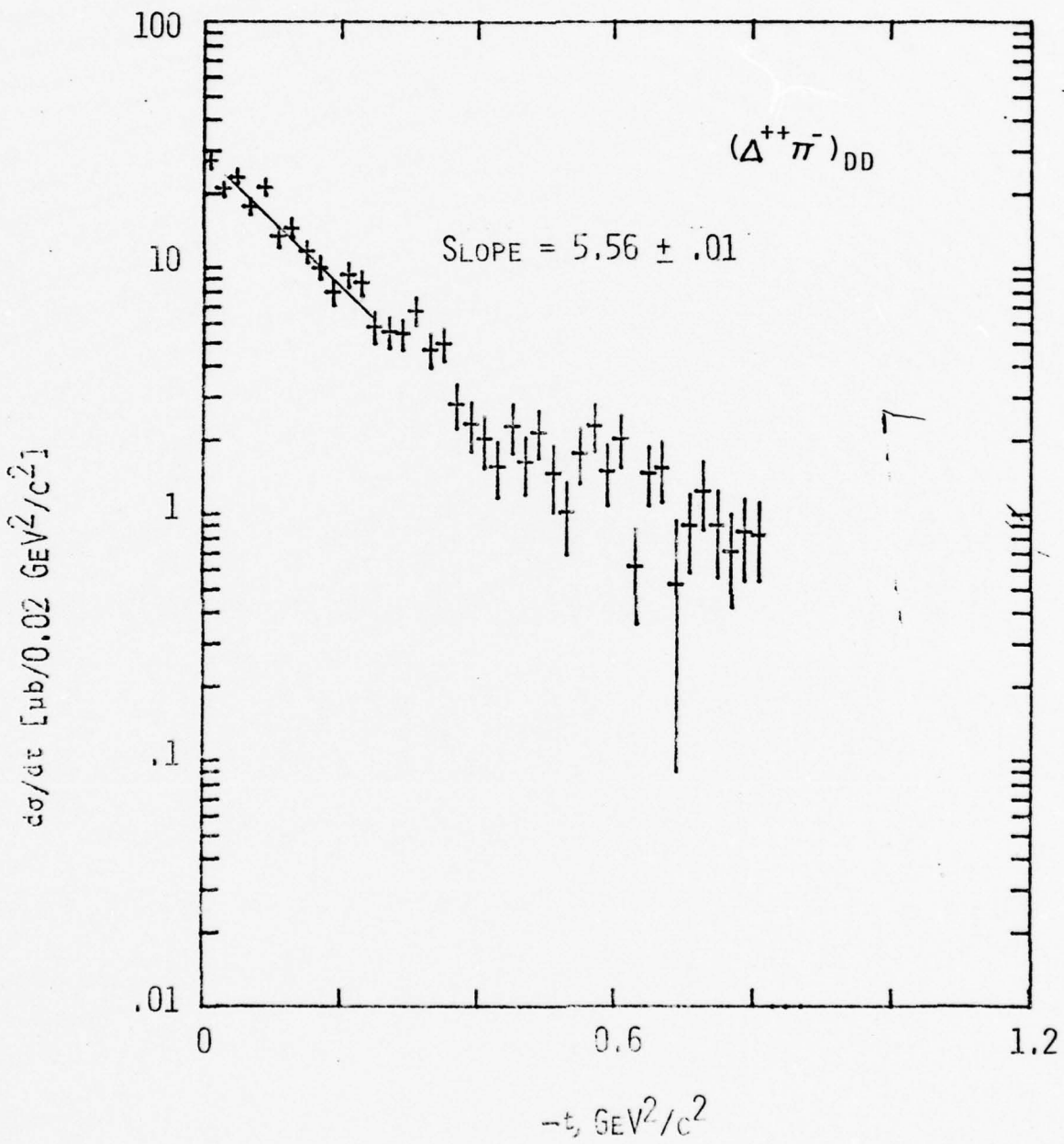


Figure 7

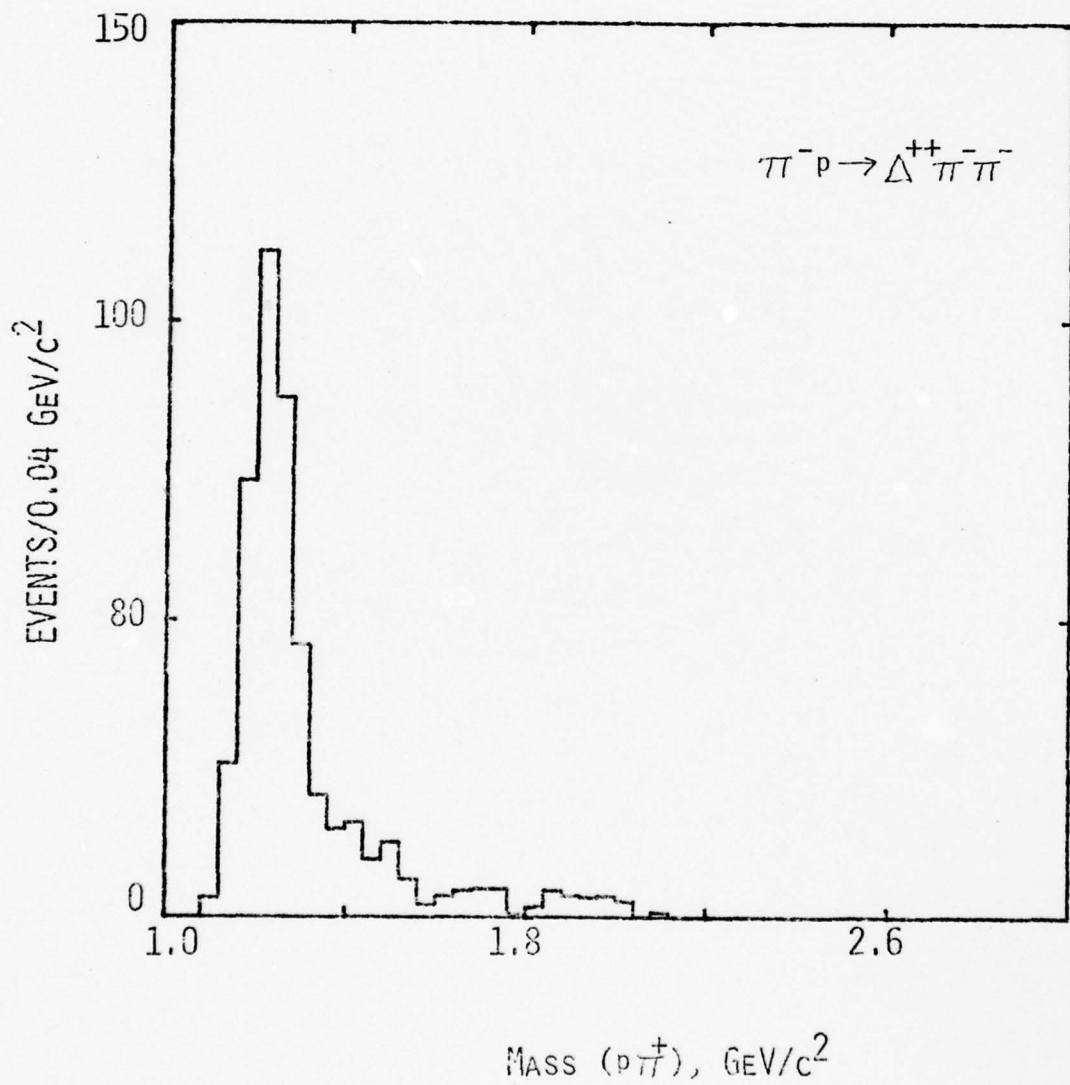


Figure 8

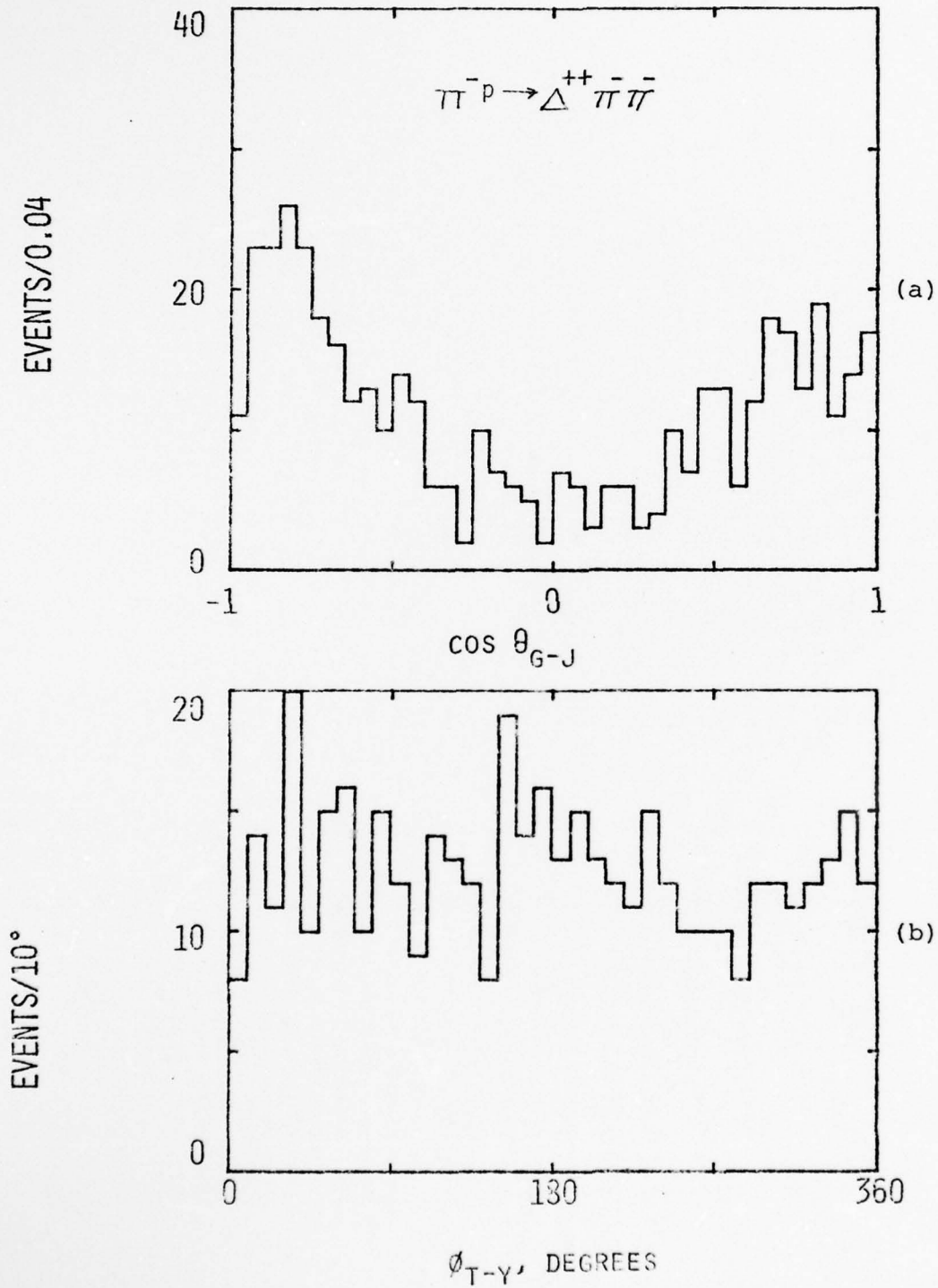


Figure 9

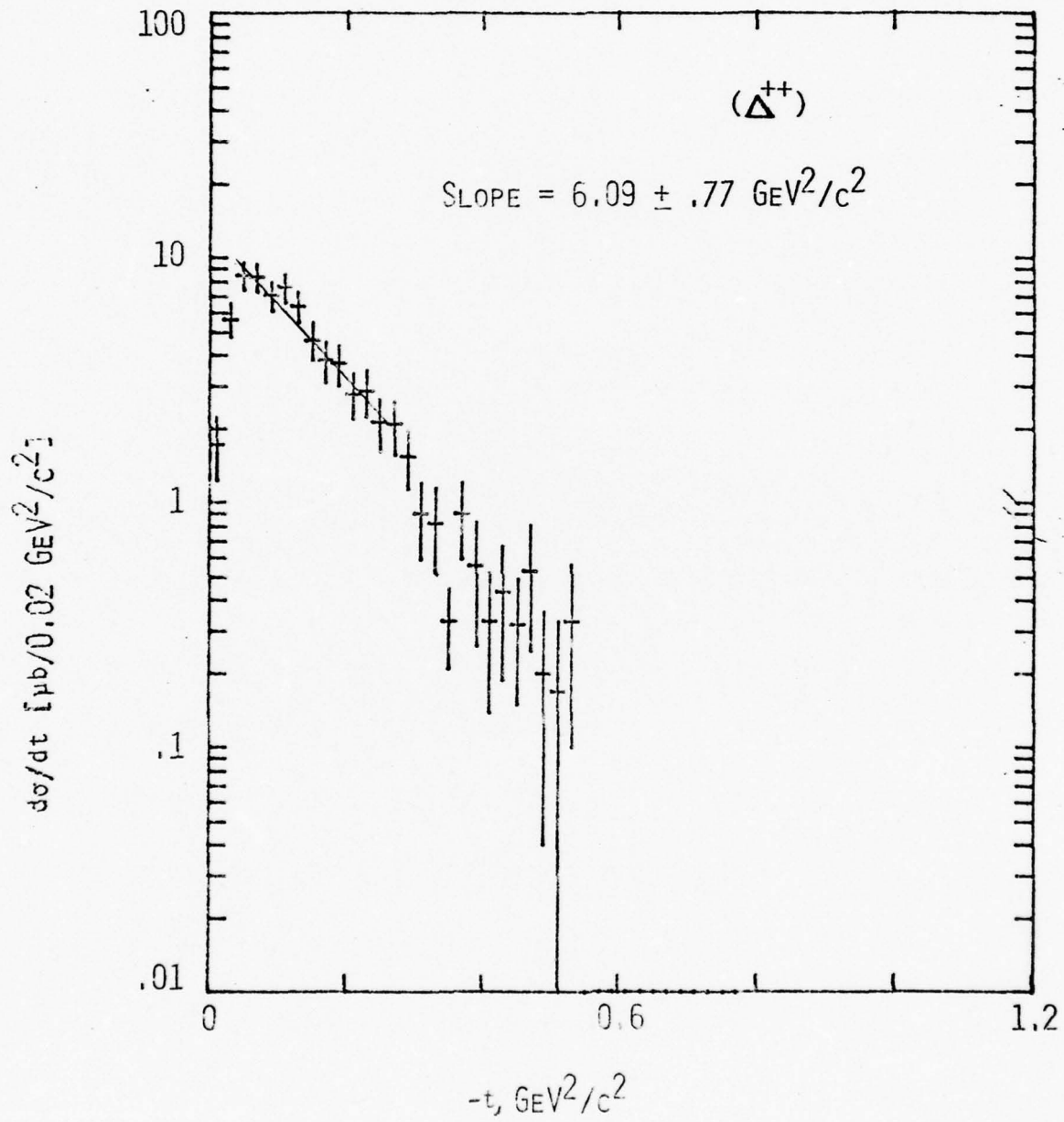


Figure 10

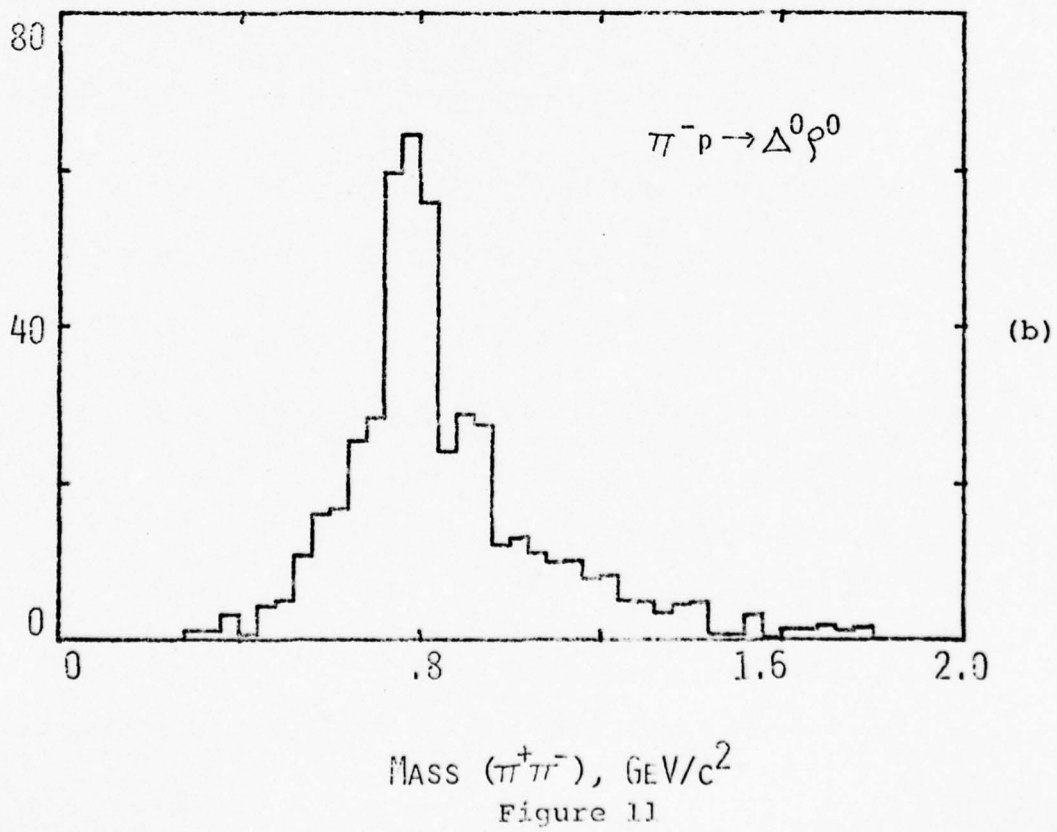
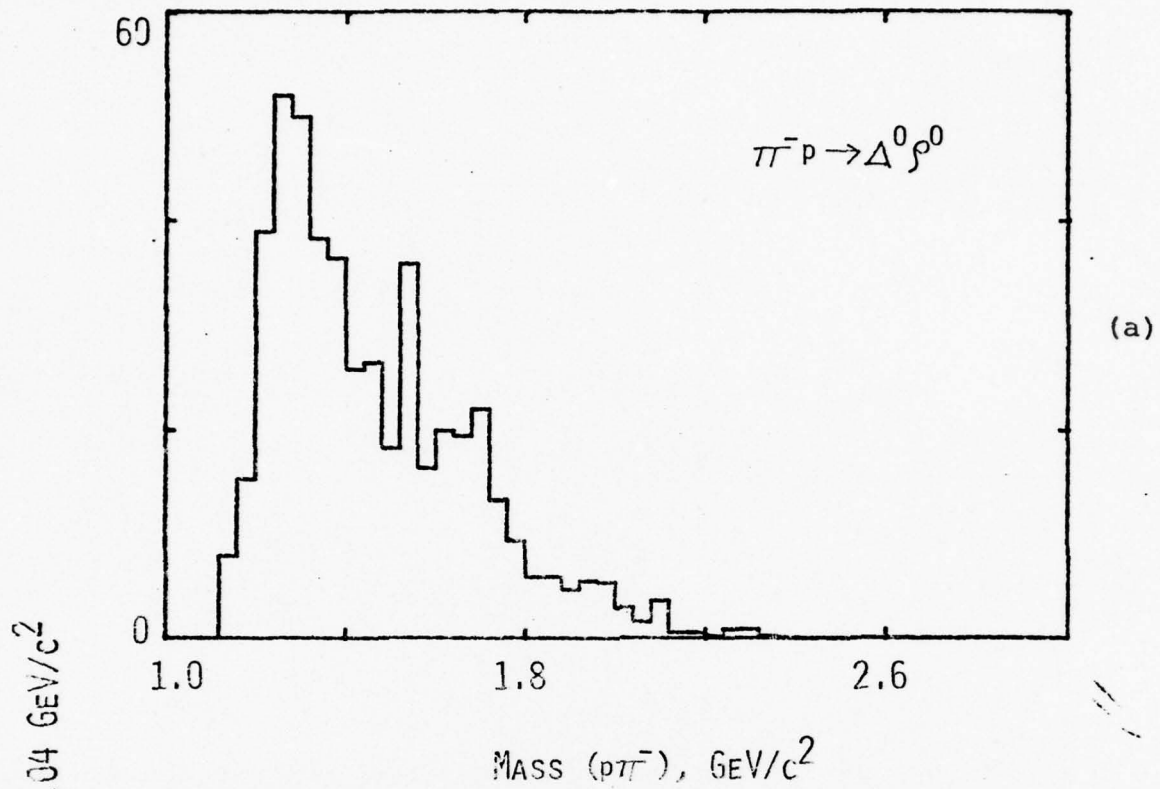


Figure 11

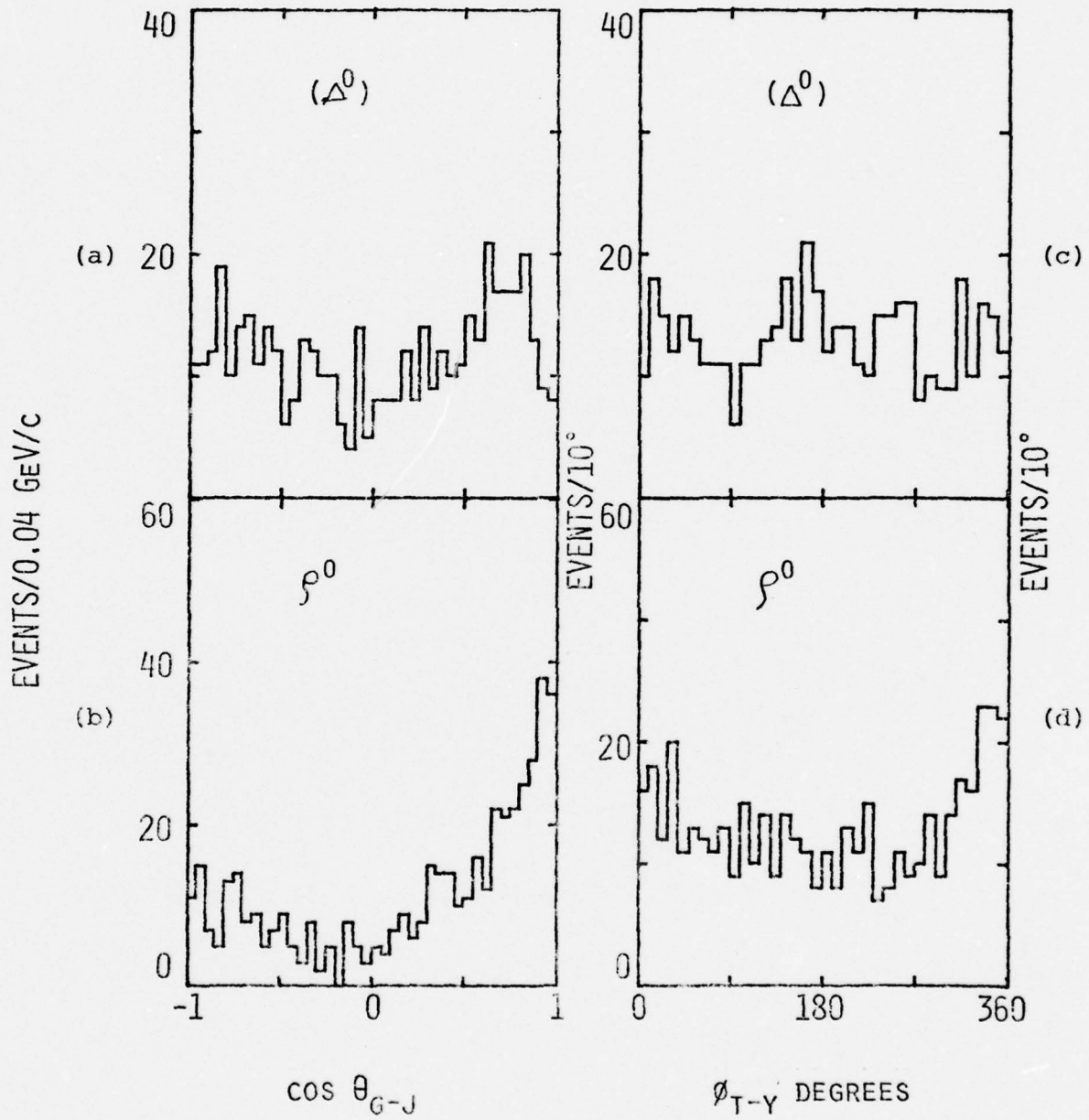
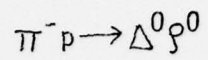


Figure 12

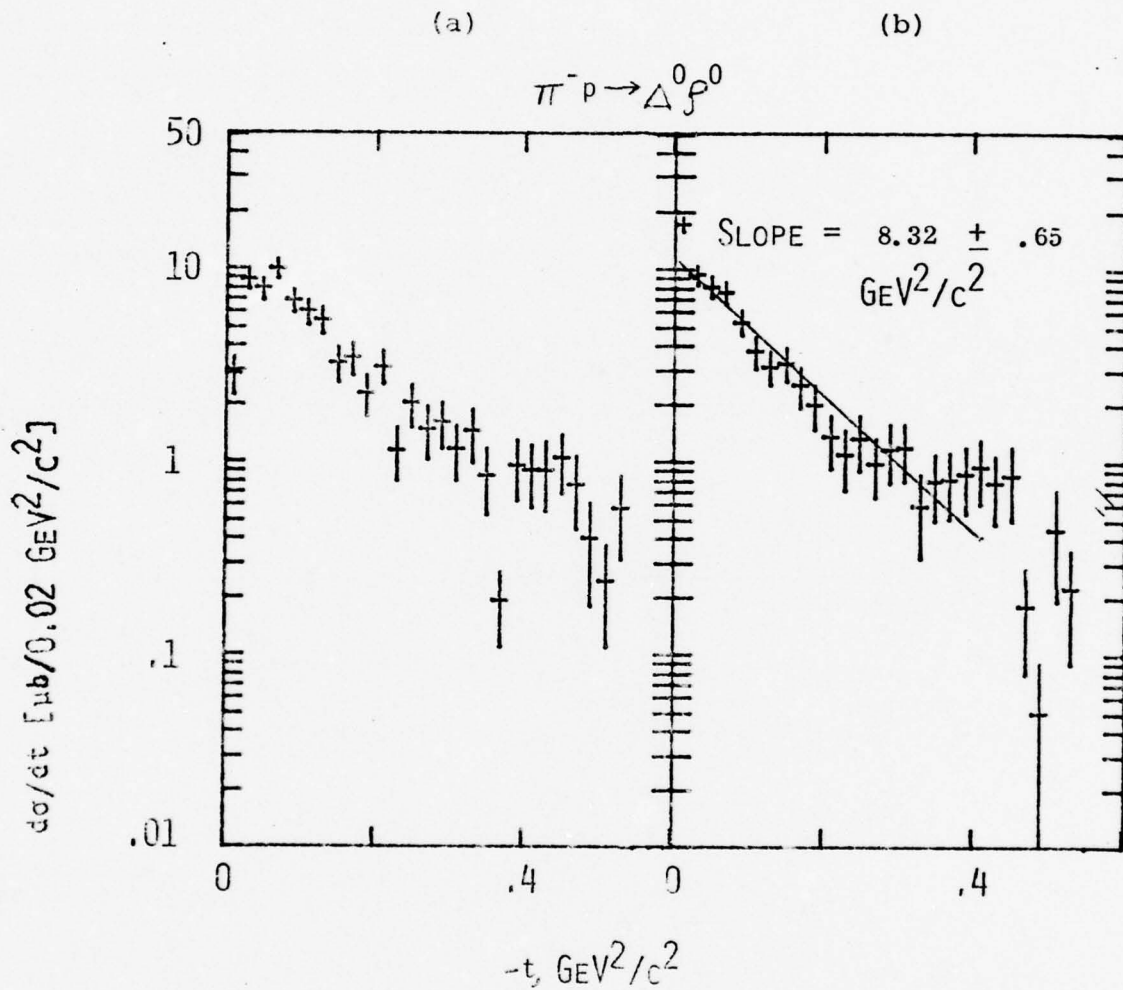


Figure 13

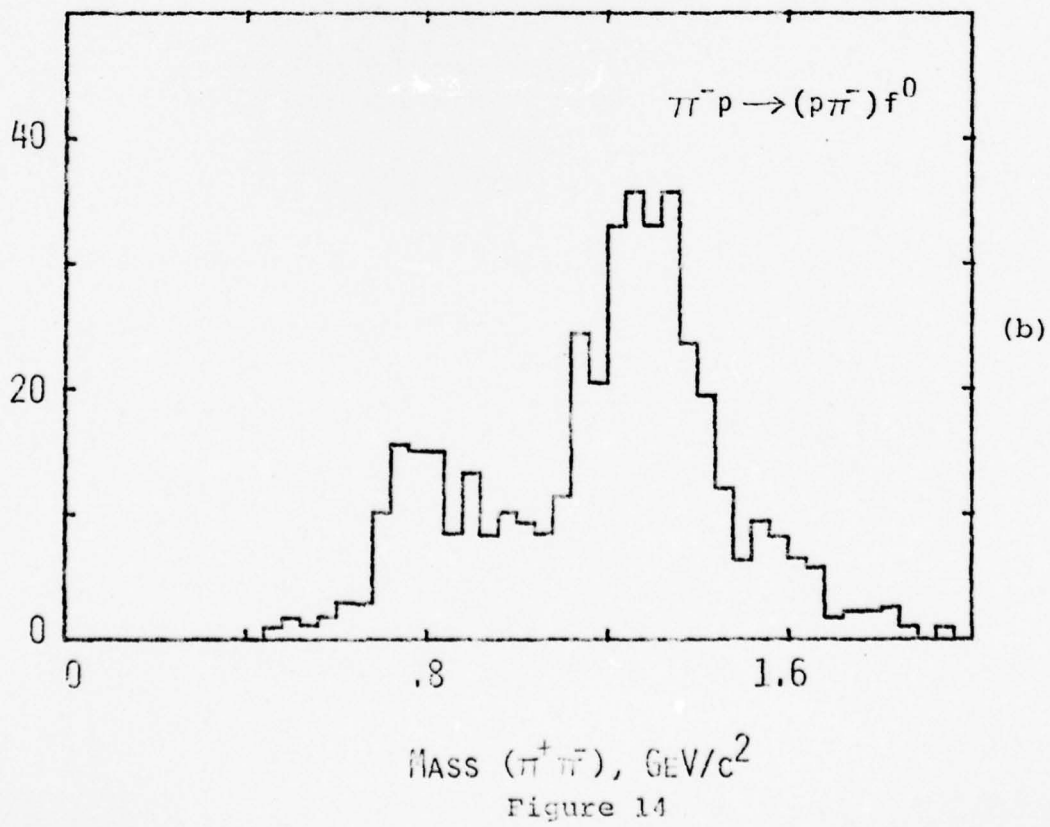
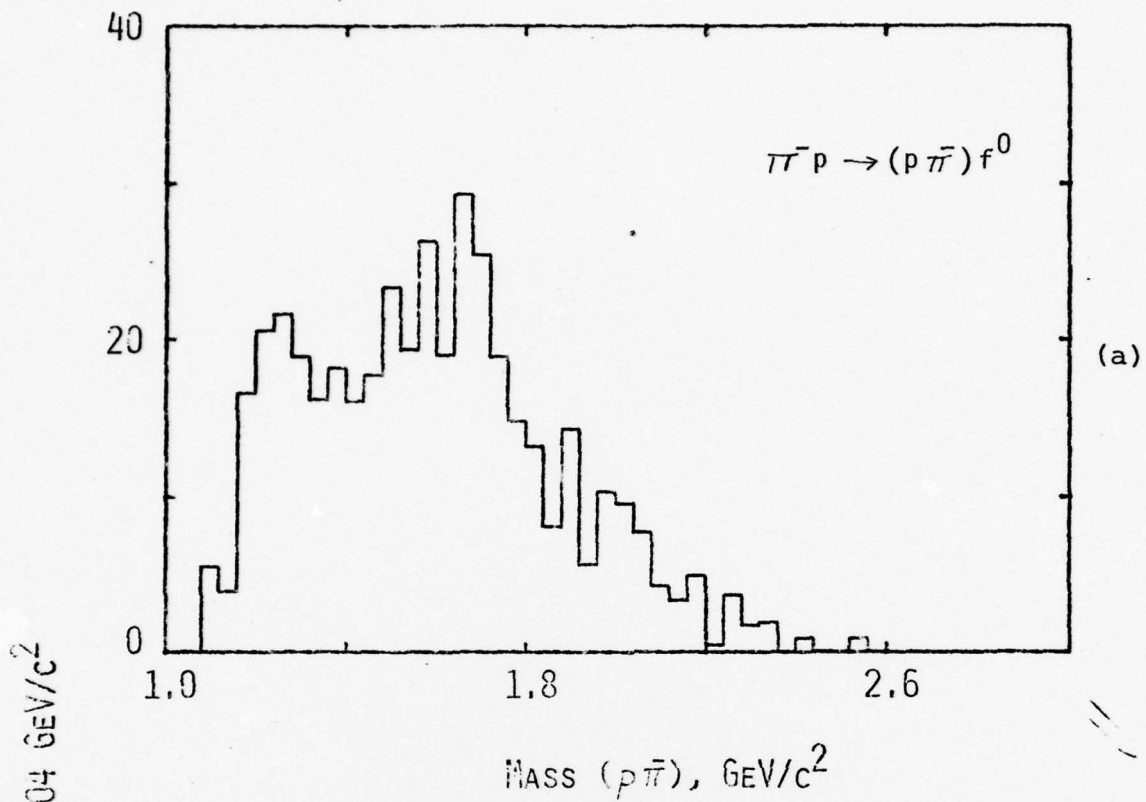


Figure 14

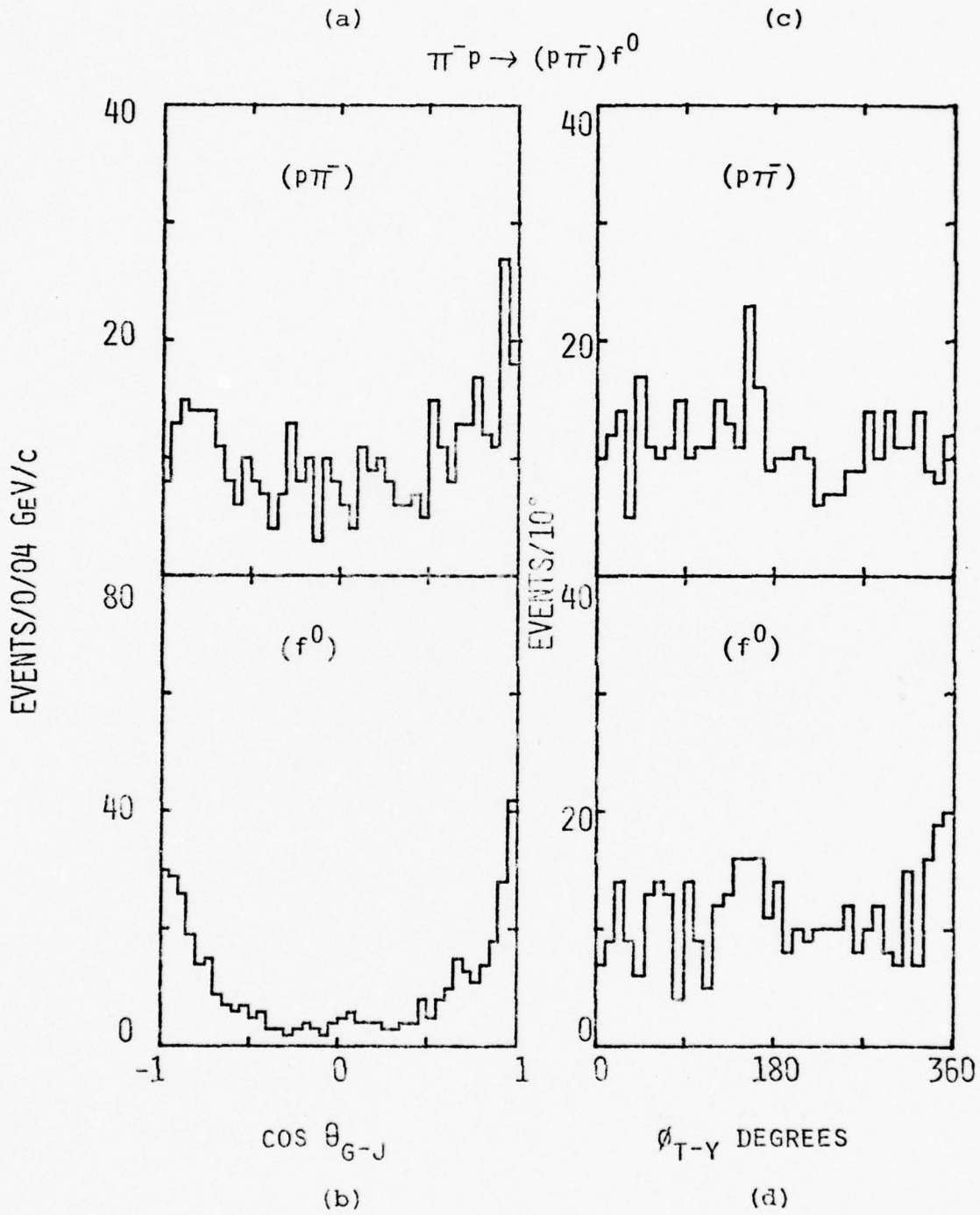


Figure 15

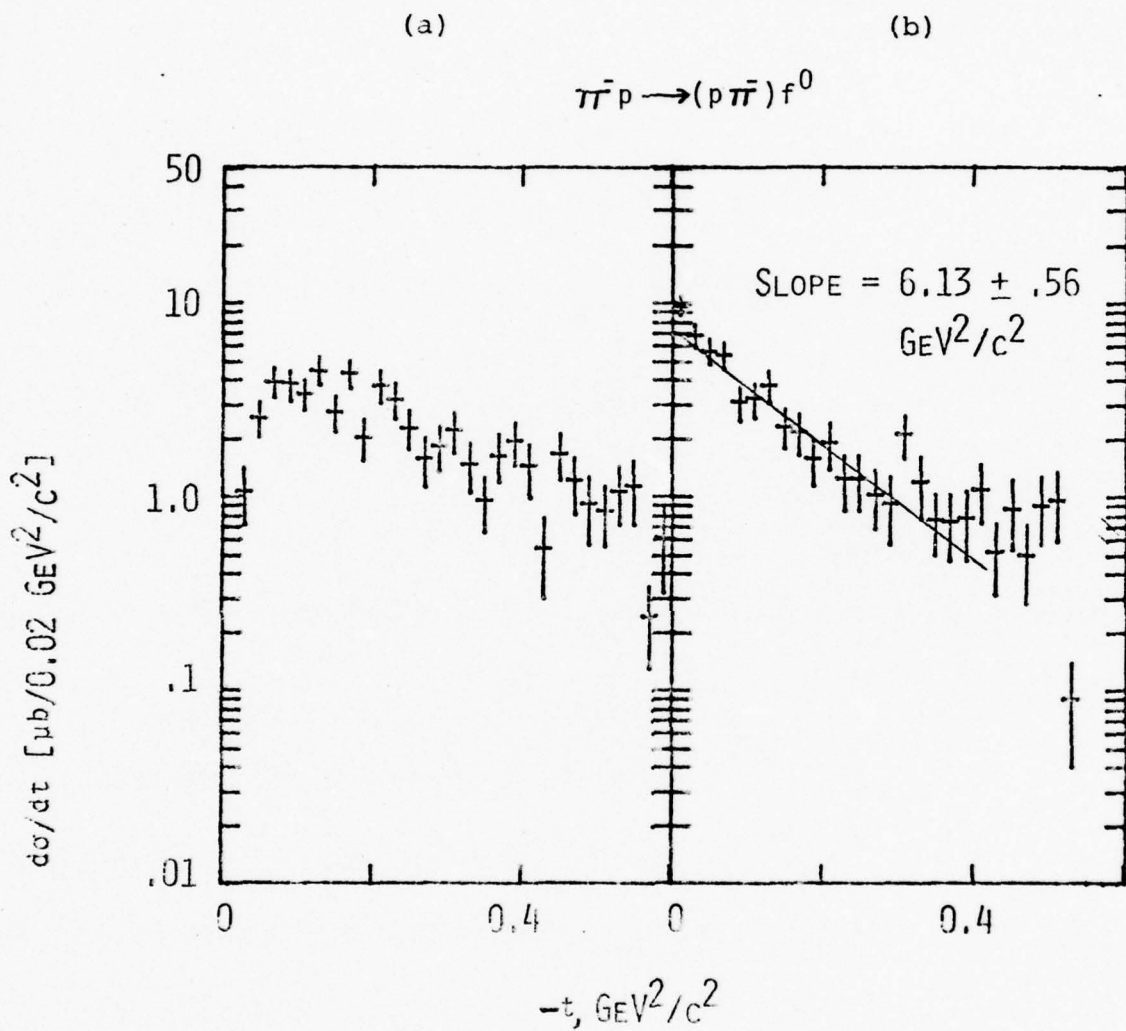


Figure 16

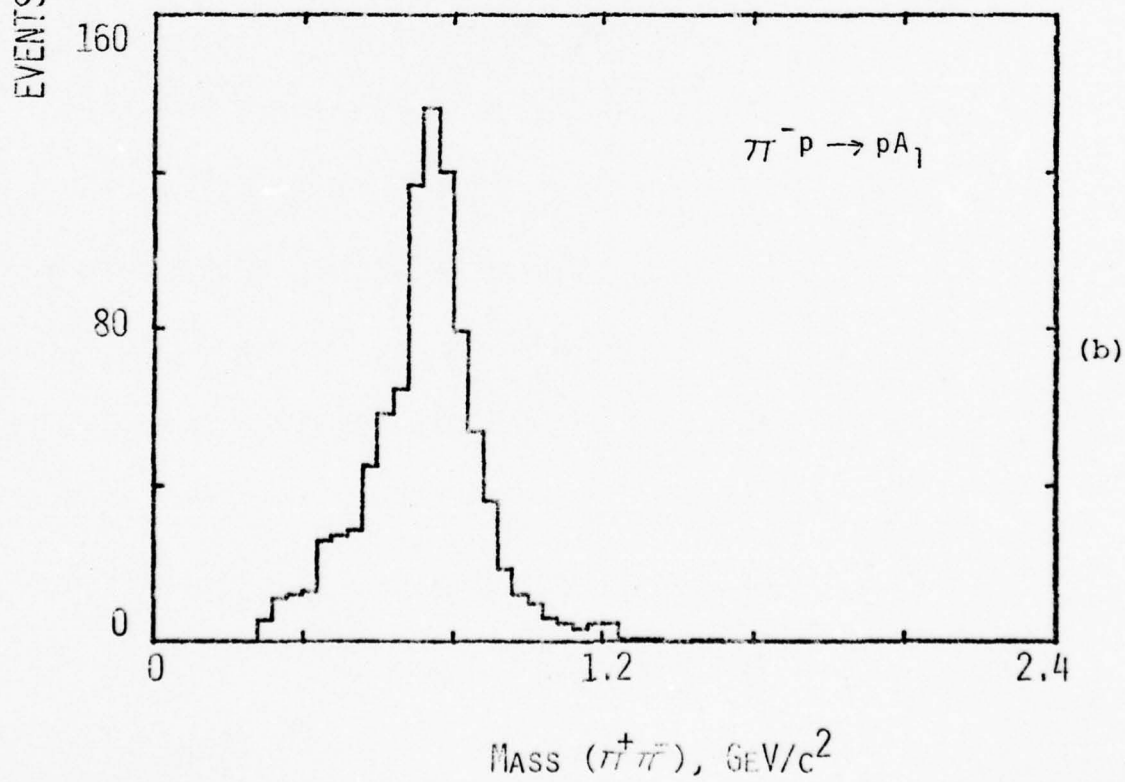
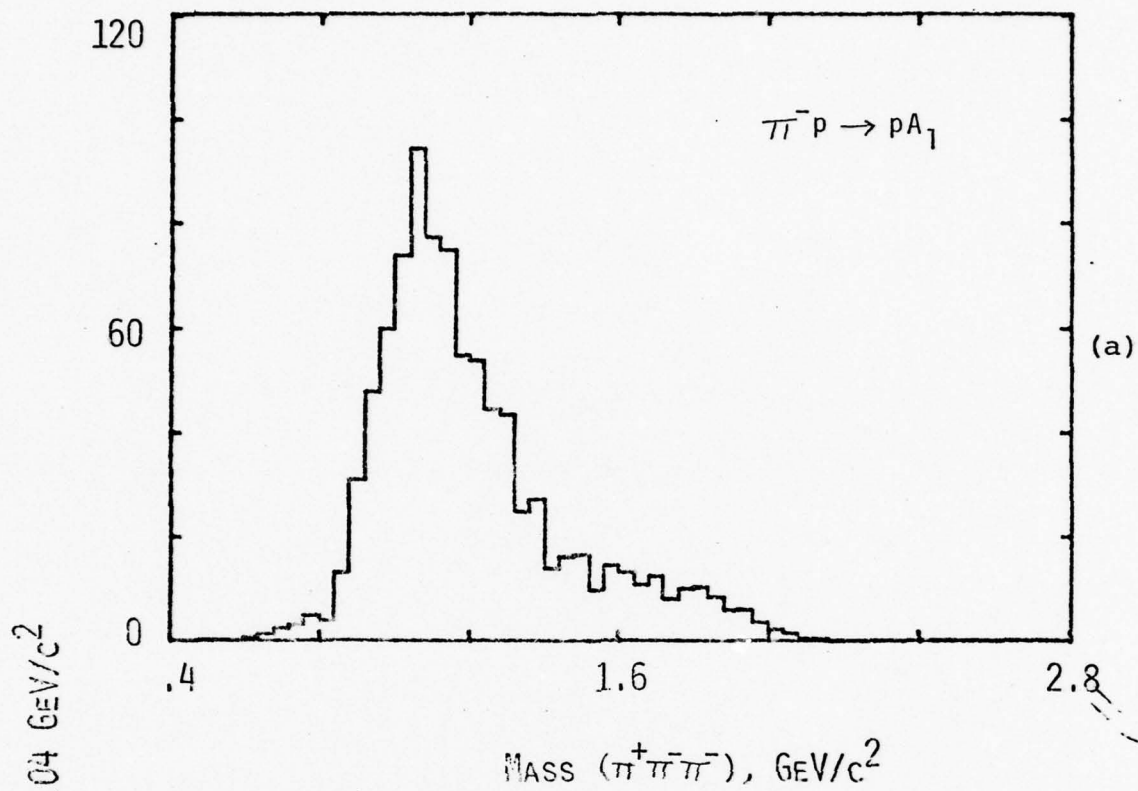


Figure 17

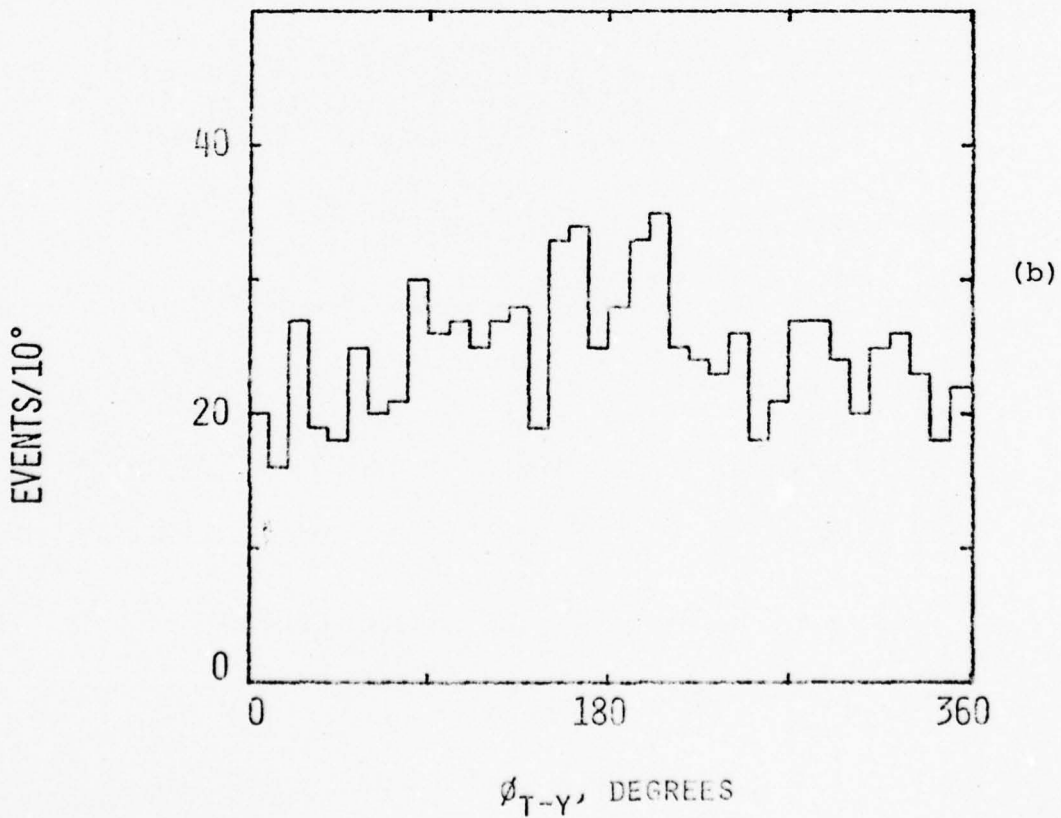
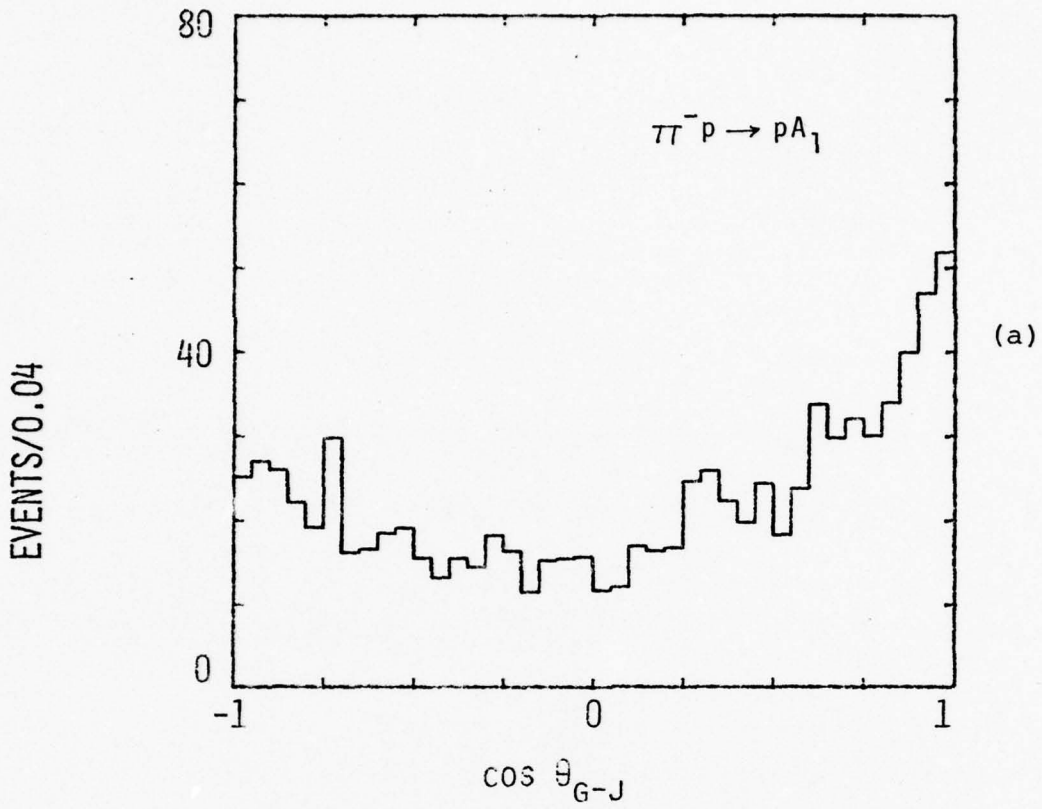


Figure 18

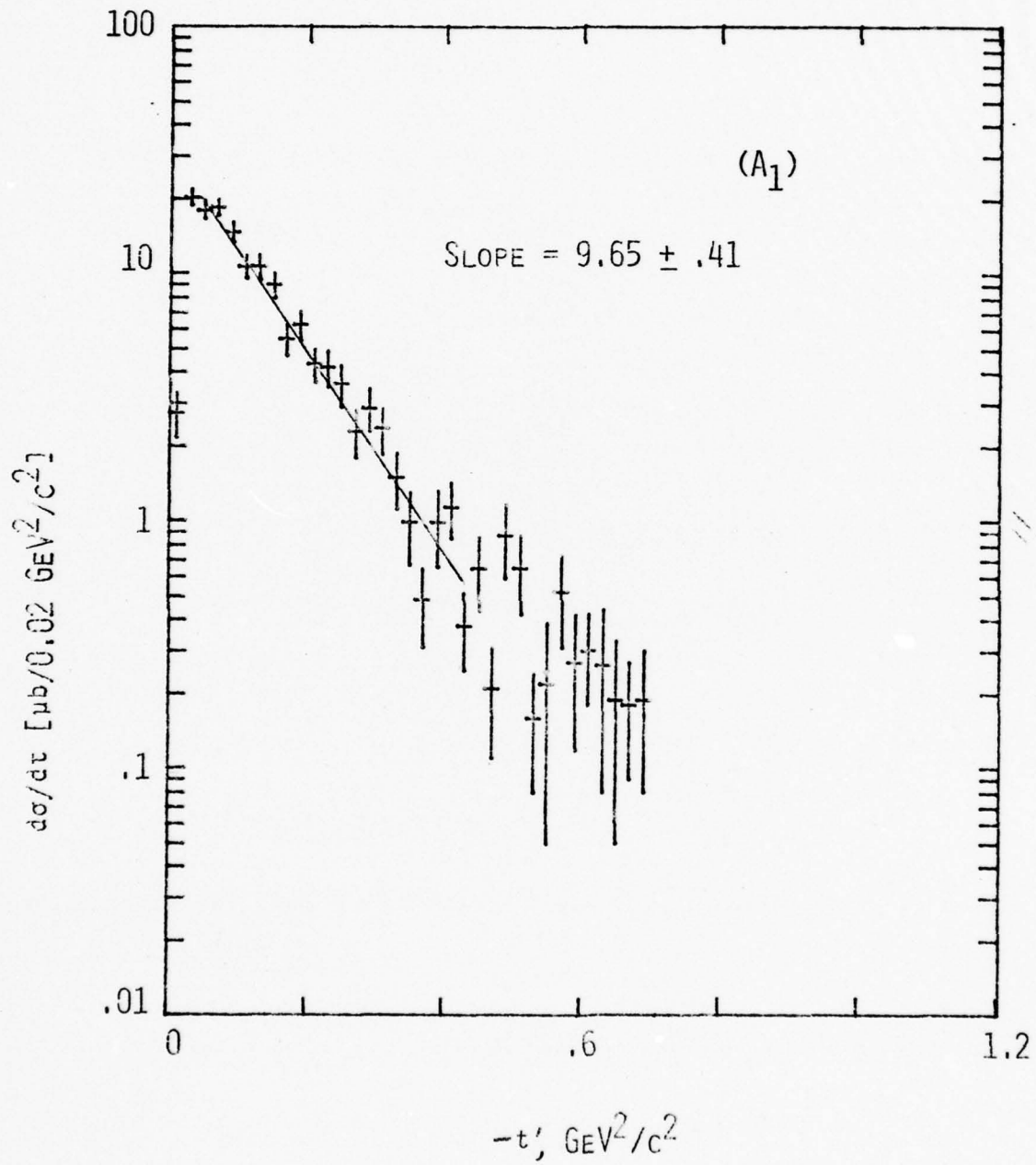


Figure 19

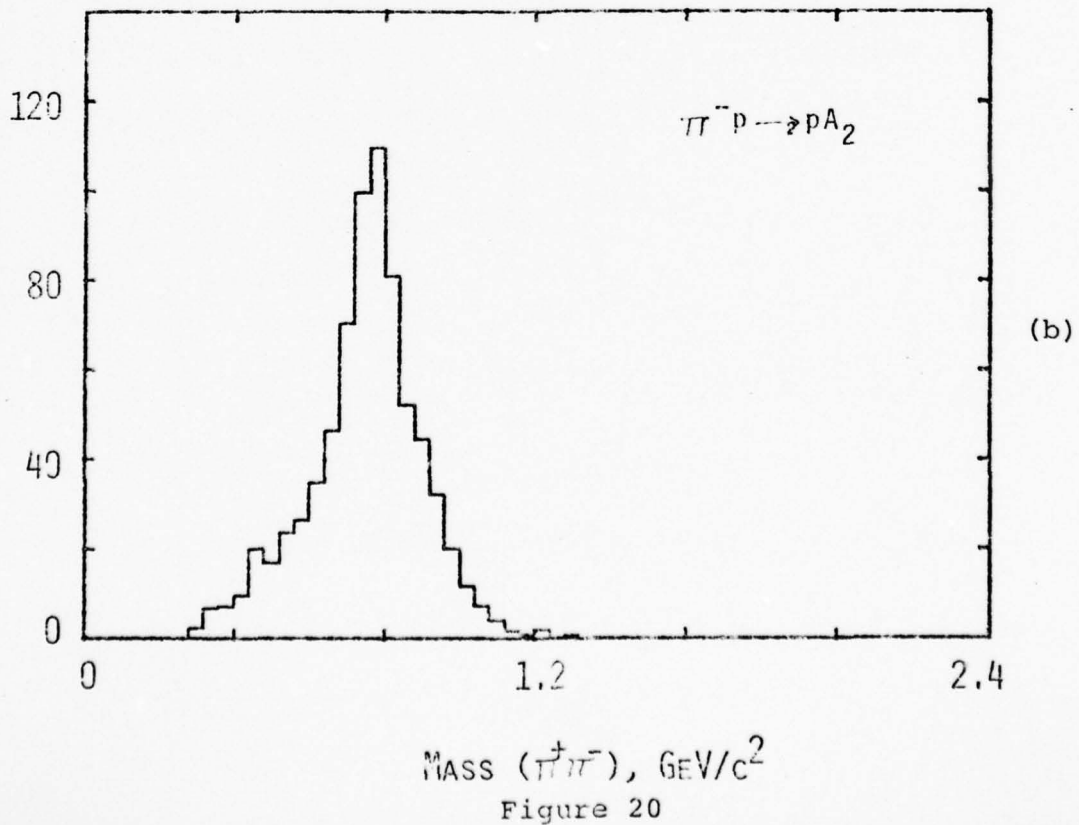
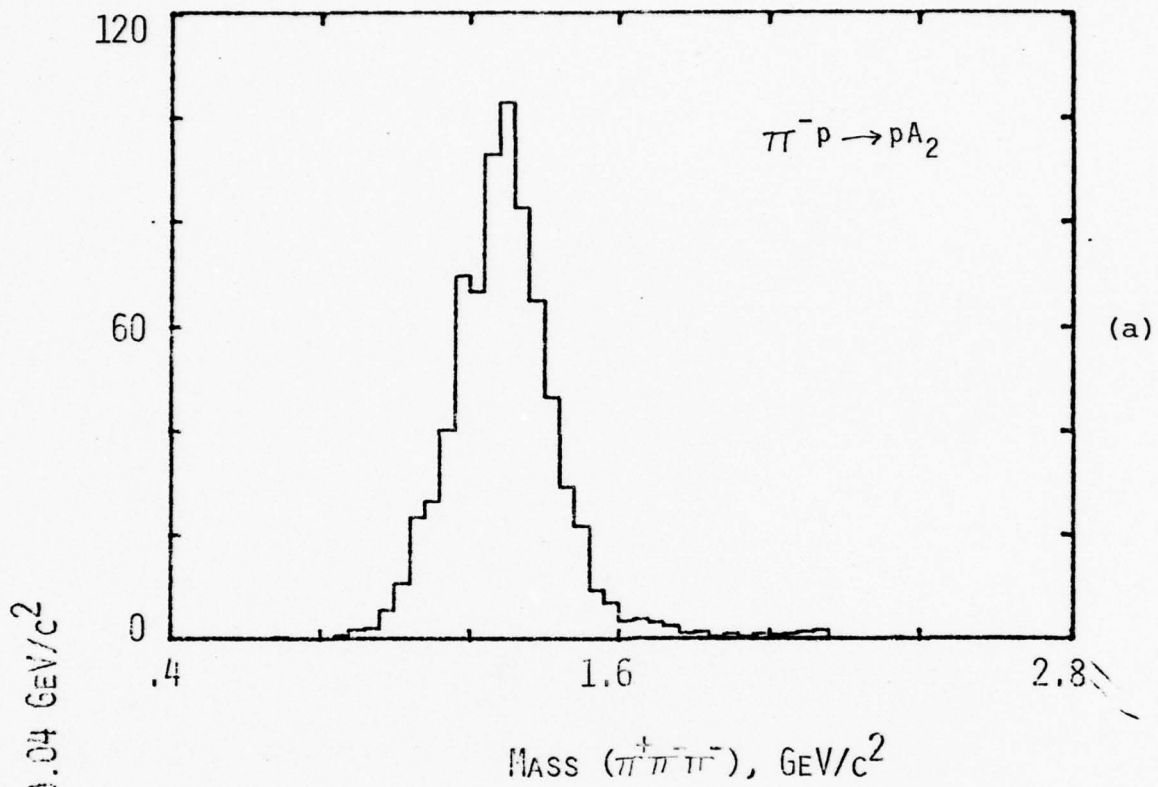


Figure 20

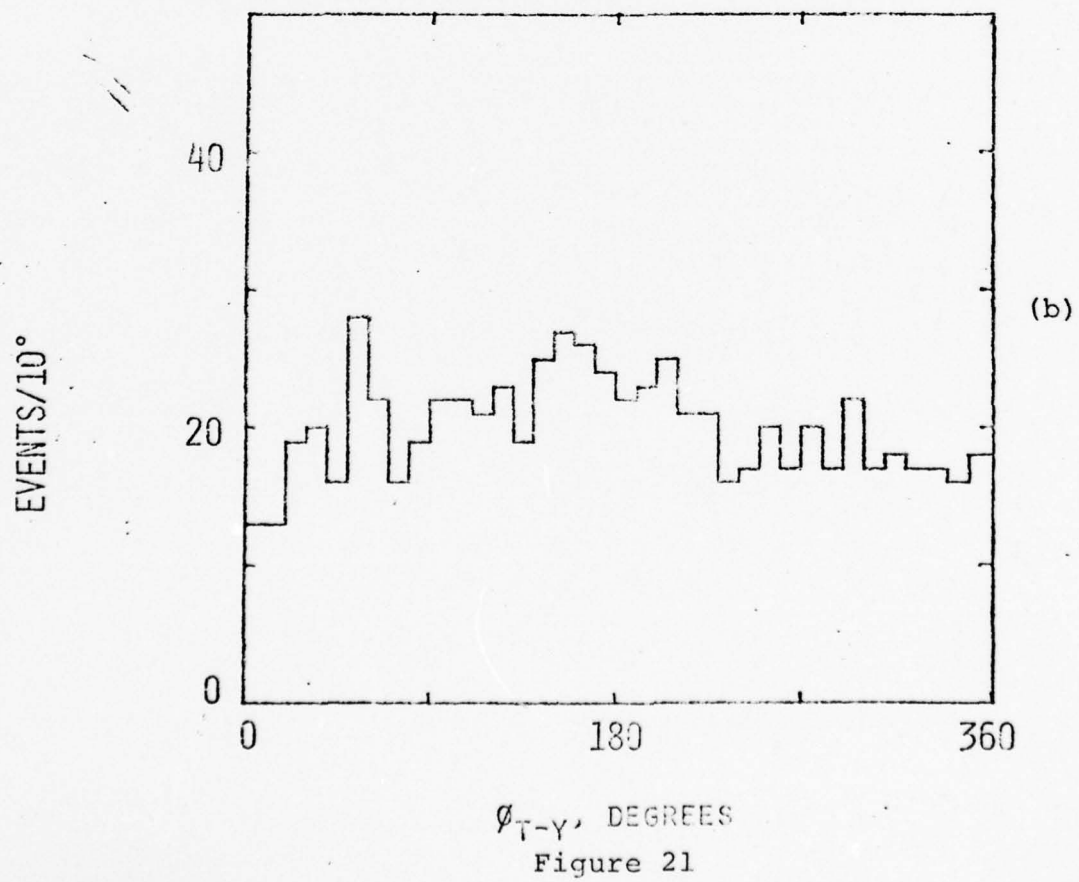
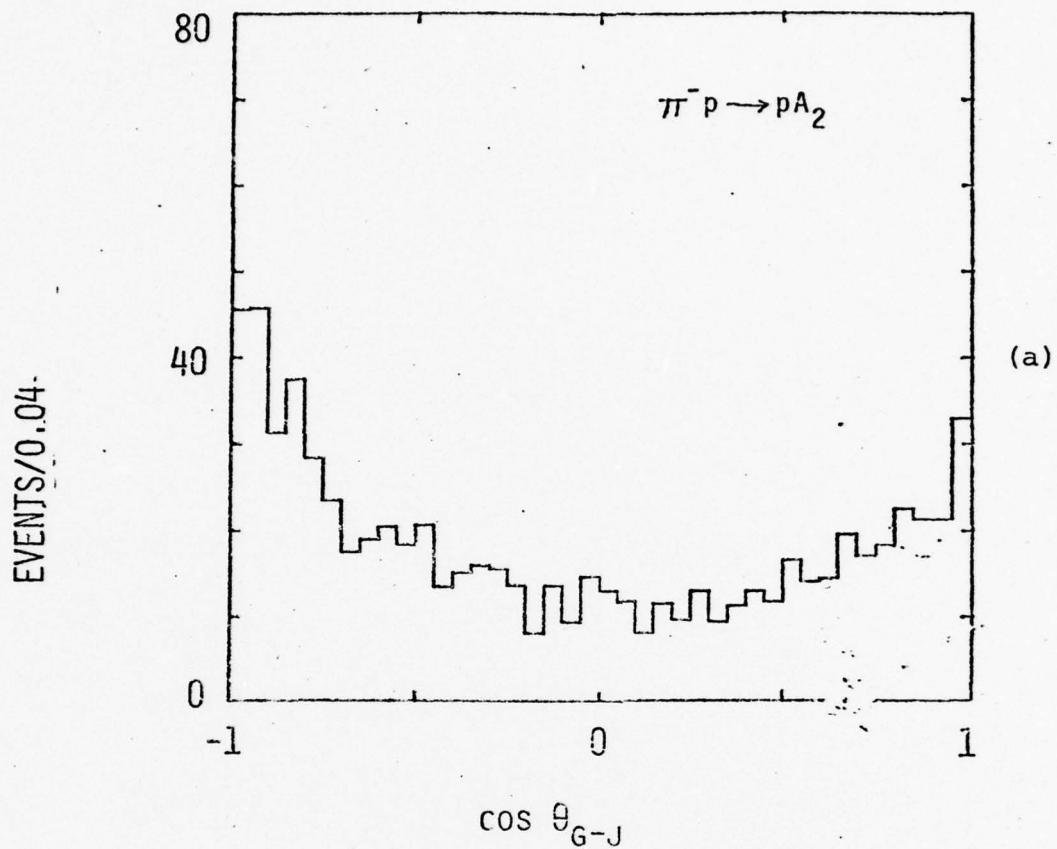


Figure 21

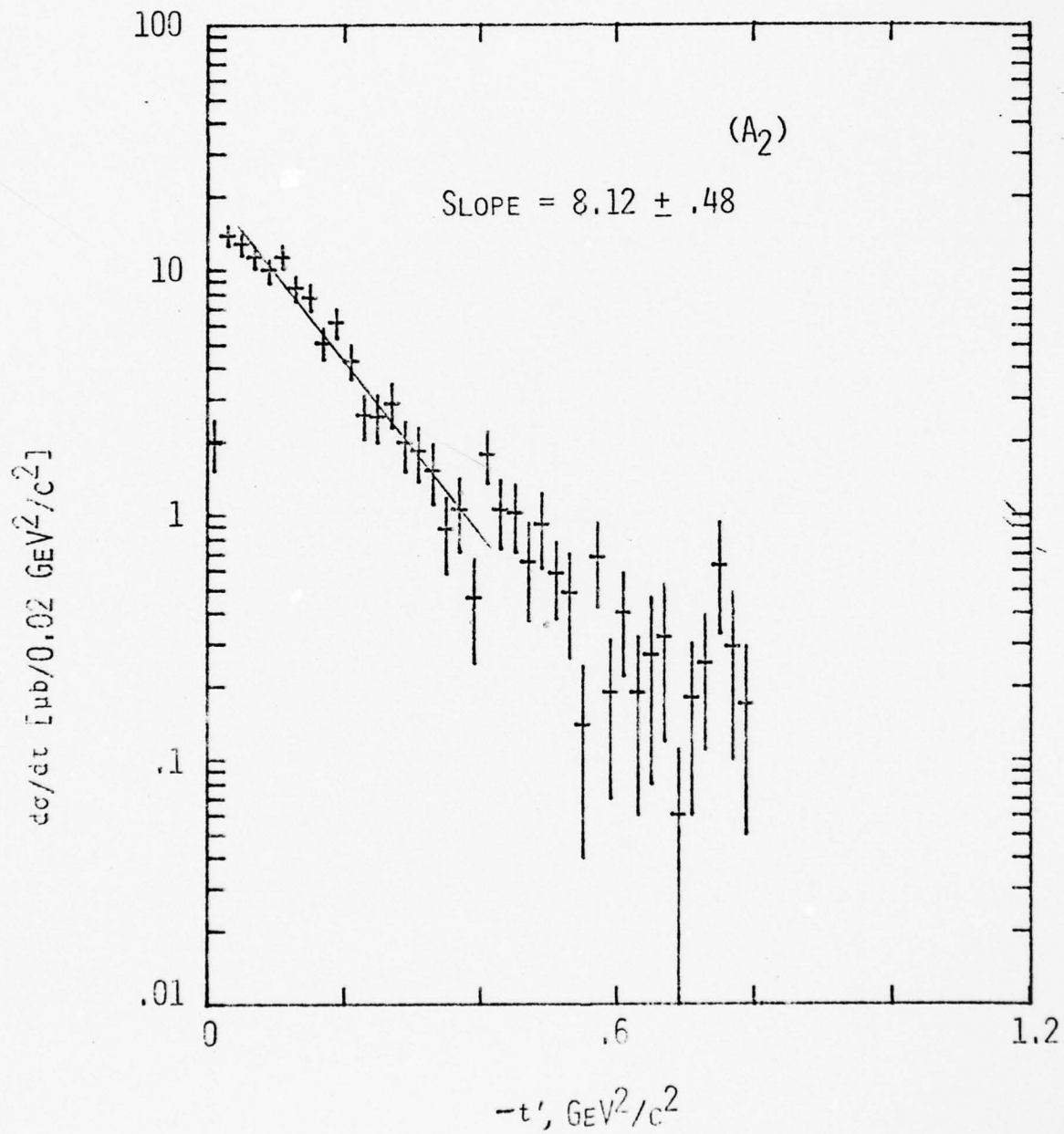


Figure 22

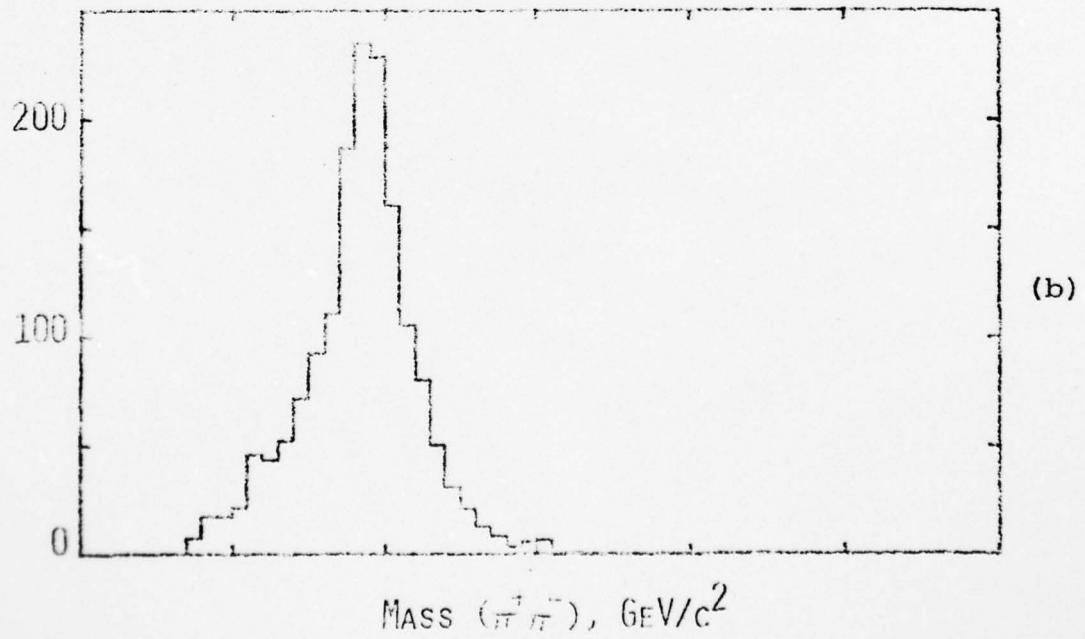
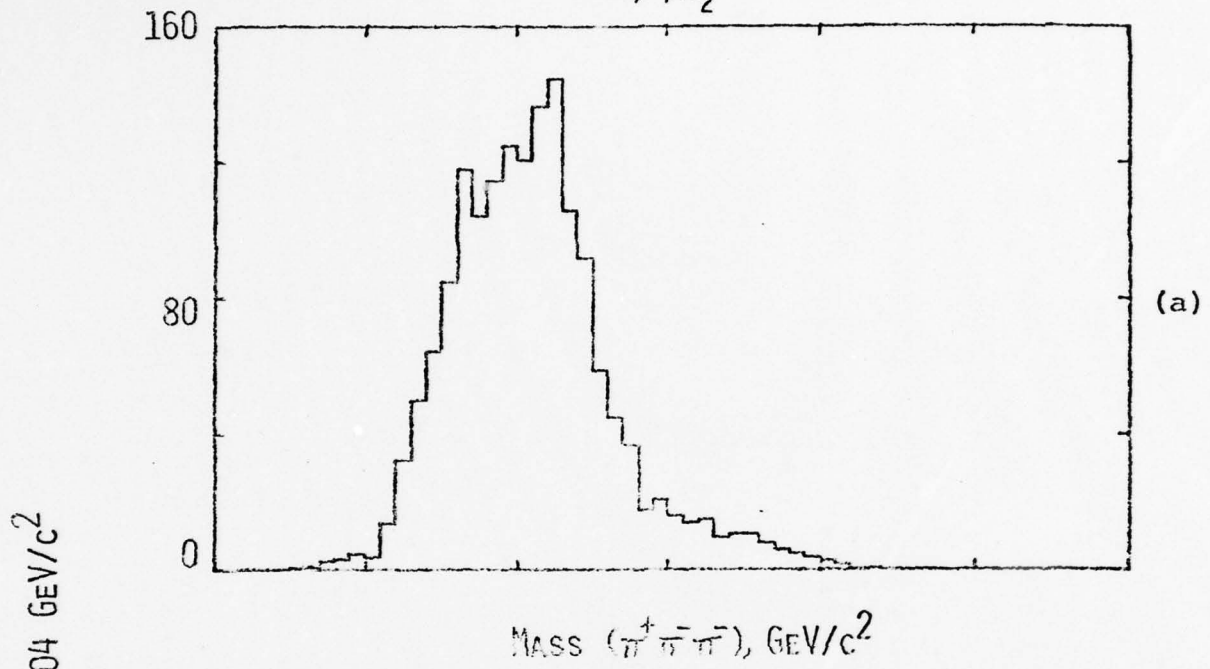
$\pi^- p \rightarrow pA_1$   
 $\rightarrow pA_2$ 

Figure 23

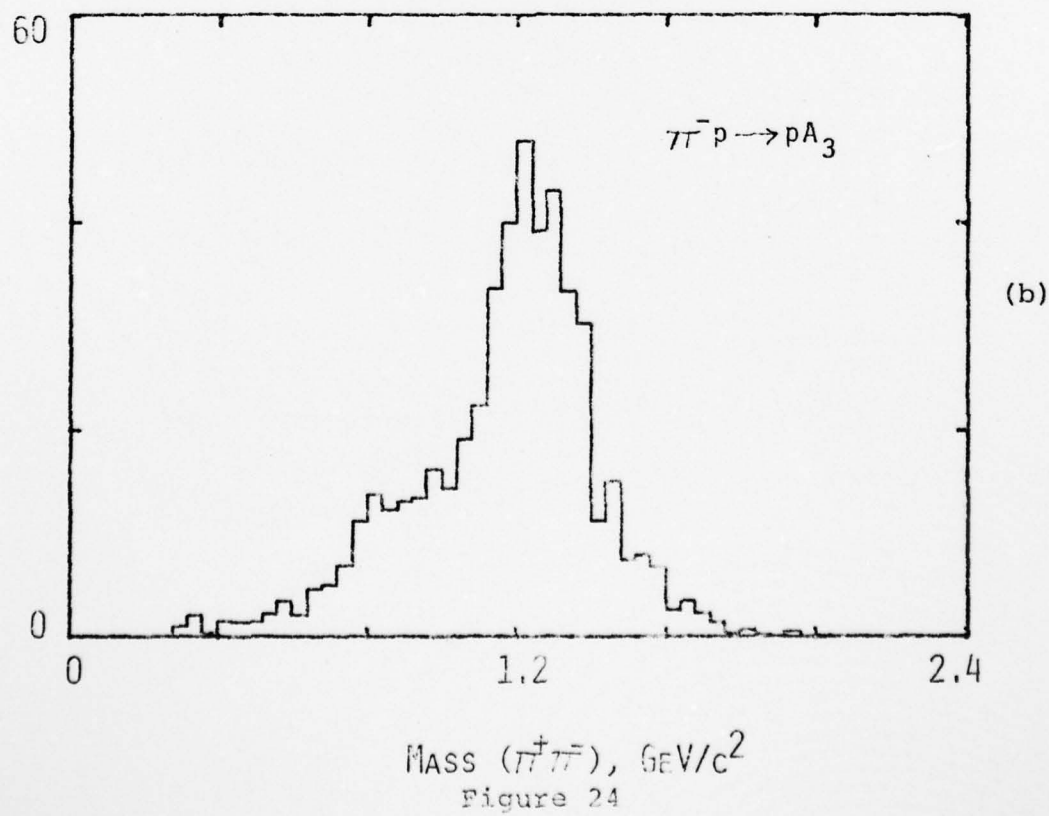
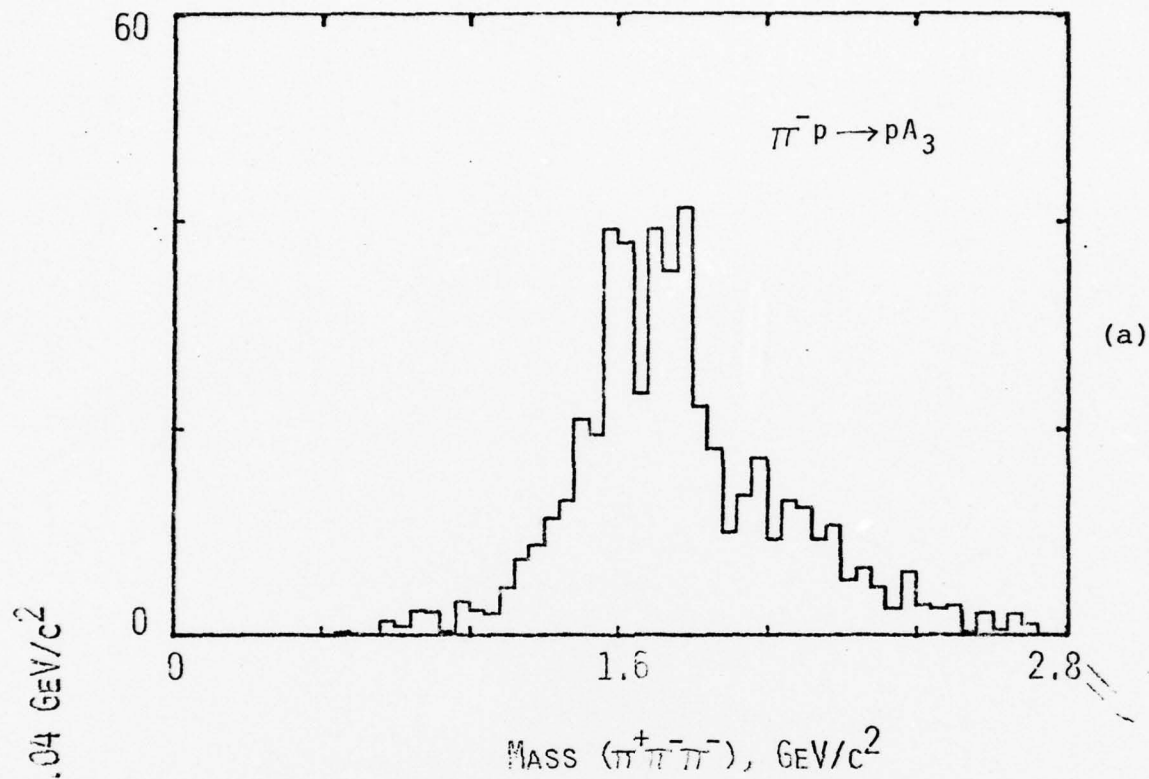


Figure 24

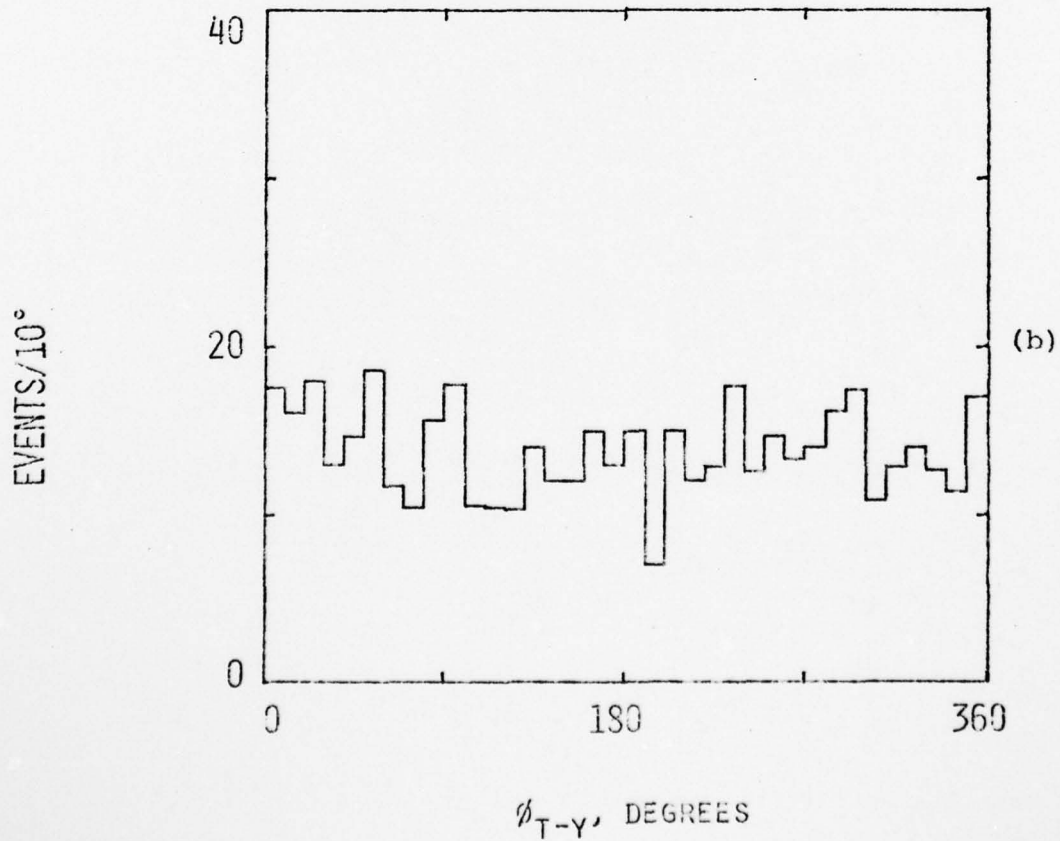
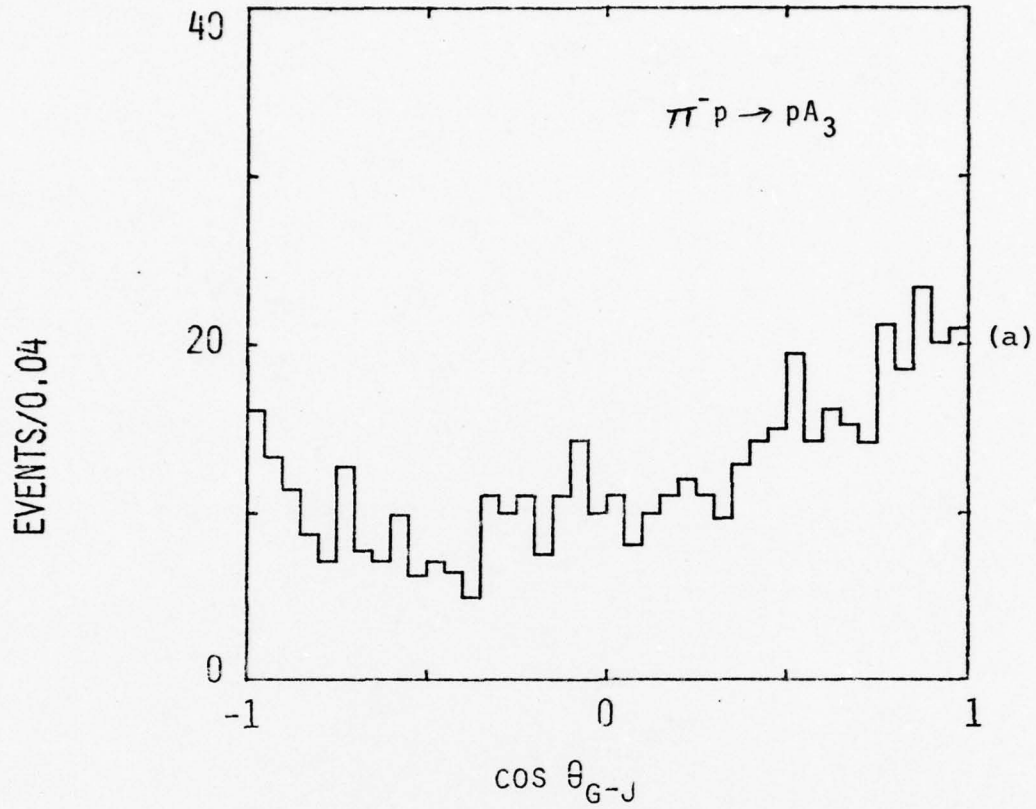


Figure 25

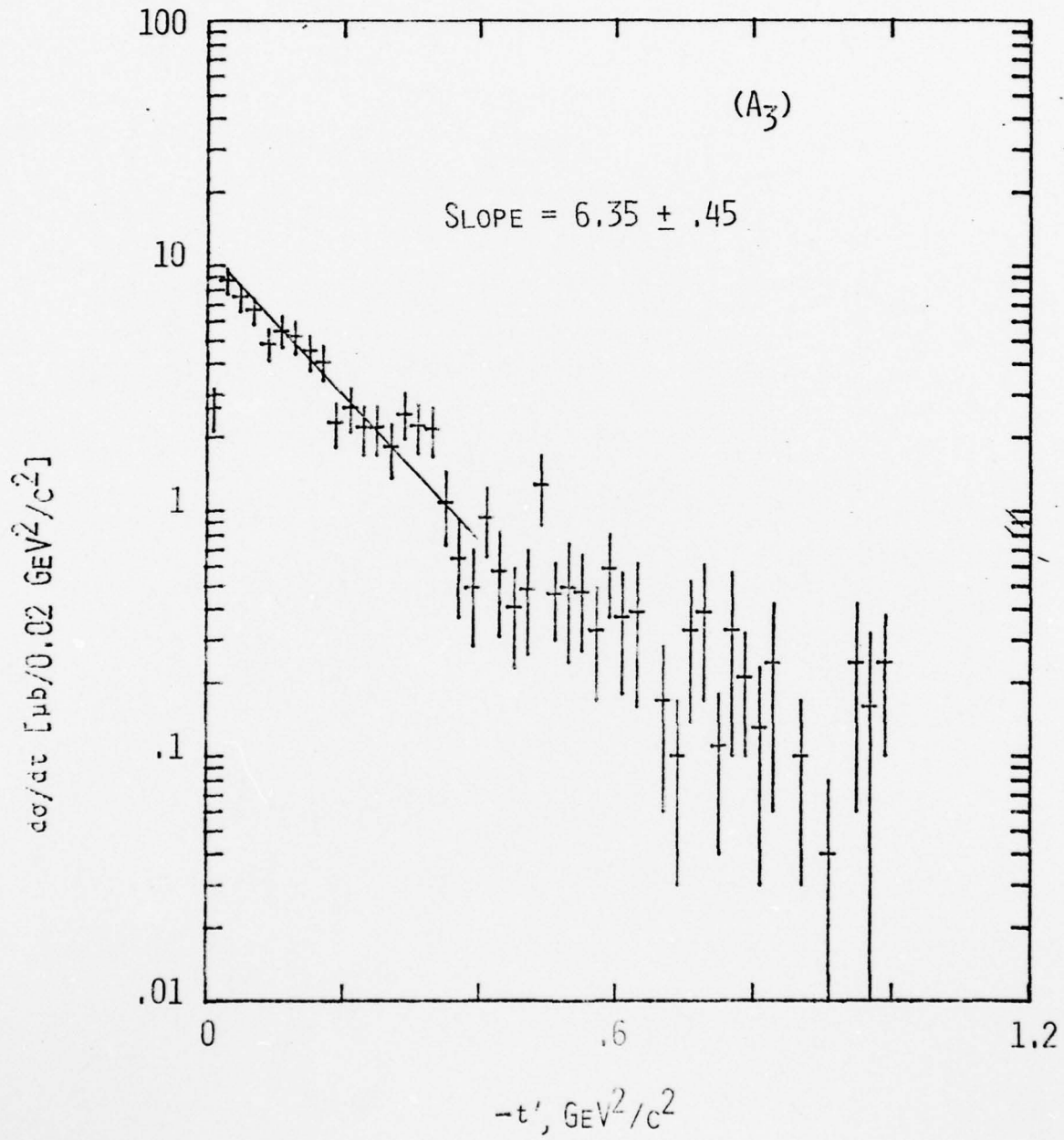


Figure 26

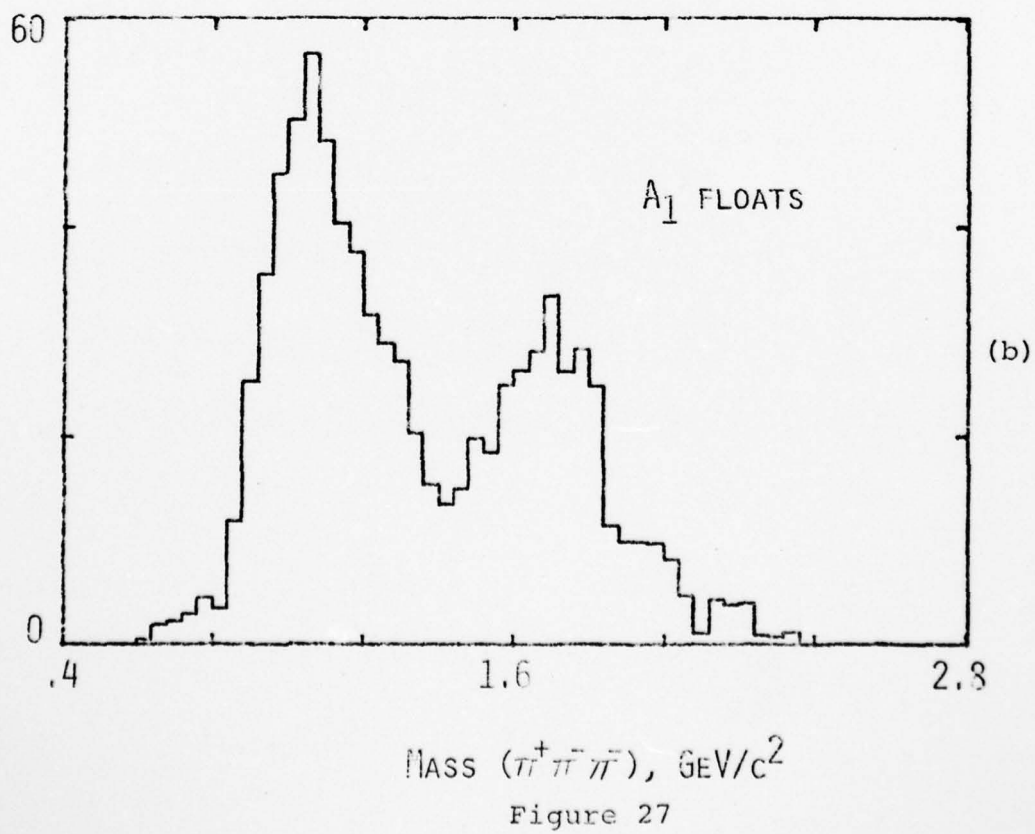
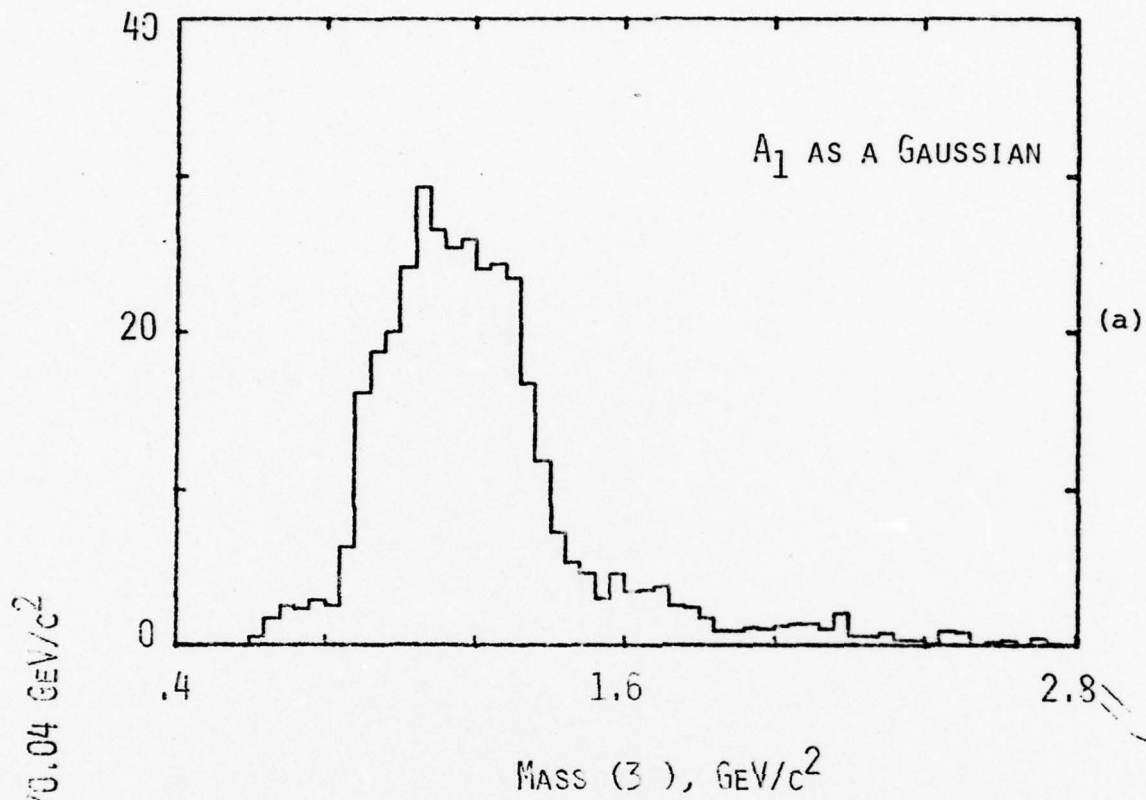


Figure 27

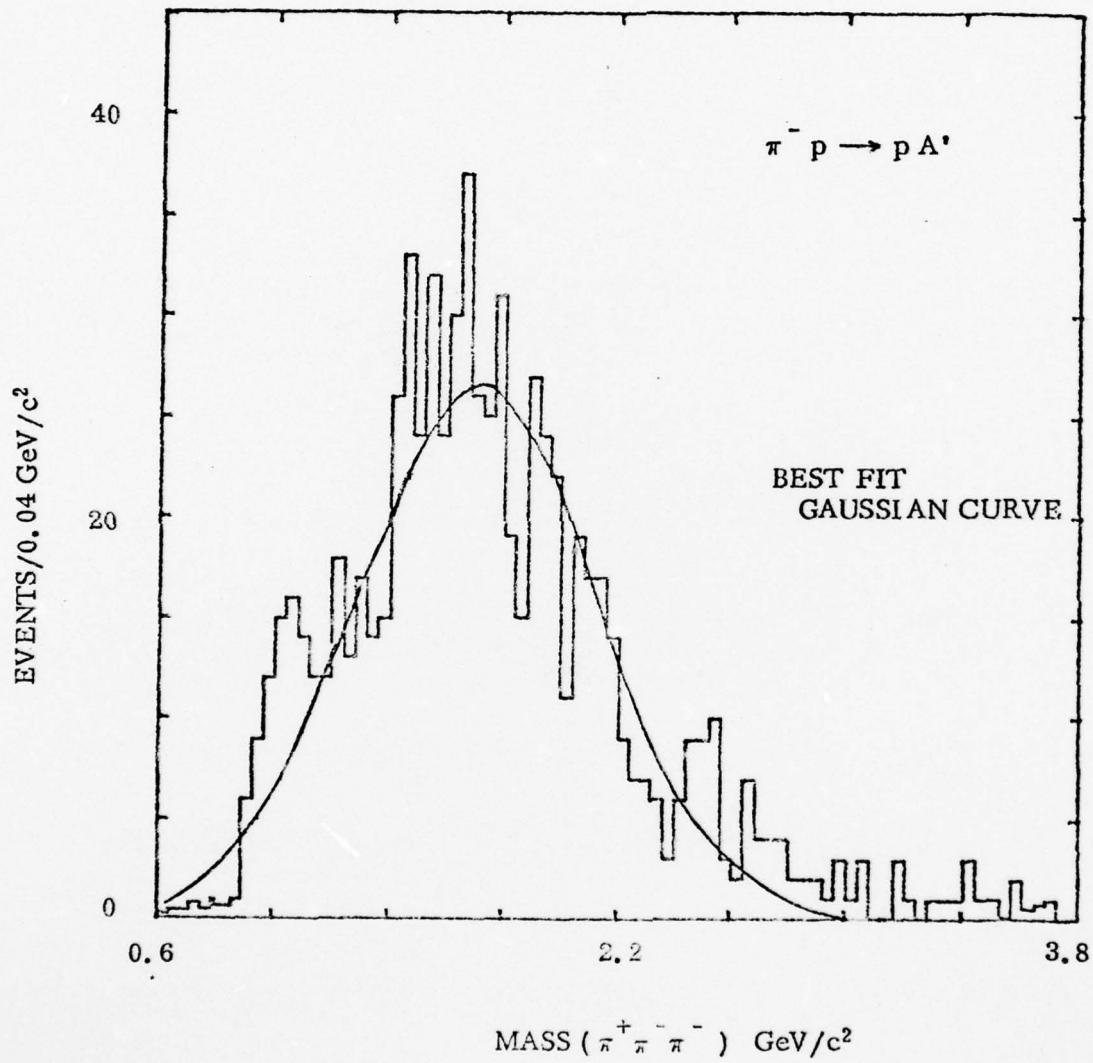


Figure 28

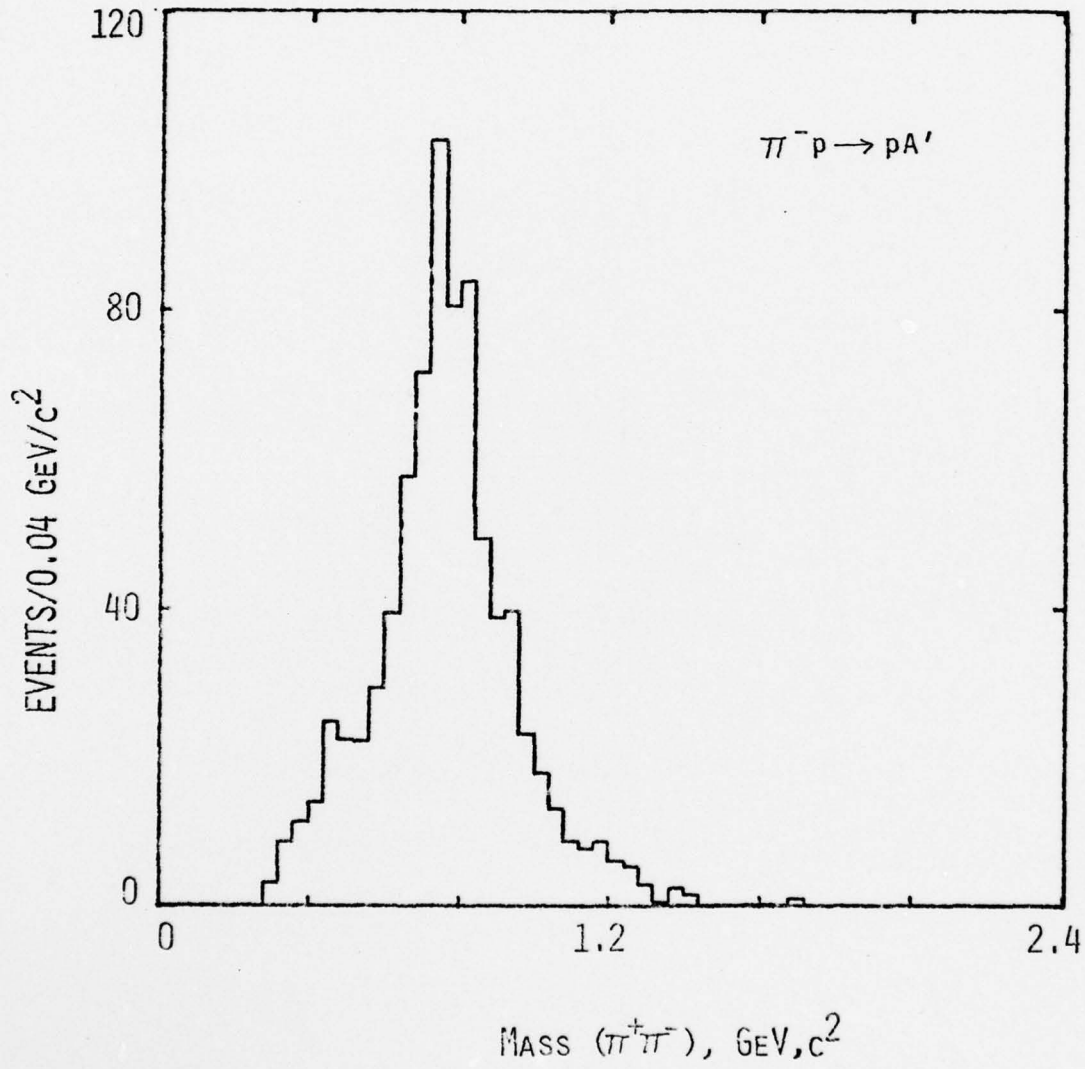


Figure 29

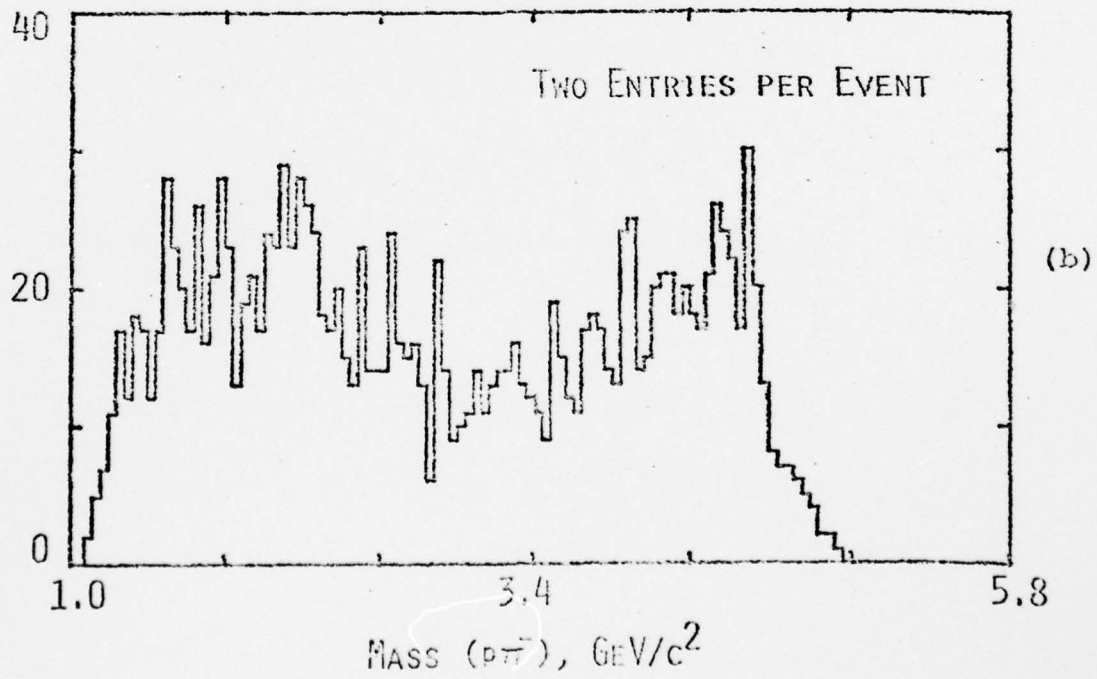
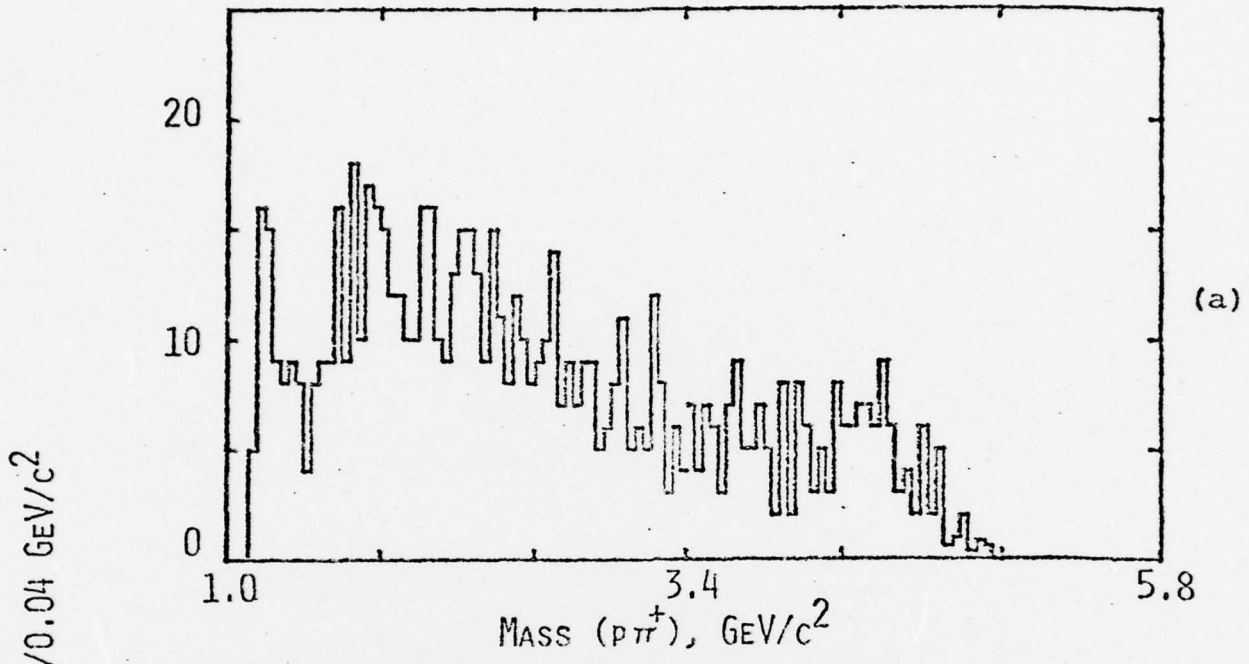
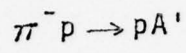


Figure 30

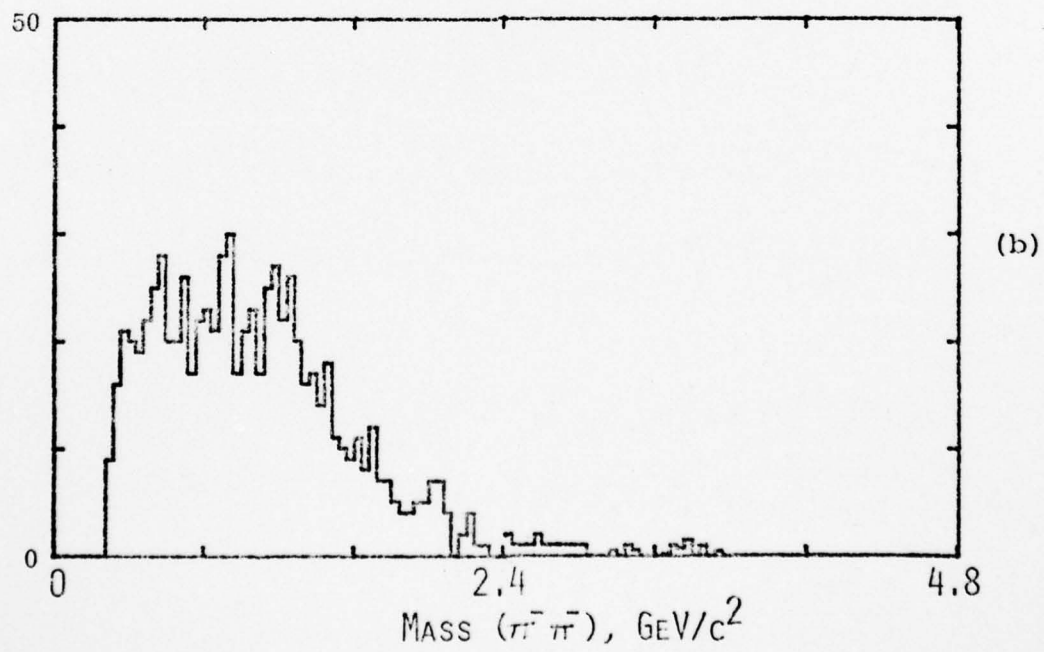
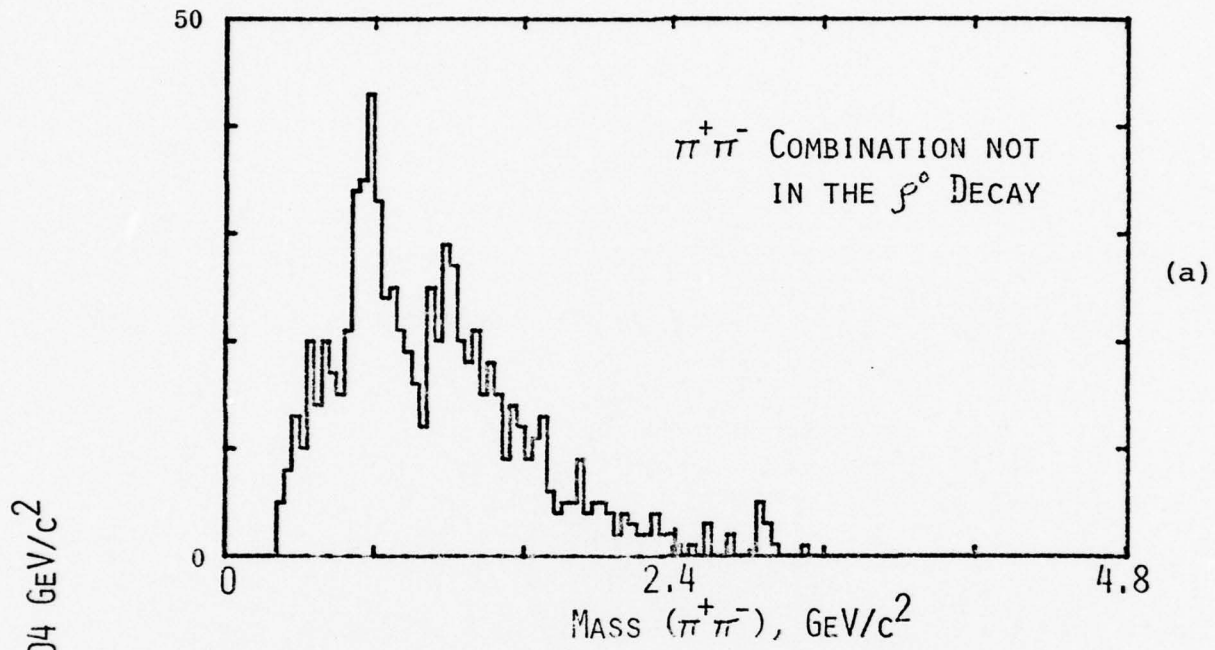
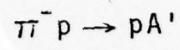
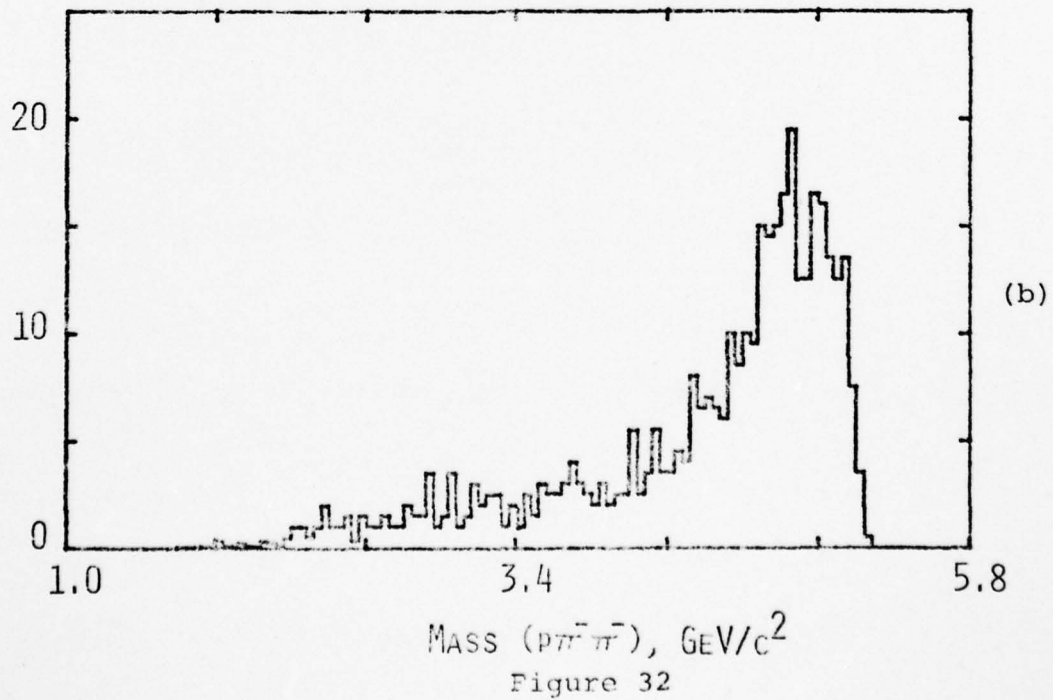
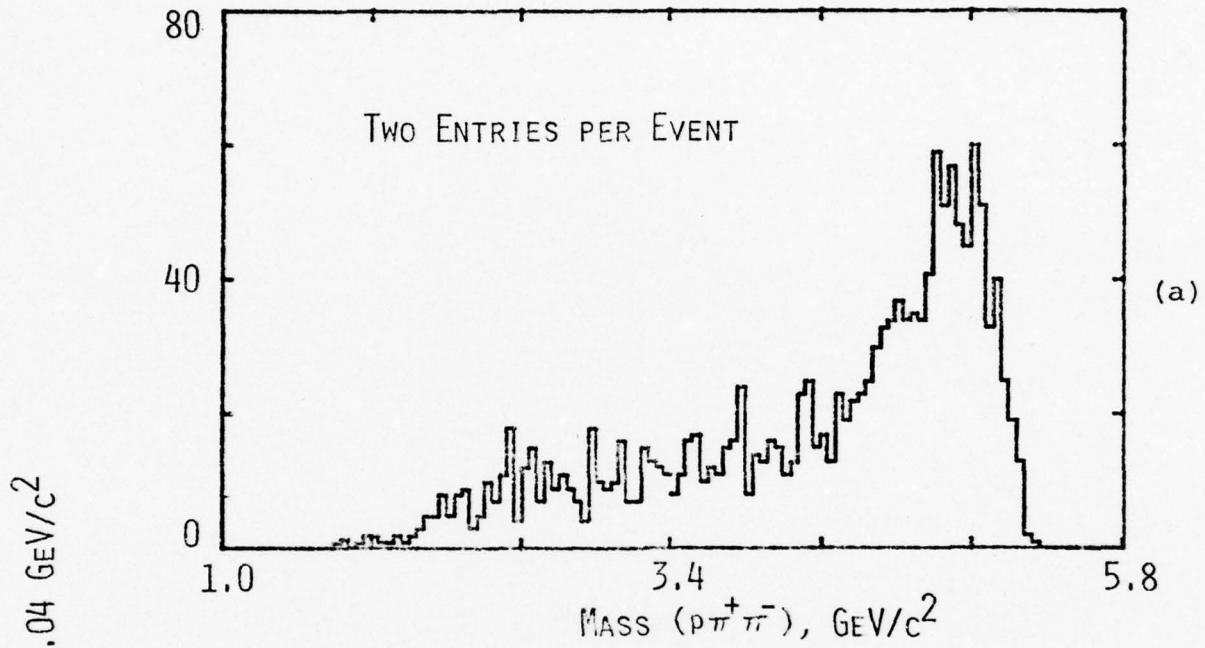


Figure 31

$\pi^- p \rightarrow pA'$ 

ALL VECTORS ARE AS SEEN IN REST  
FRAME OF A'

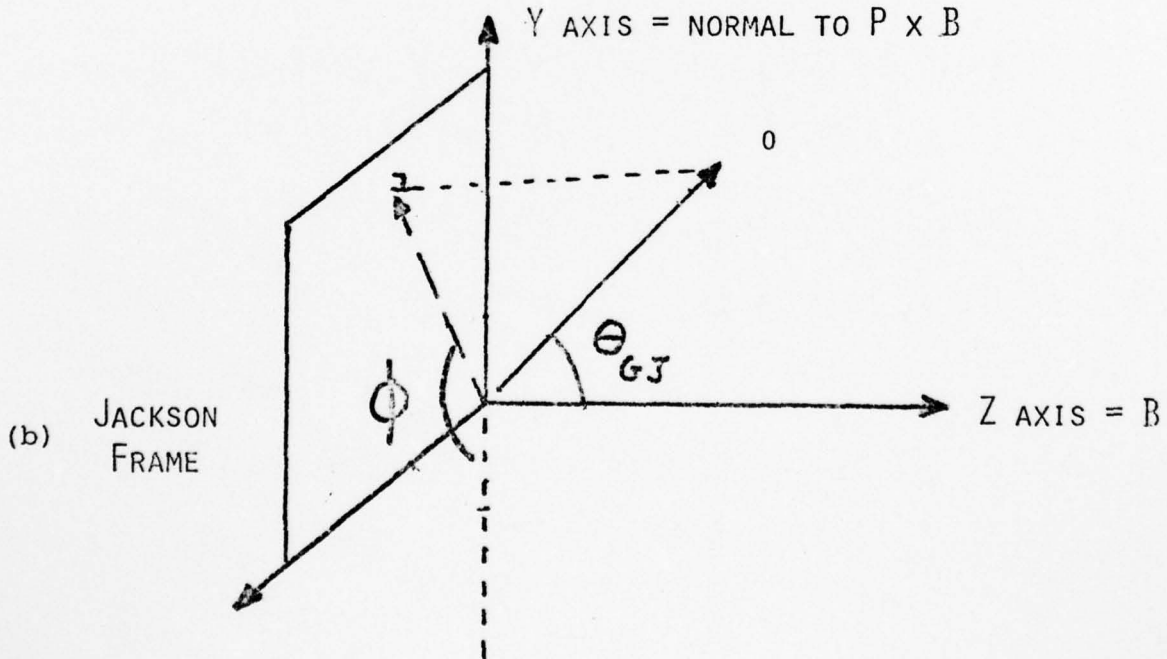
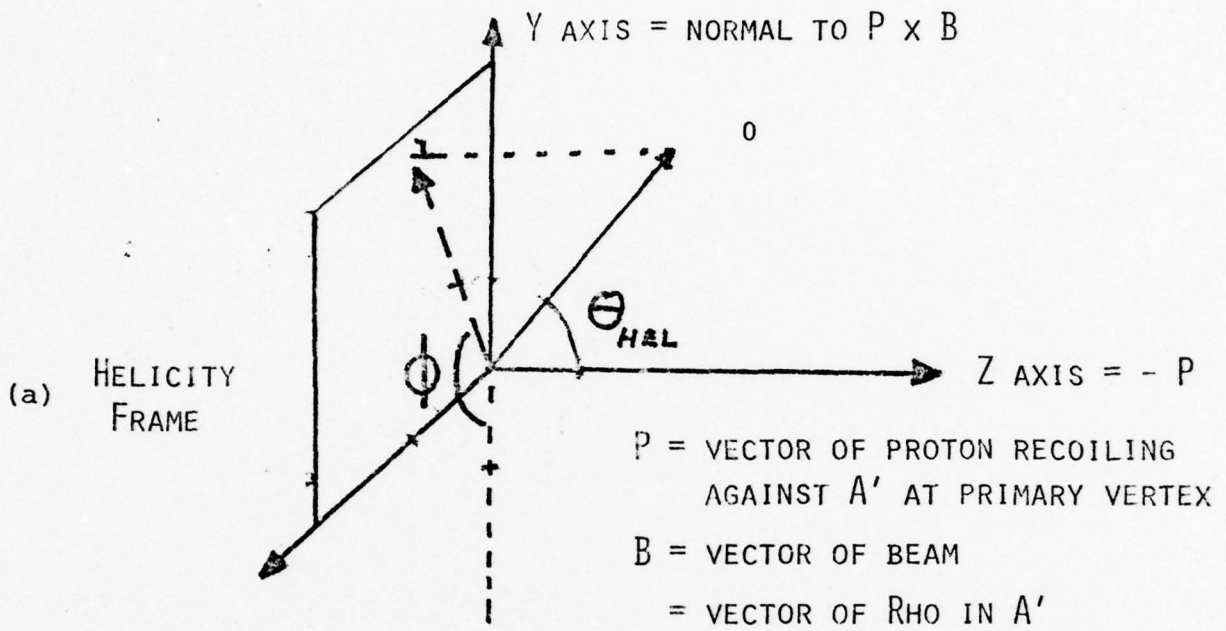
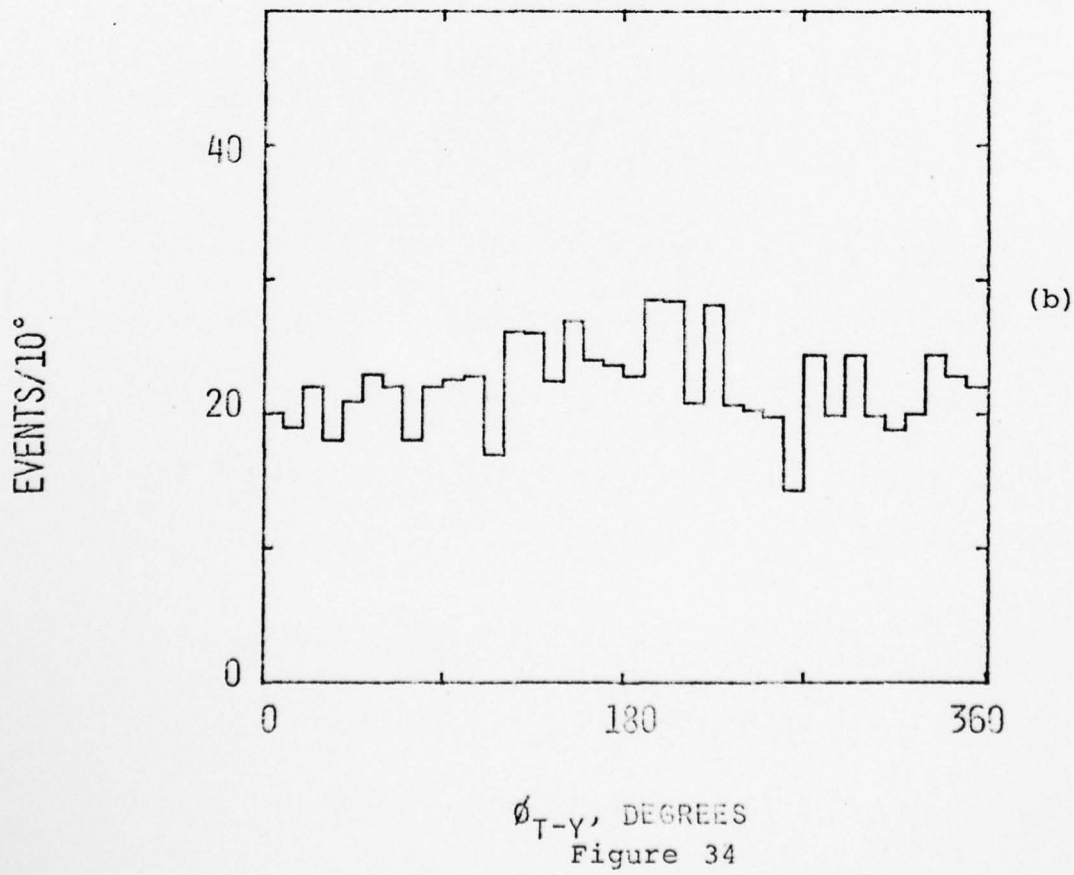
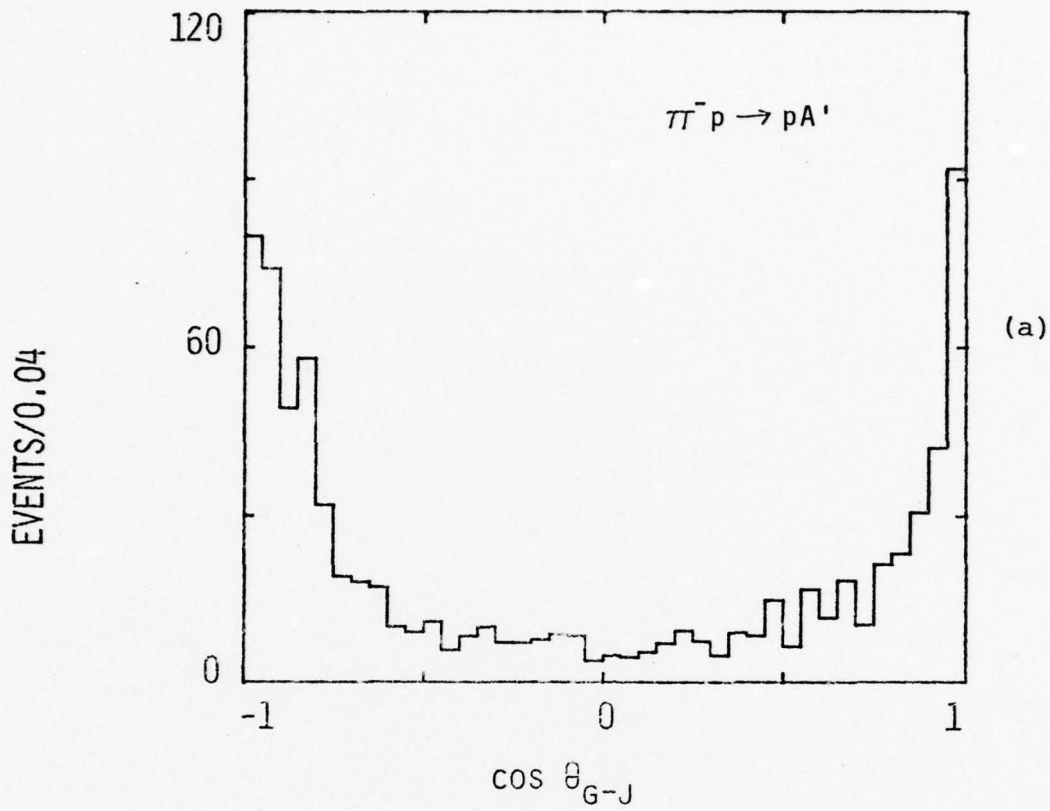


Figure 33



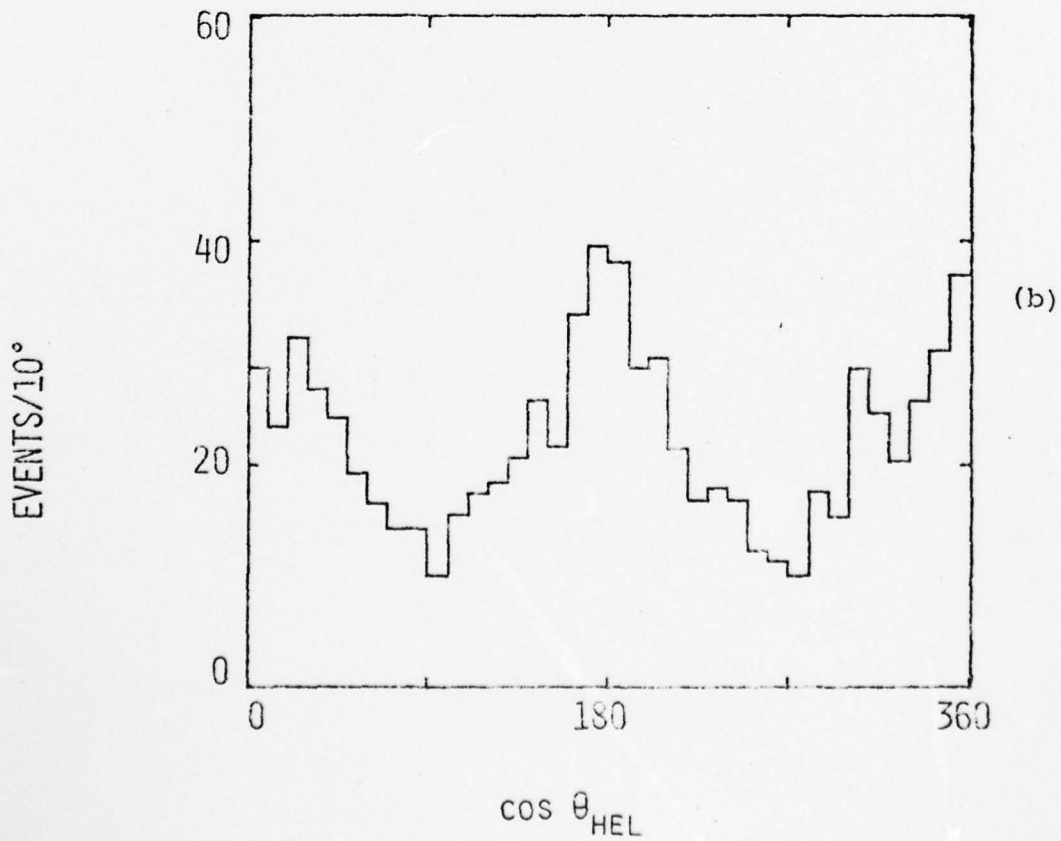
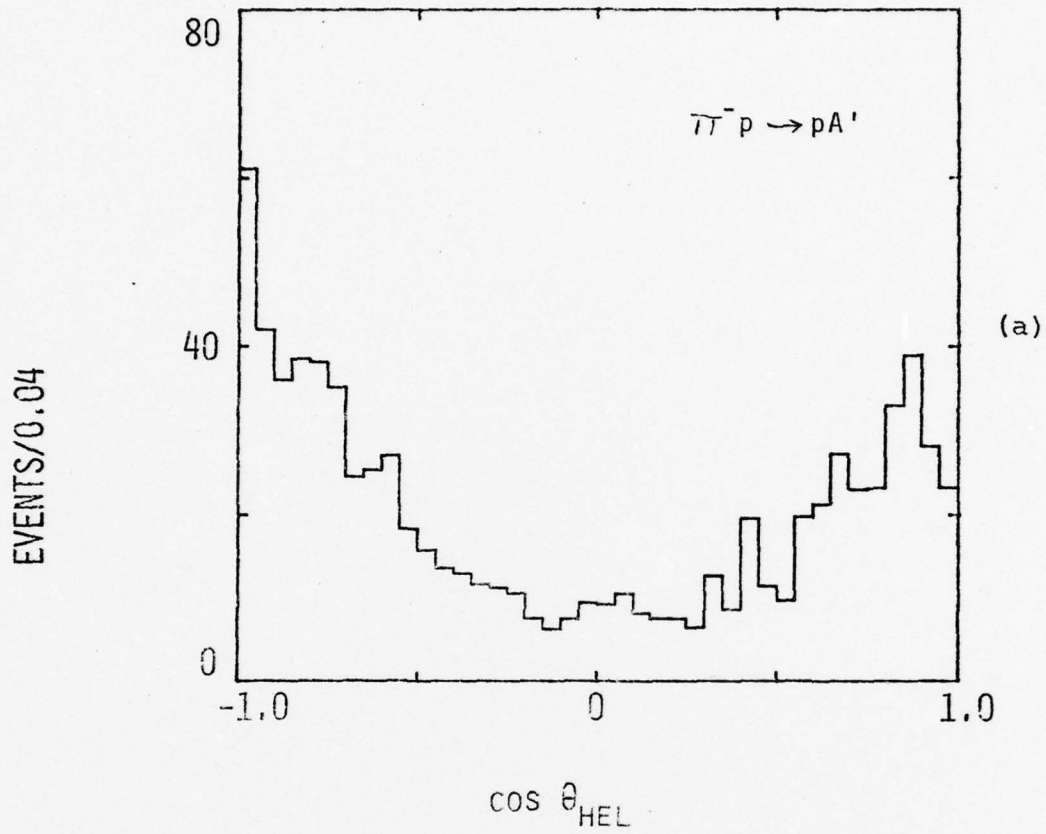


Figure 35

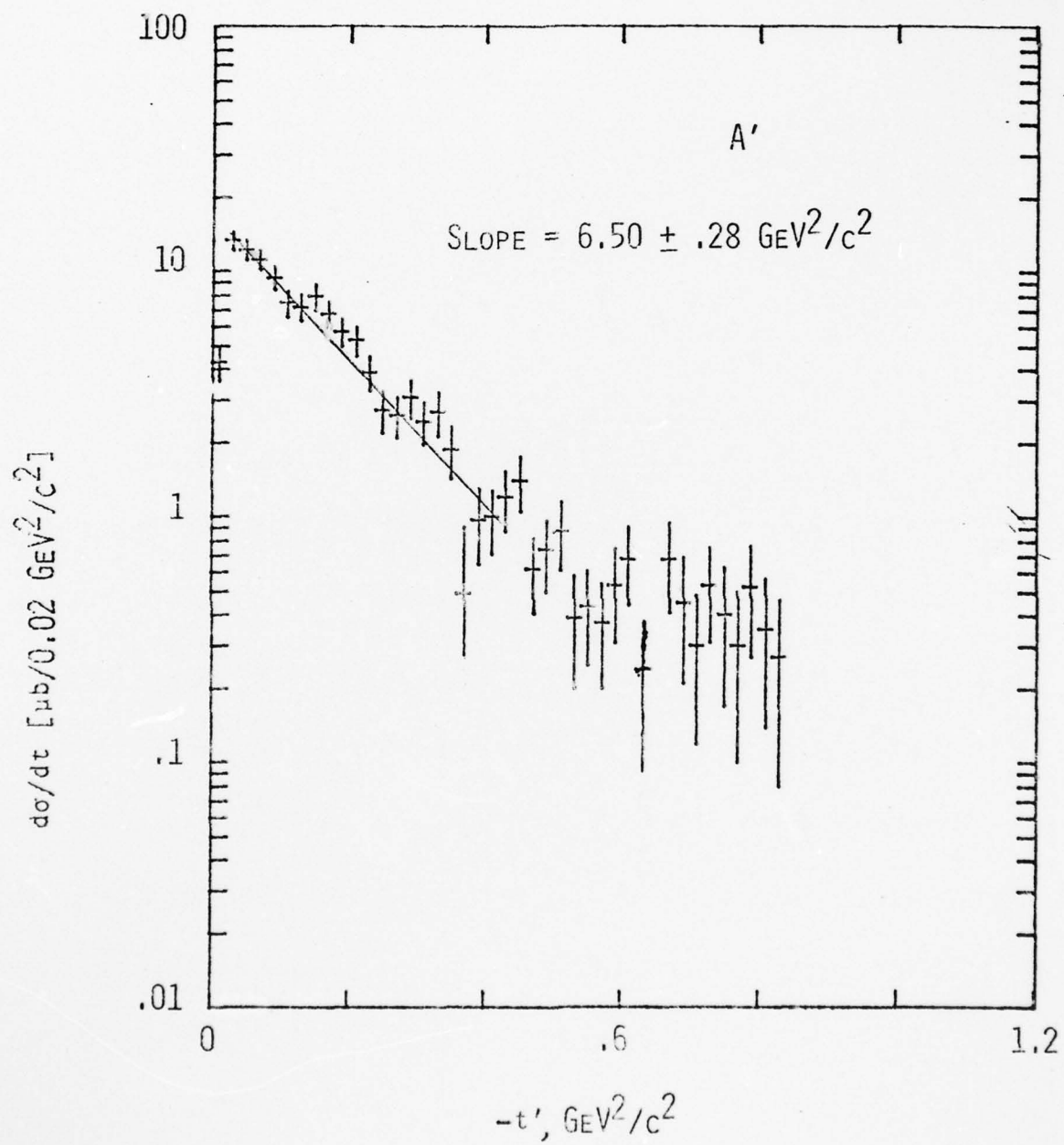


Figure 36

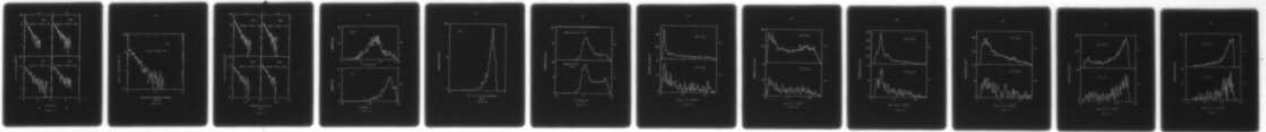
AD-A053 520

MASSACHUSETTS INST OF TECH CAMBRIDGE DEPT OF PHYSICS F/G 20/8  
PRISM PLOT ANALYSIS OF THE REACTION  $\pi(-)P$  YIELDS  $P \pi(+)\pi(-)P$ --ETC(U)  
MAY 77 T LAINIS

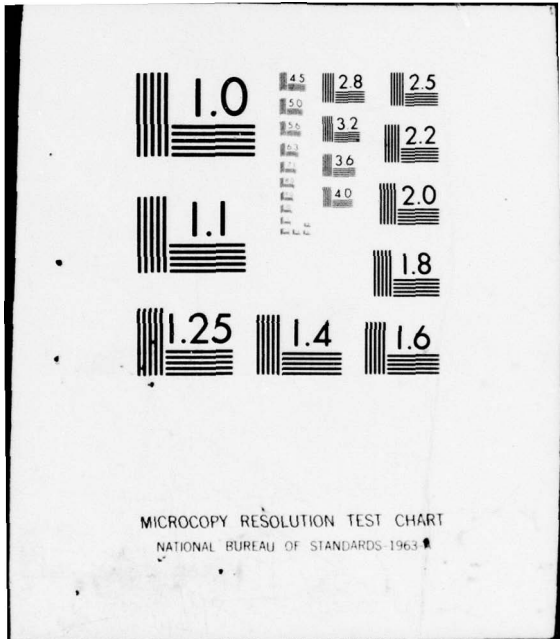
UNCLASSIFIED

NL

2 OF 2  
AD  
A053520



END  
DATE  
FILMED  
6-78  
DDC



MICROCOPY RESOLUTION TEST CHART  
NATIONAL BUREAU OF STANDARDS-1963-A

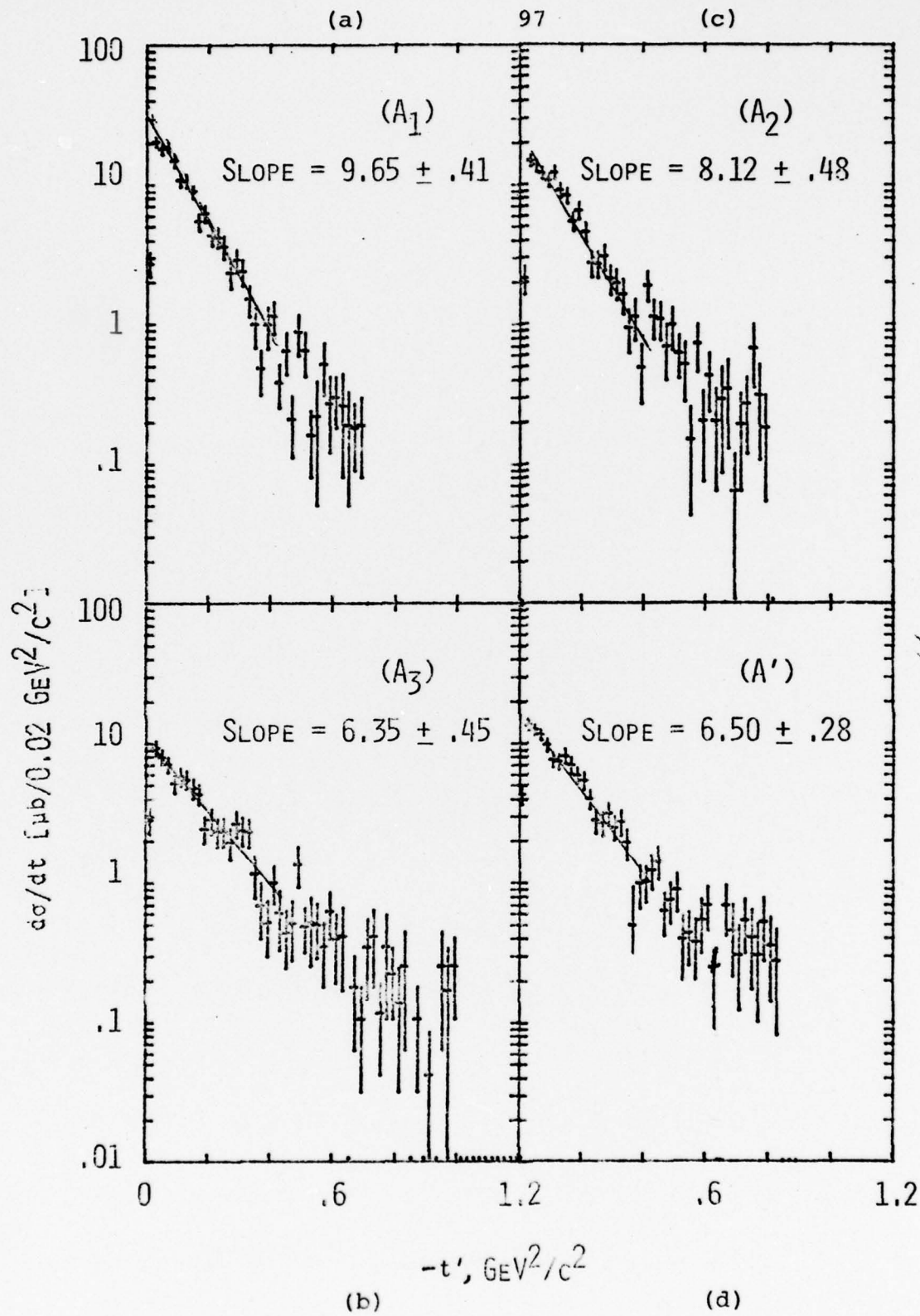


Figure 37

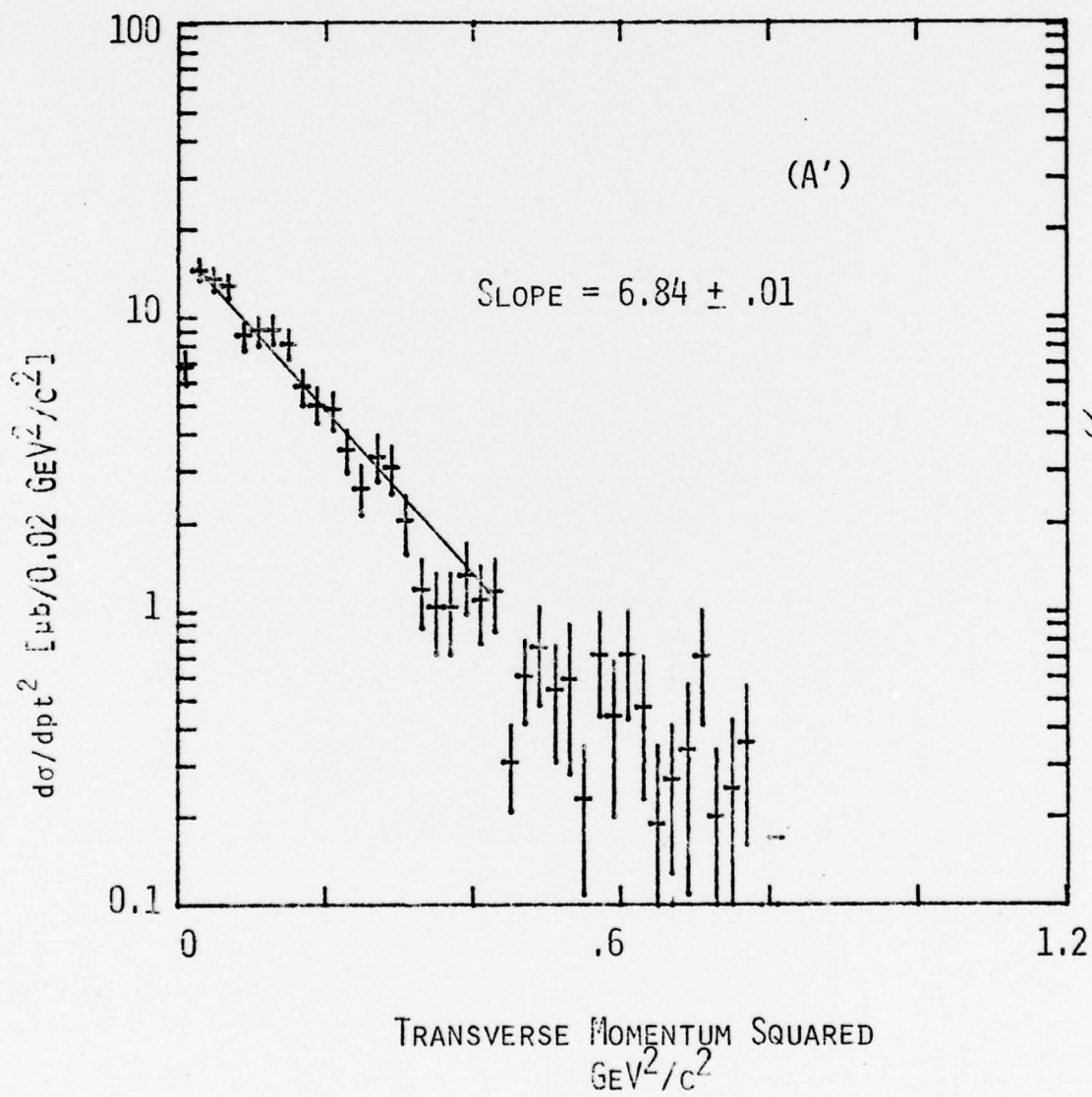


Figure 38

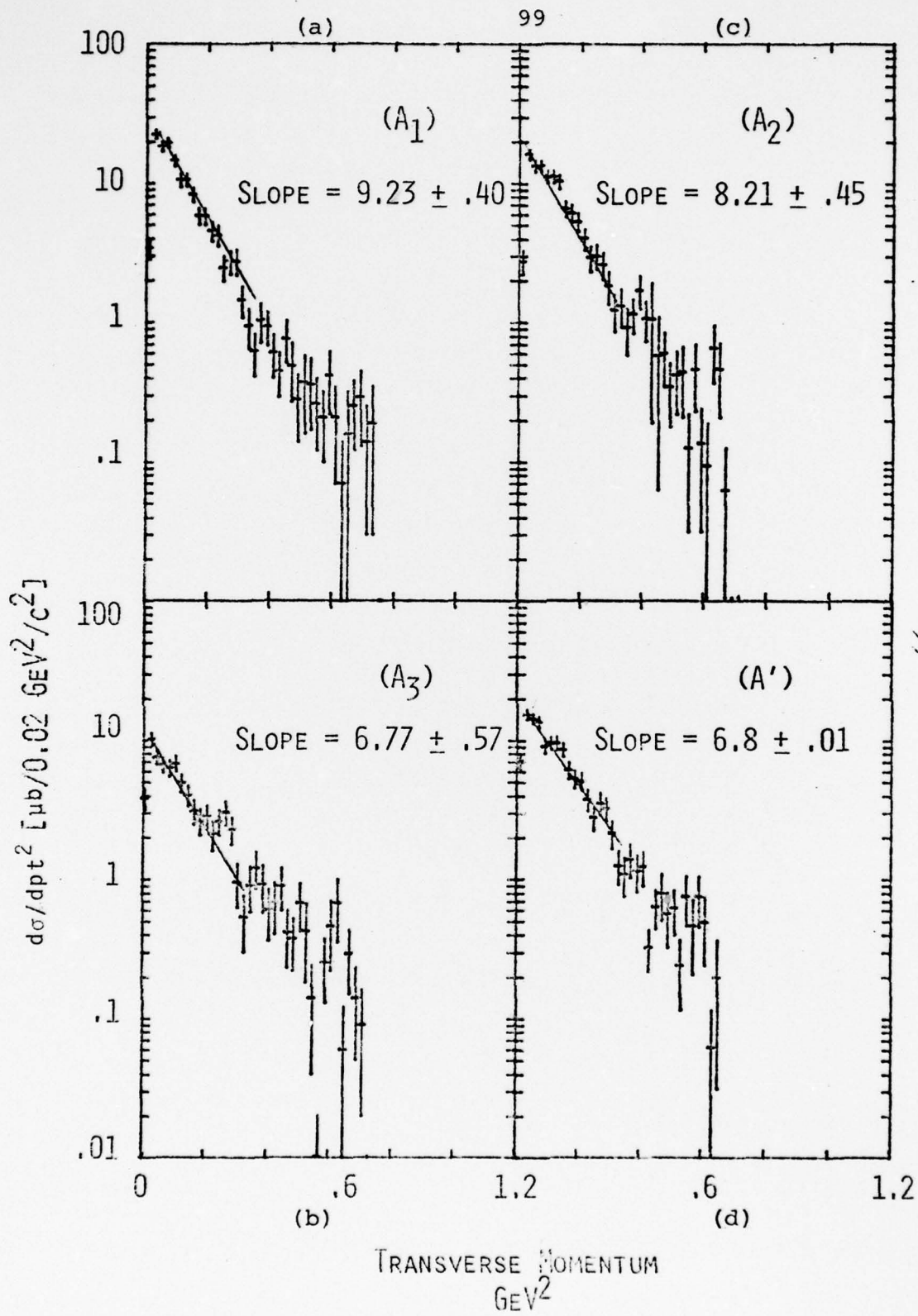


Figure 39

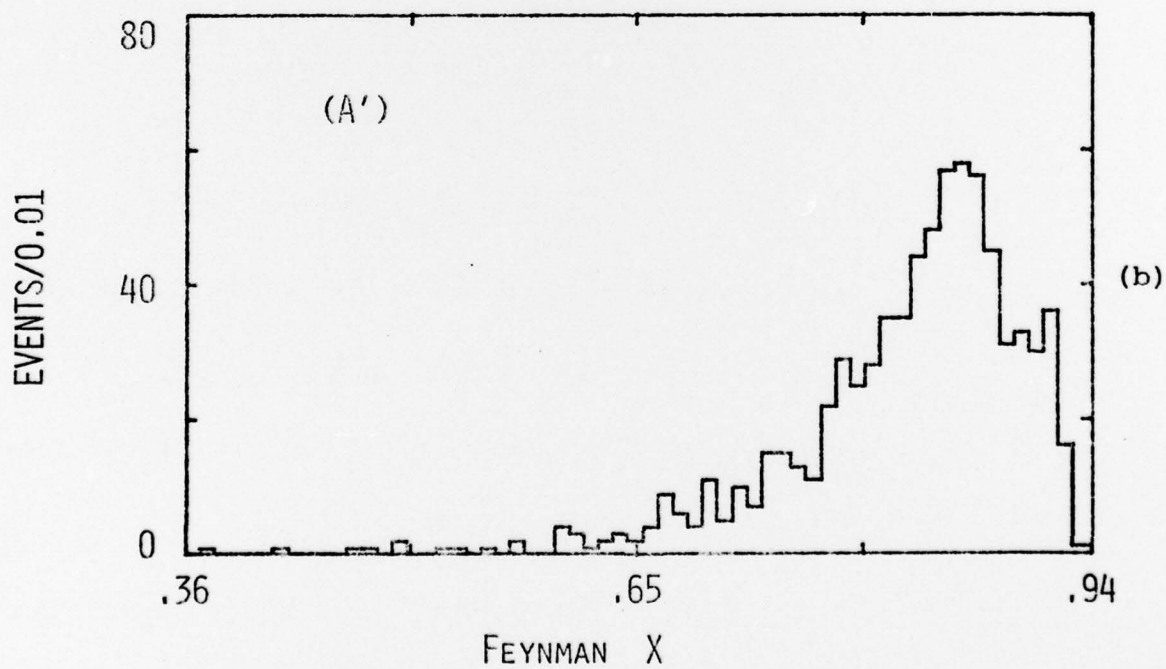
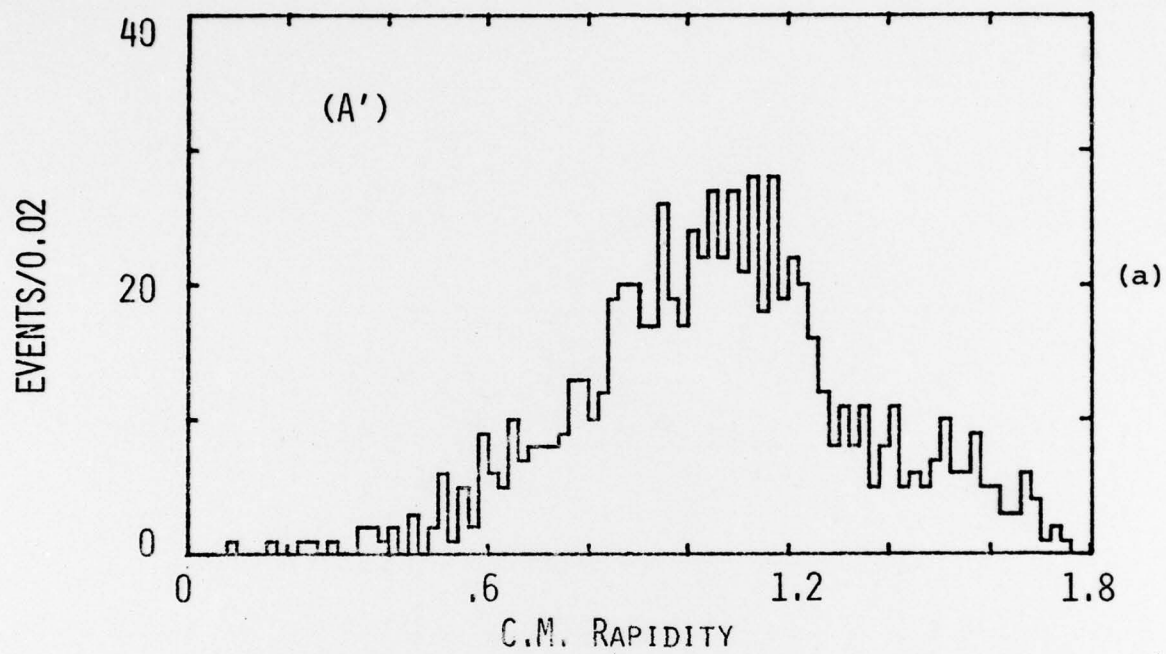


Figure 40

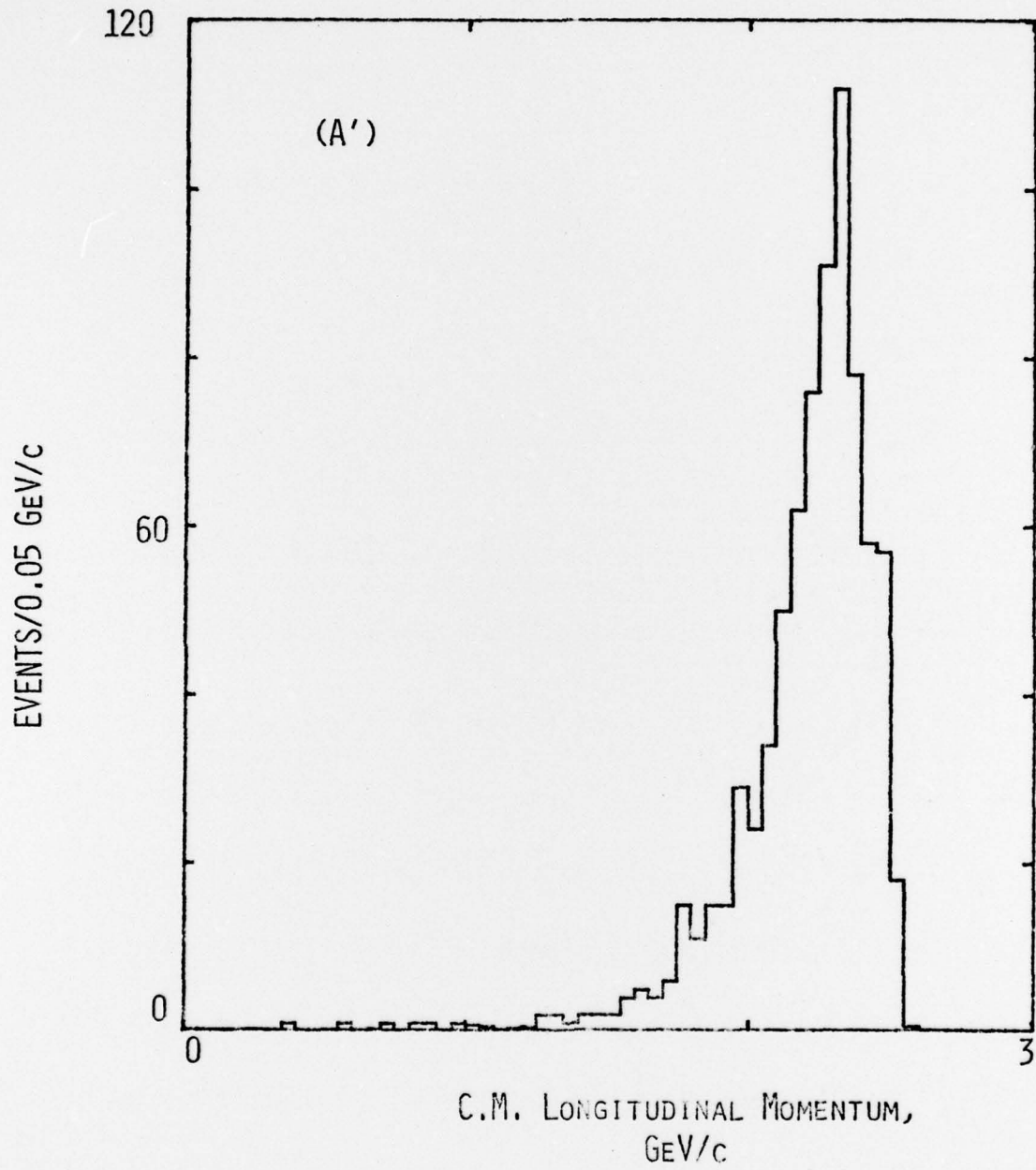


Figure 41

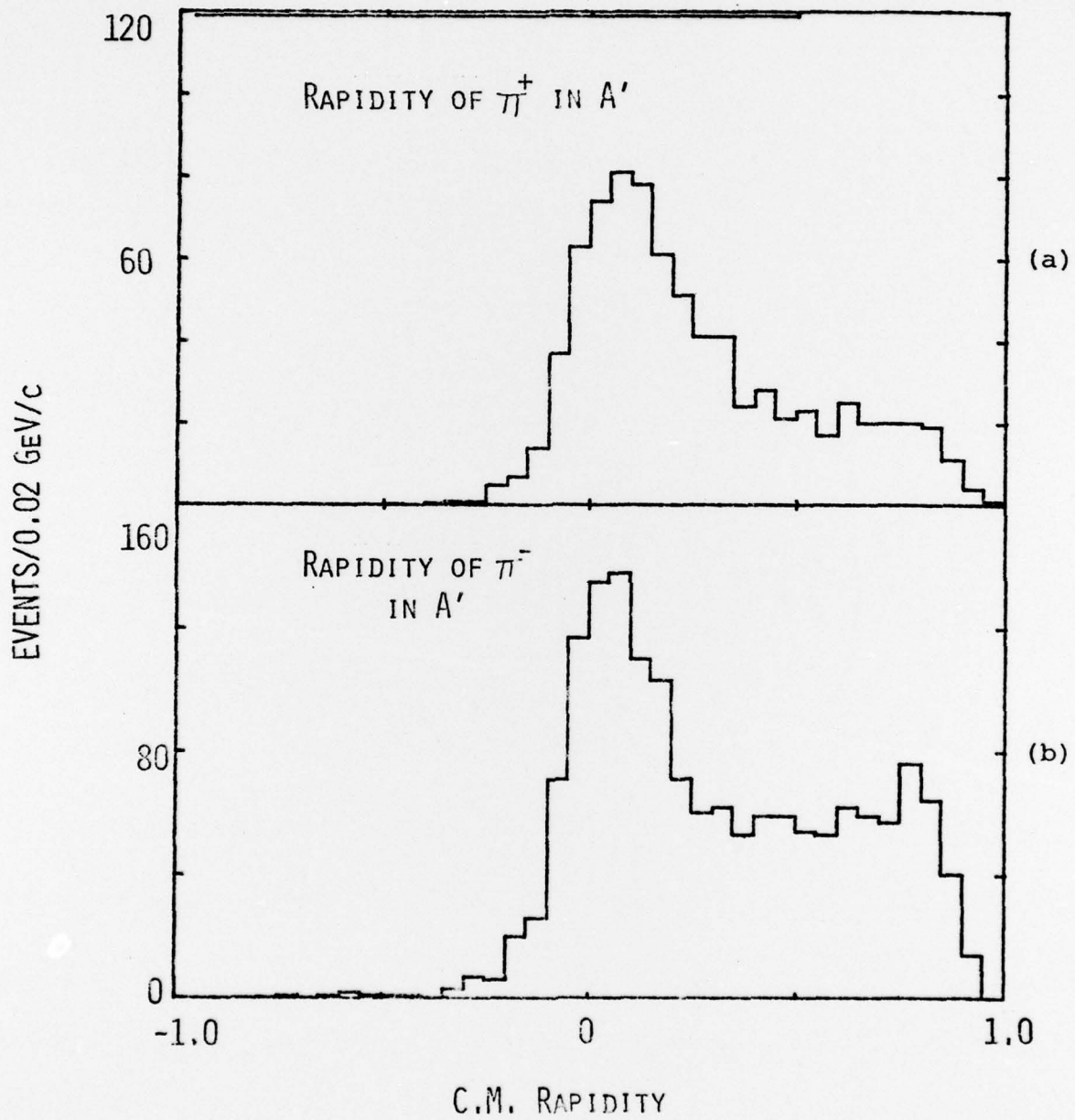


Figure 42

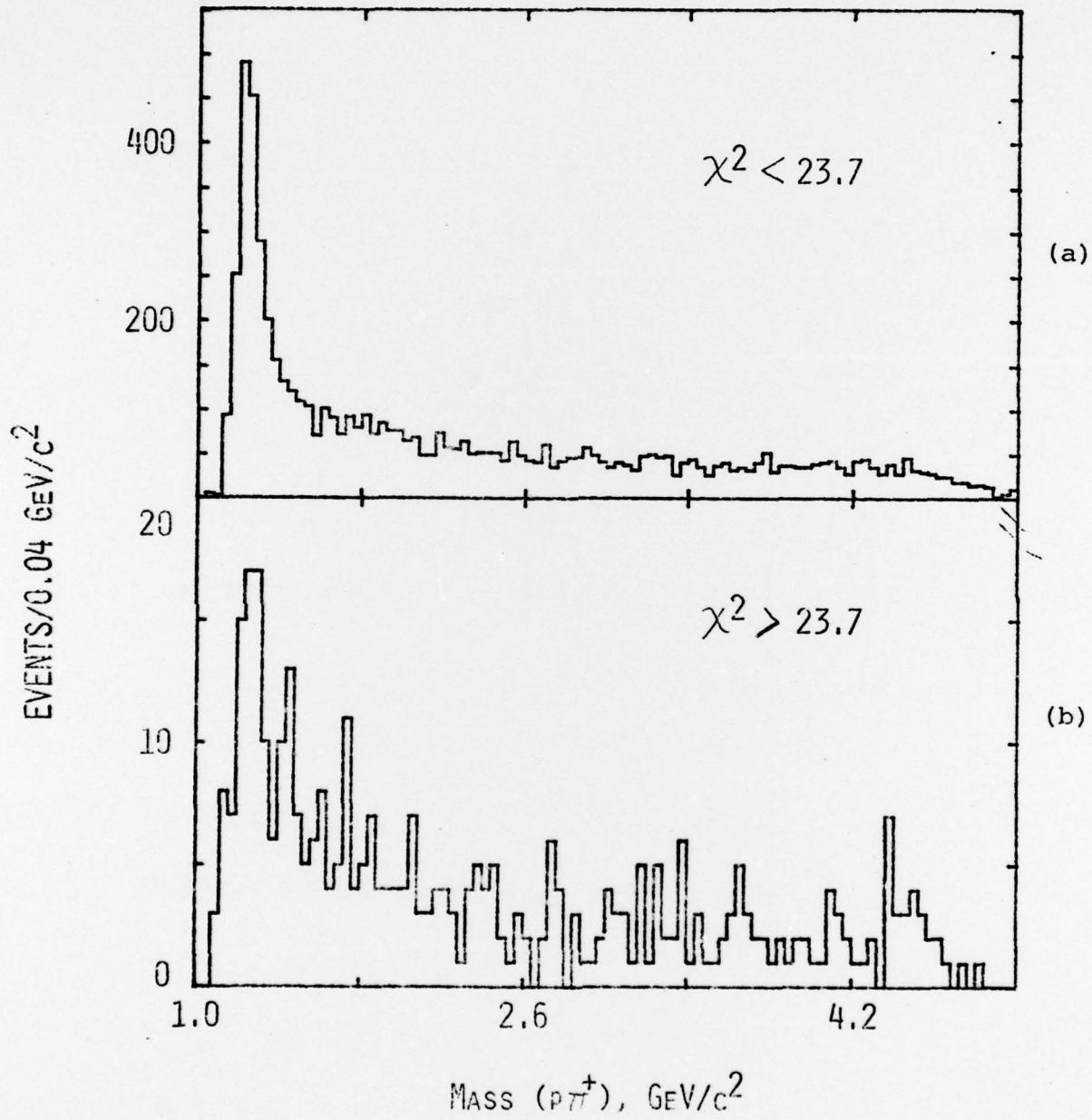


Figure 43

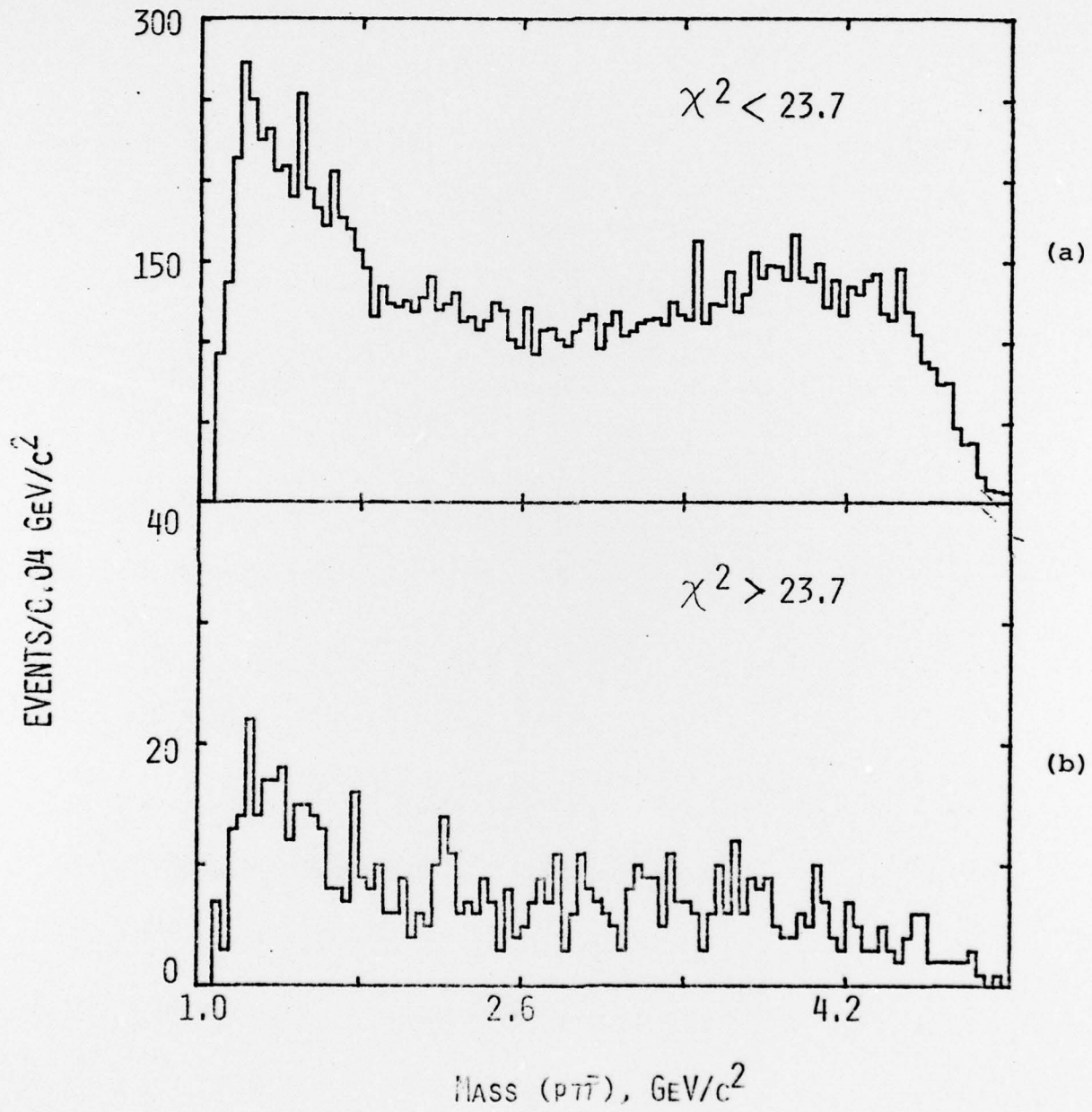


Figure 44

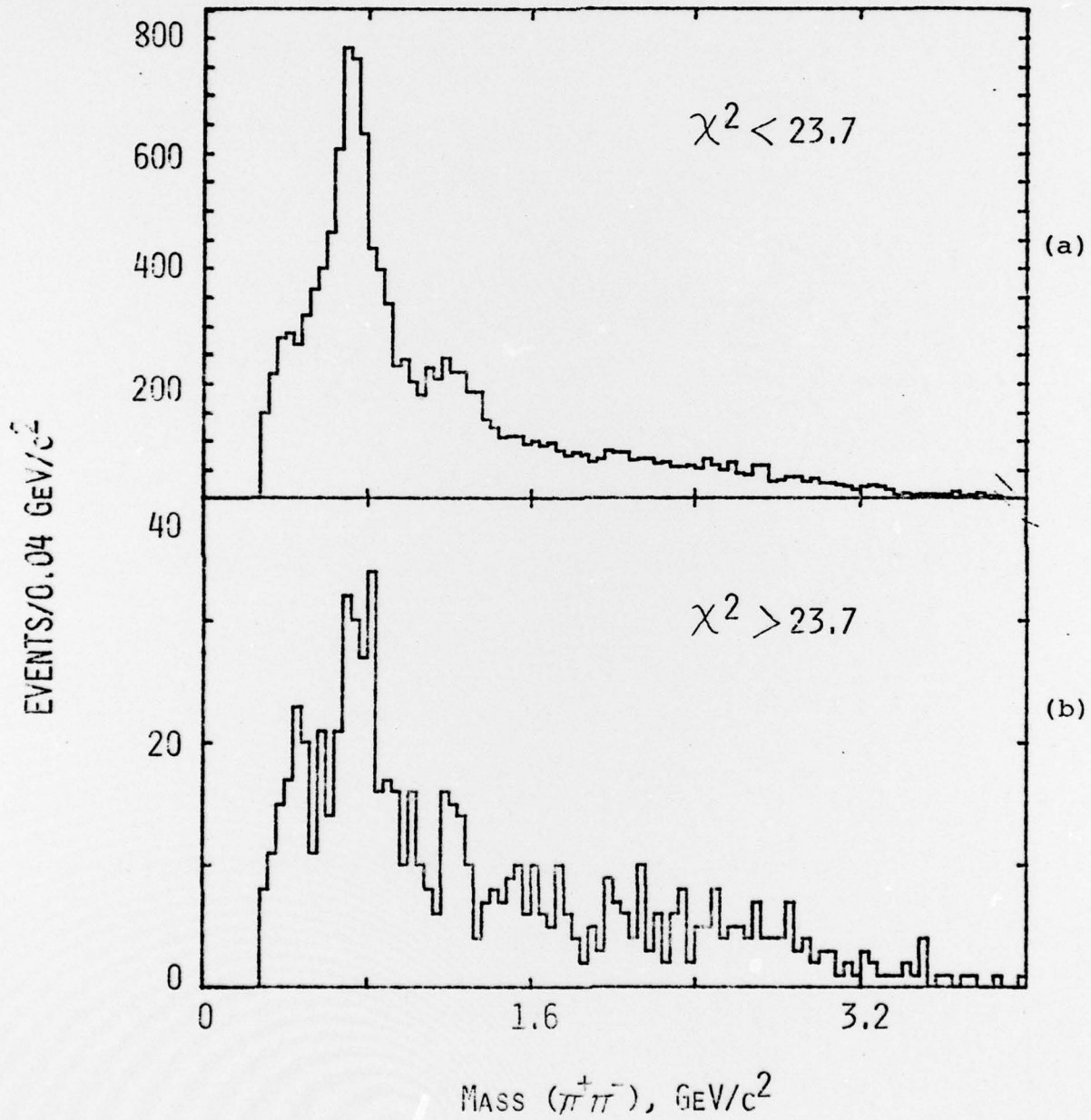


Figure 45

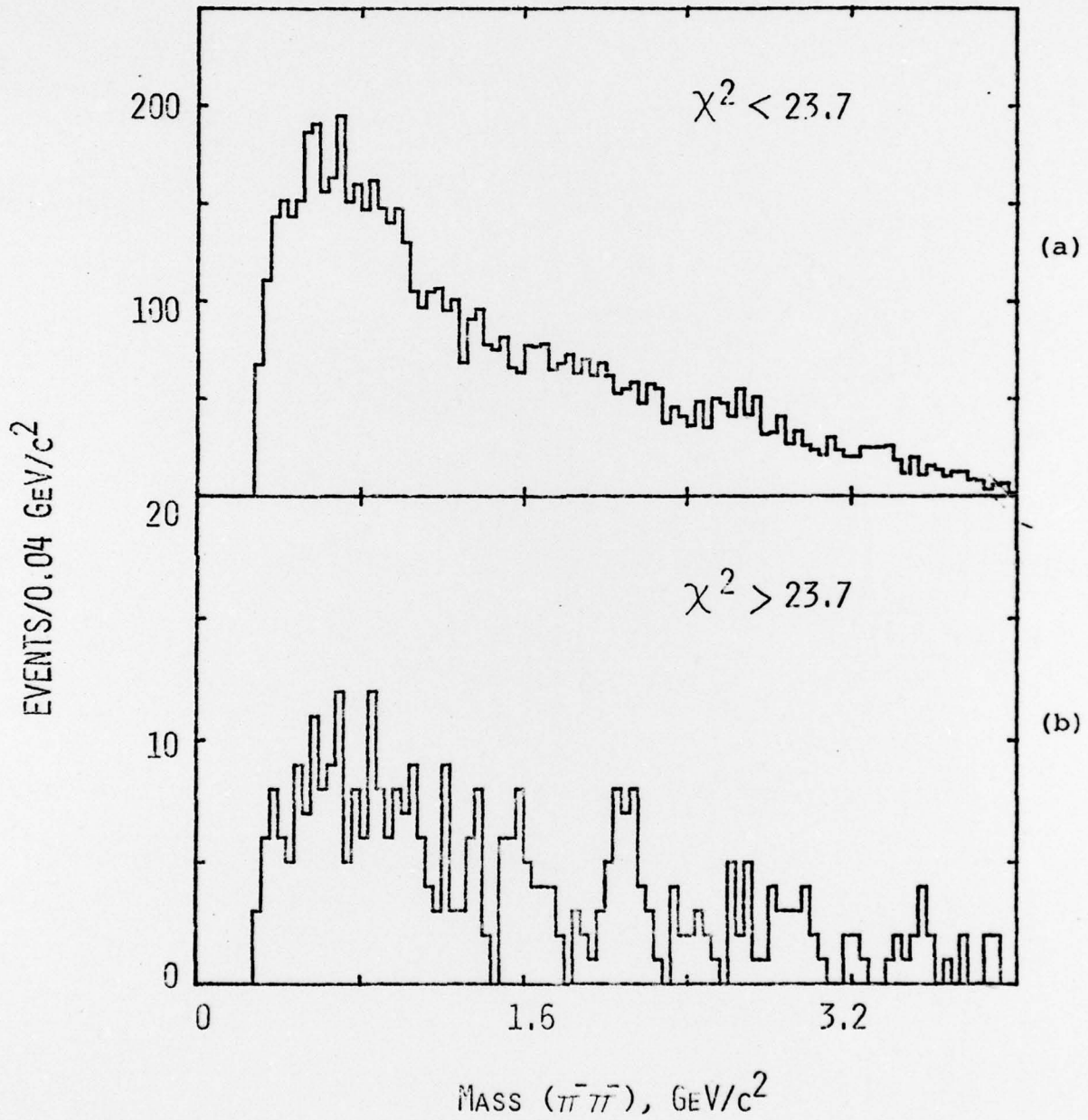


Figure 46

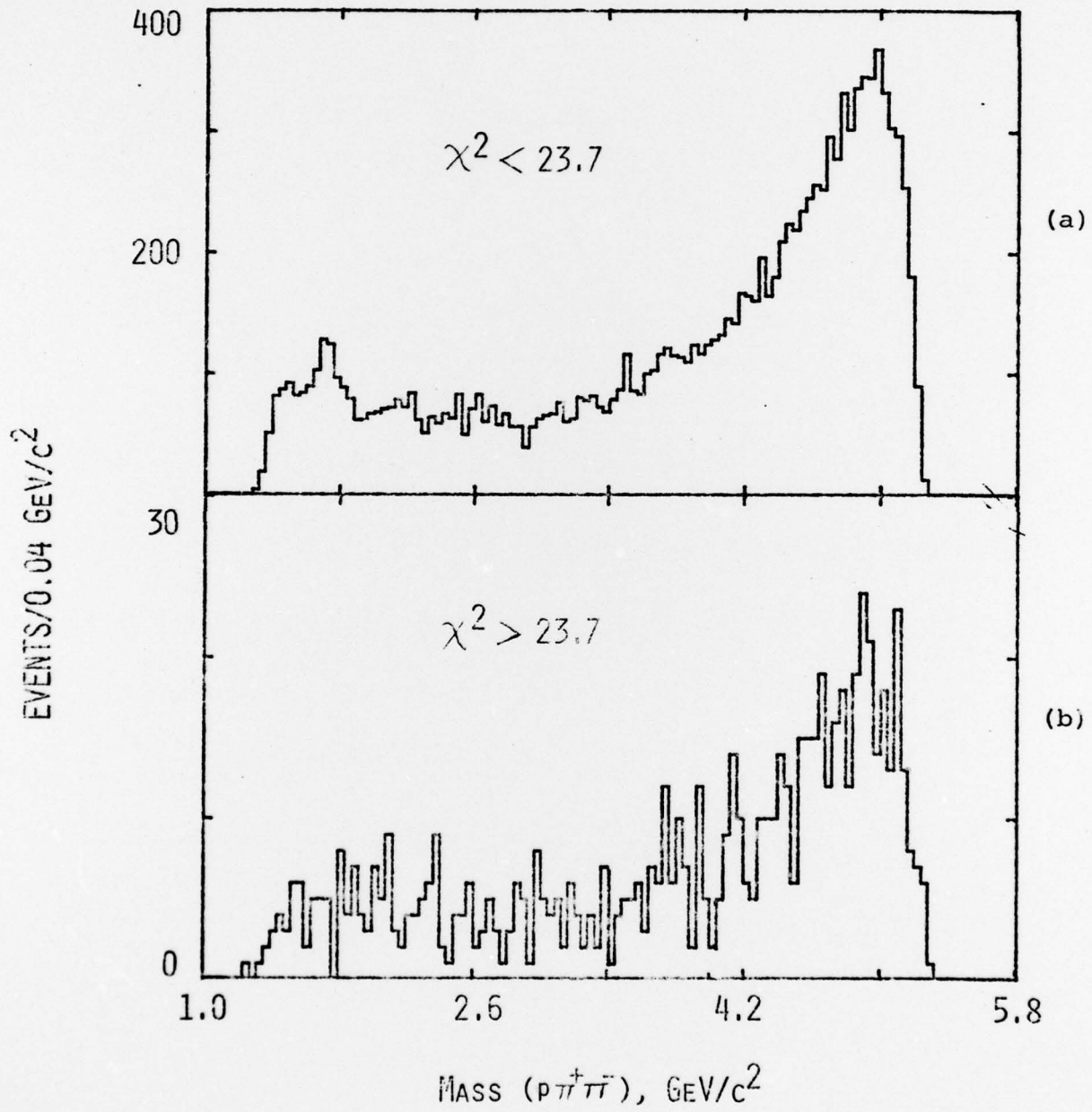


Figure 47

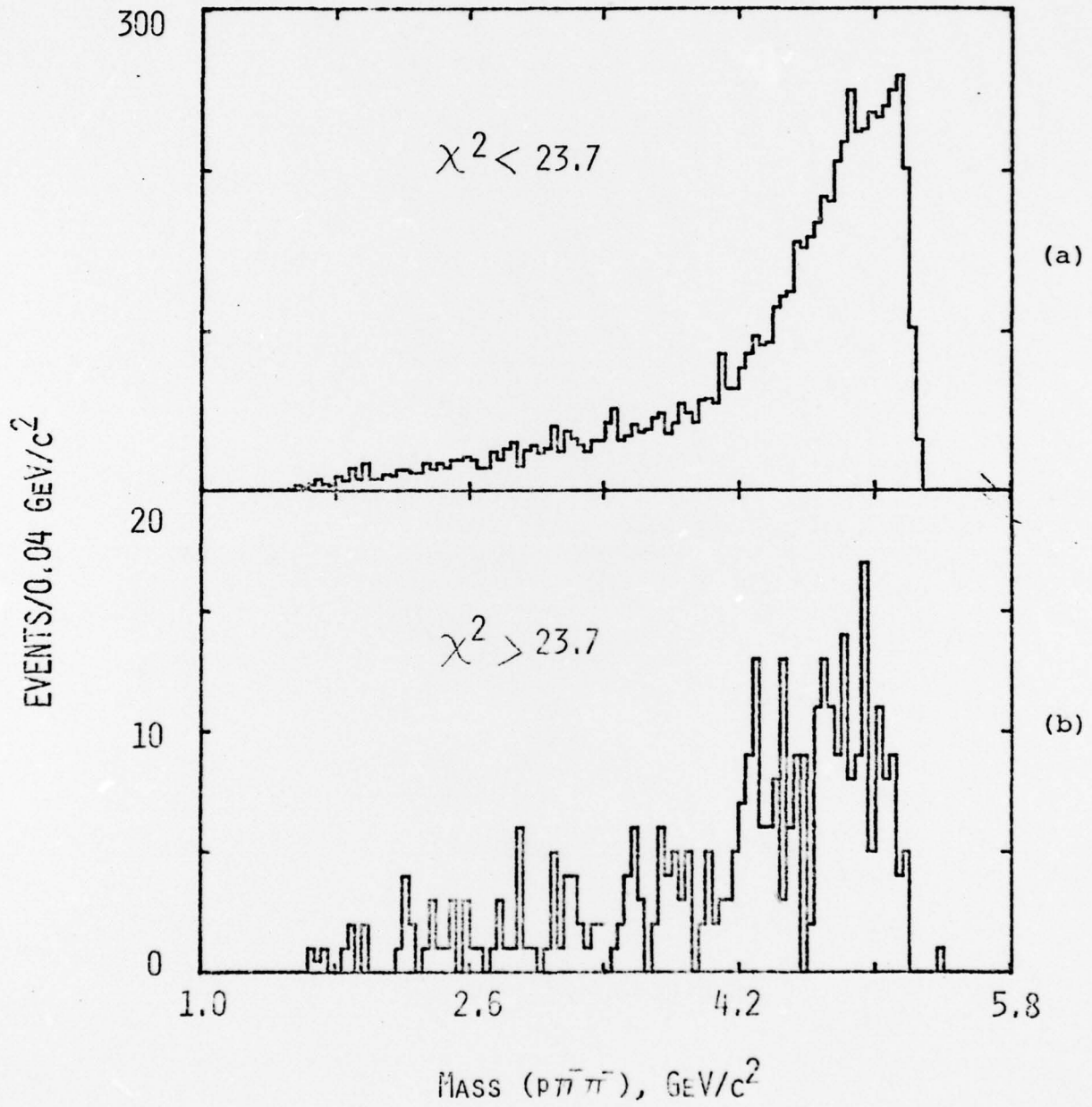


Figure 48

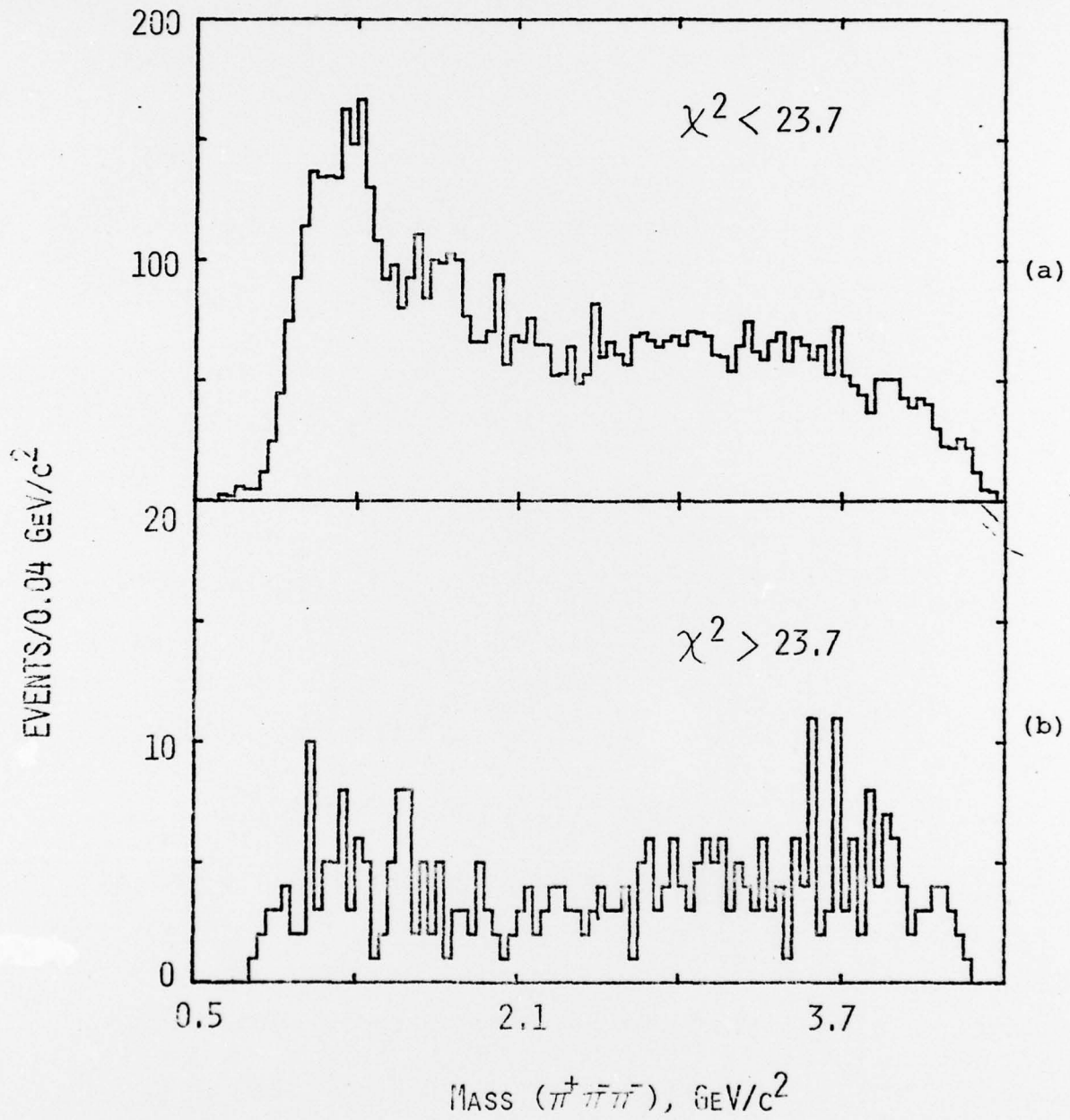


Figure 49

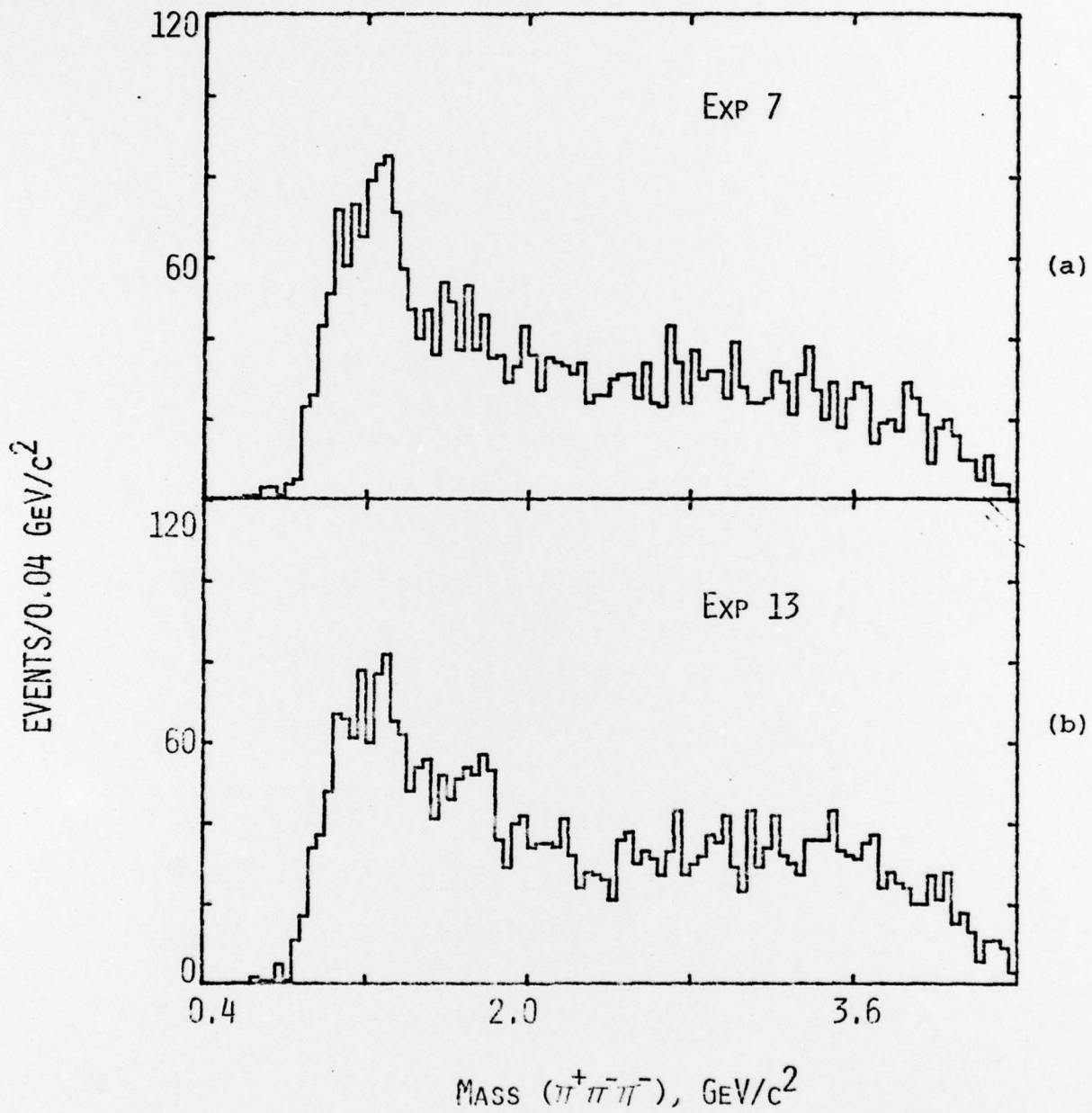


Figure 50

CHANNELS INCREASED FROM  
5 TO 11

CHANNEL

+ ( $\Delta^{++} \pi^-$ )

□  $A_2$

●  $A_3$

△  $A_1$

▽  $\Delta^0 \rho^0$

■ PHASE SPACE

PHASE SPACE DROPPED  
 $A_1$  AND  $A_3$  FLOATED,  $A'$   
DROPPED

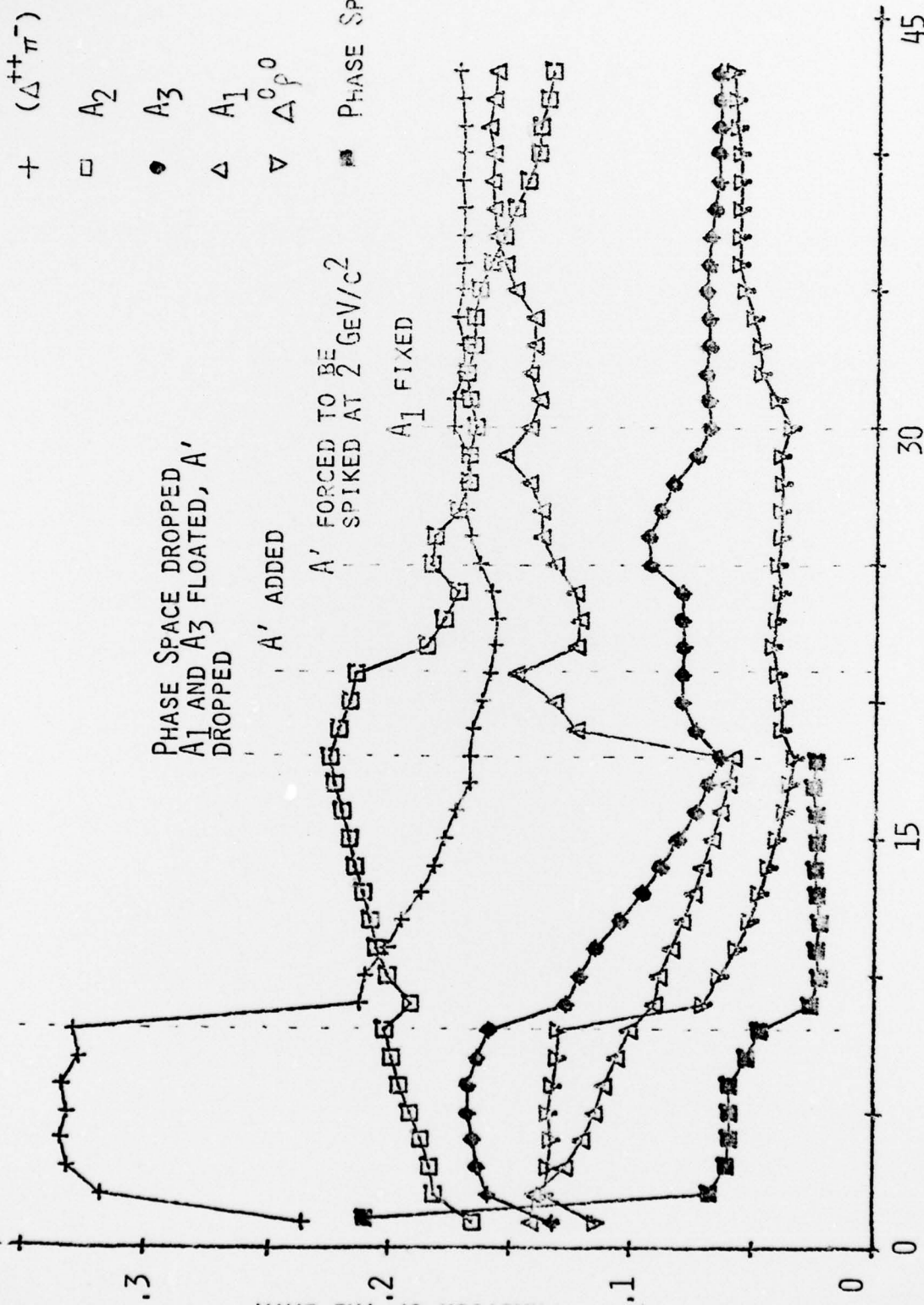
$A'$  ADDED

$A'$  FORCED TO BE  
SPIKED AT 2 GEV/ $c^2$

$A_1$  FIXED

111

FRACTION OF THE DATA



ITERATION NUMBER  
Figure 51

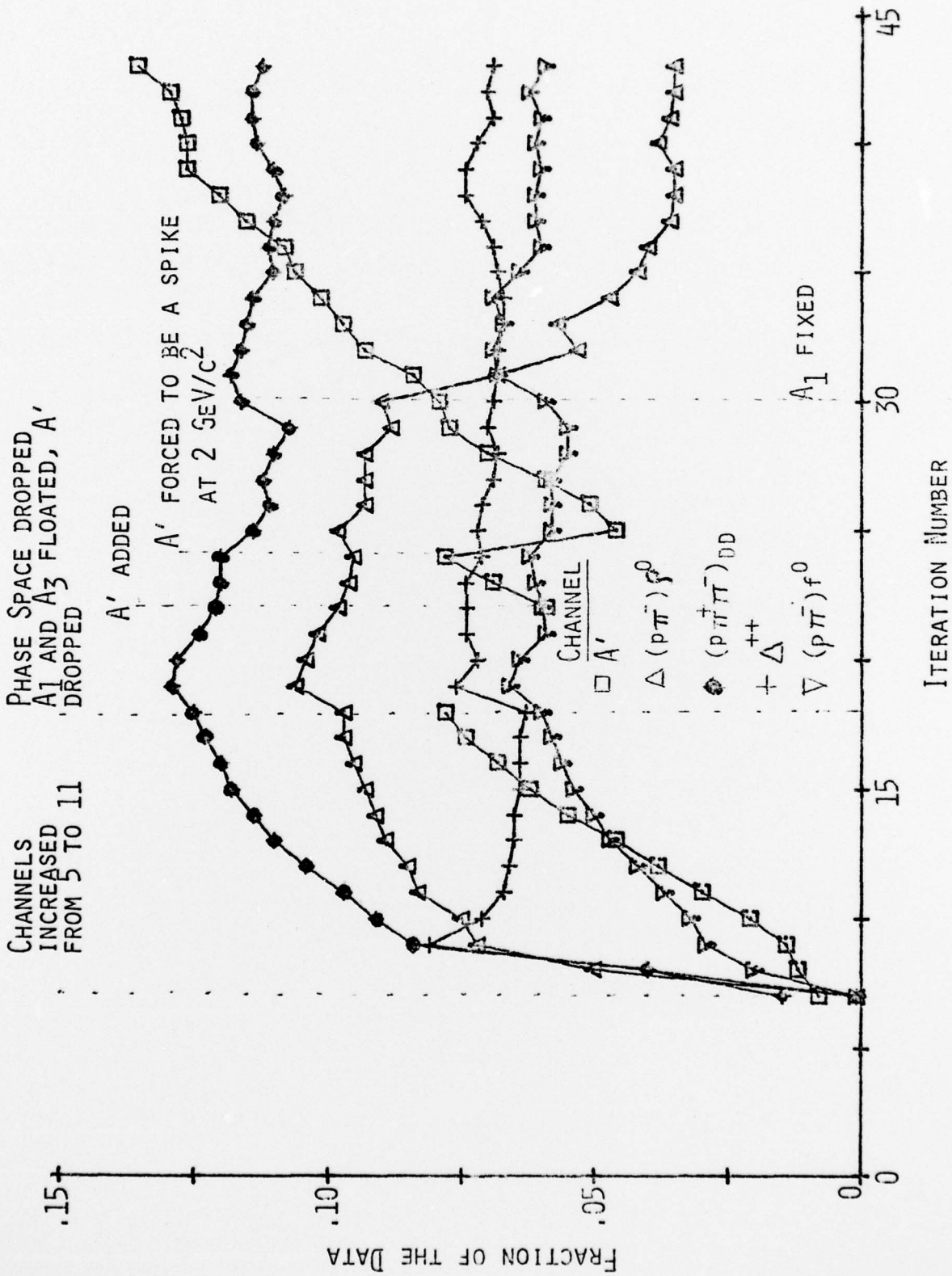


Figure 52

## VARYING BOX TECHNIQUE USED

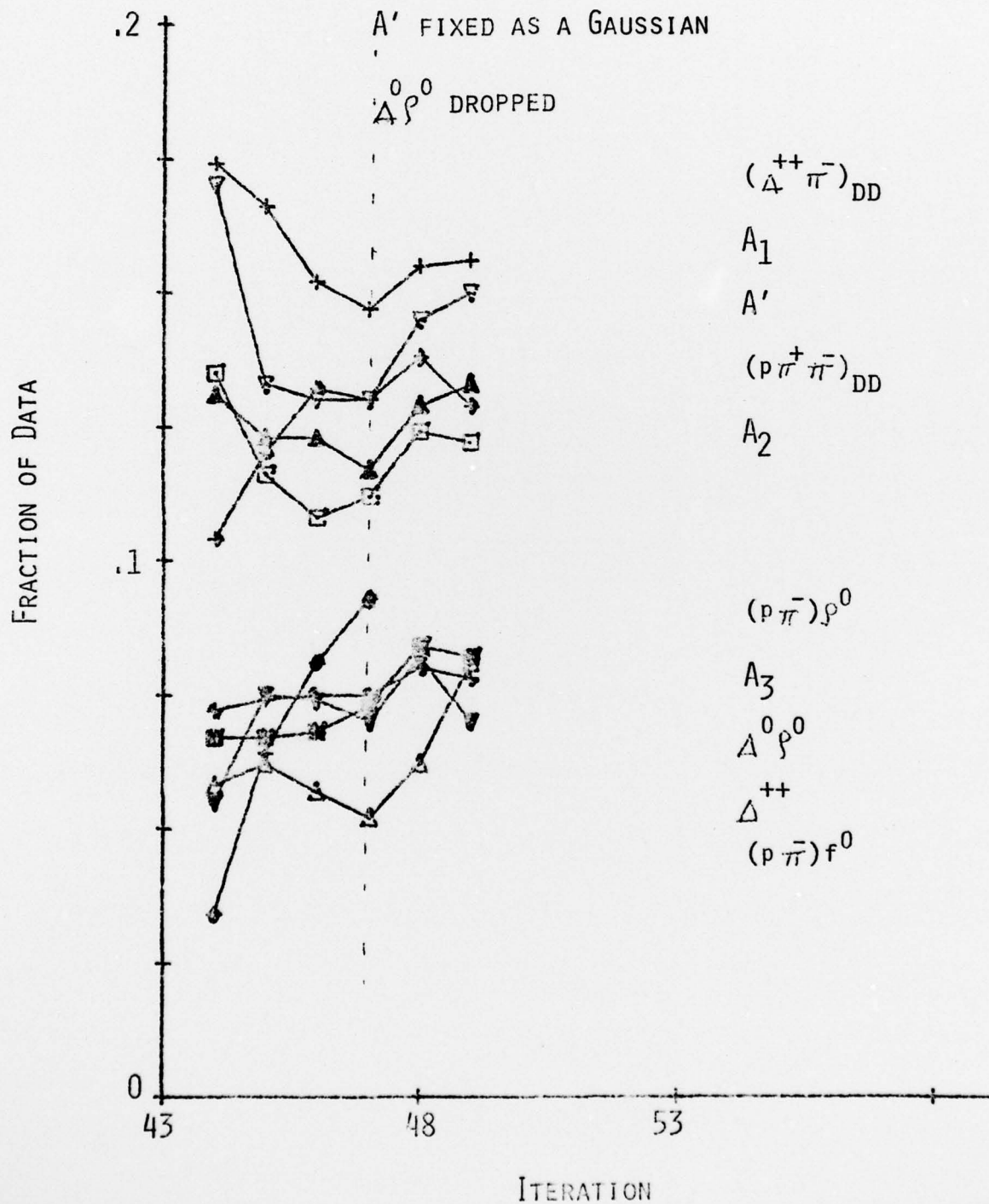


Figure 53